Nanomanufacturing
University of Michigan
ME599-002 | Winter 2010

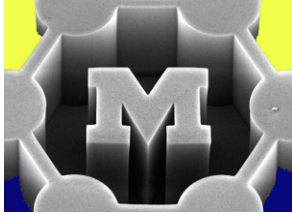

15: **Nanowire/nanotube synthesis; bulk production and top-down integration**

March 15, 2010

John Hart
ajohnh@umich.edu
http://www.umich.edu/~ajohnh

Announcements

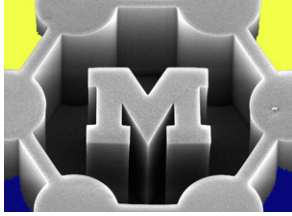

- Video due 5pm today (Mar/15)
  - Please bring file on USB stick Wednesday
  - Peer review info TBA (due Mar/26)
- PS3 due Wed (Mar/17)
  - Q2, Q3 → qualitative answers OK; ask questions during lecture today
- PS2 returned Wed, also HW3 solution to be posted Wed

Recap: NP growth kinetics – size broadening and focusing

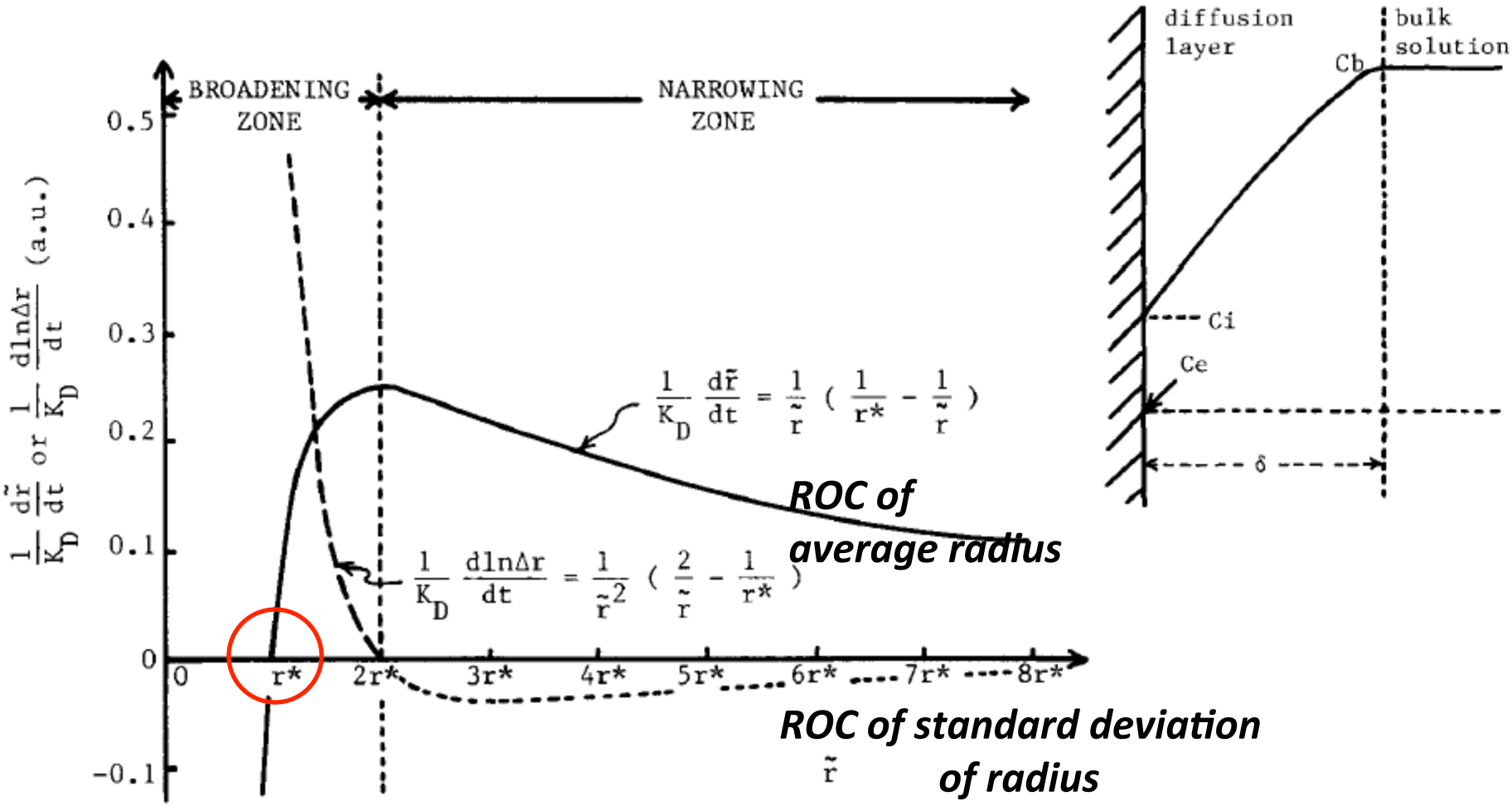

Fig. 3. $[d\tilde{r}/dt]/K_D$ or $[d\ln(\Delta r)/dt]/K_D$ as a function of r for diffusion-controlled growth with the infinite diffusion layer; the size distribution is broadened for $\tilde{r} < 2r^*$, while narrowed for $\tilde{r} > 2r^*$.

Sugimoto, *Adv. Colloid Interface Science* 28:65, 1987.

Good separation of nucleation and growth

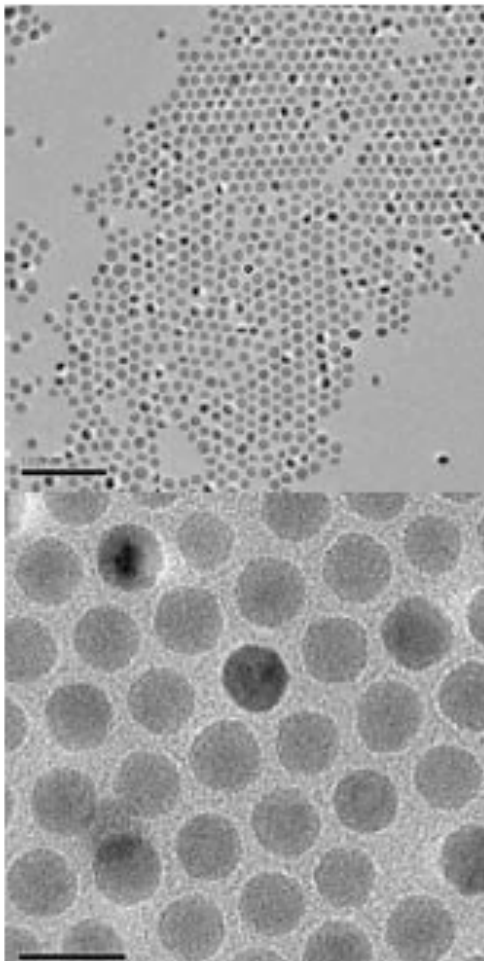

Poor separation of nucleation and growth

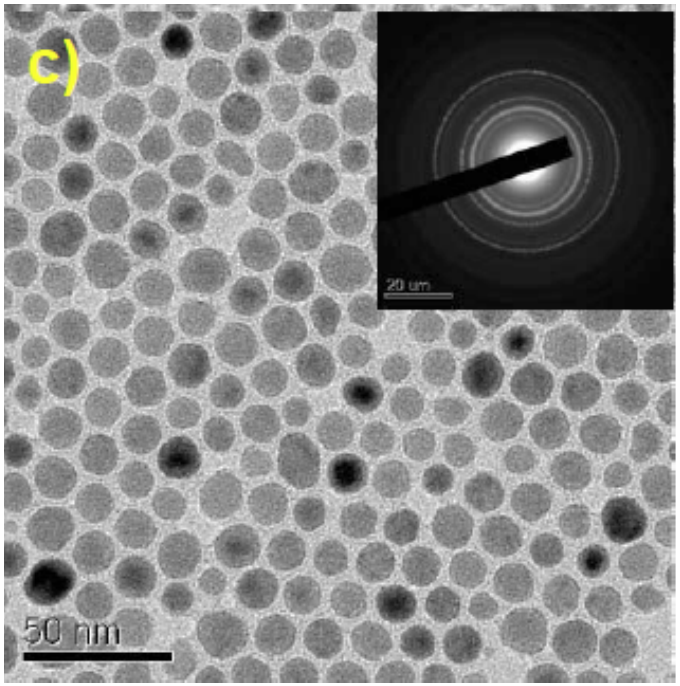

Park et al., *Nature Materials* 3:891, 2004.

Today's agenda

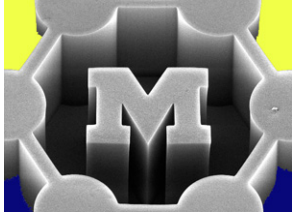

- General methods of making 1D nanostructures
- Synthesis of nanotubes and nanowires by CVD methods:
  - Basic growth mechanisms
  - Furnace designs
  - Nucleation and catalyst performance
  - Preparation and deposition of nanoparticle catalysts
  - CNT and NW growth on substrates: morphology control and parameter trends
  - Limiting mechanisms: kinetics, diffusion, impurities, defects

Readings for lectures 13-15

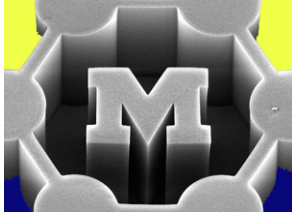

Nominal: (ctools)

- AJH written notes (one file for today and wednesday)
- Sugimoto, "Preparation of monodispersed colloidal particles"
  - Through page 73, needed as backup to lecture notes only
- Peng et al., "Kinetics of II-VI and III-V colloidal semiconductor nanocrystal growth: focusing of size distributions"

- Kodambaka et al., "Growth kinetics of Si and Ge nanowires"
- Hochbaum et al., "Controlled growth of Si nanowire arrays for device integration"
- Terranova et al., "The world of carbon nanotubes: an overview of CVD growth methodologies"
- Wirth et al., "Diffusion- and reaction-limited growth of carbon nanotube forests"

Readings for lectures 13-15

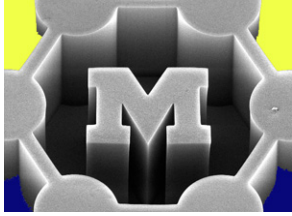

Extras: (ctools)

- Burda et al., excerpt from "Chemistry and properties of nanocrystals of different shapes"

  → More detail on chemical methods of NP synthesis, self-assembly

- Xia et al., "One-dimensional nanostructures: synthesis, characterizaton, and applications"

  → Broad overview of top-down and bottom-up NW/NT synthesis

- Wagner and Ellis, "The vapor-liquid-solid method of crystal growth and its application to silicon"
- Hofmann et al., "Ledge-flow-controlled catalyst interface dynamics during Si nanowire growth"
- Harutyunyan et al., "Preferential growth of single-walled carbon nanotubes with metallic conductivity"

Building blocks

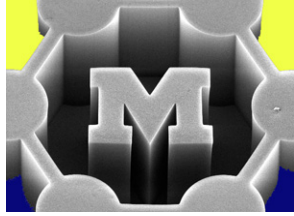

0-D

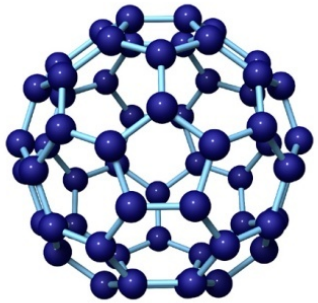

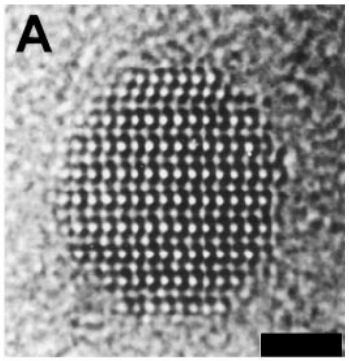

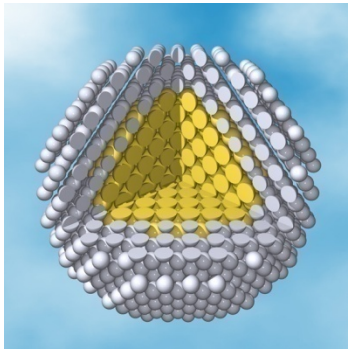

Nanoclusters

Magic #'s of atoms

≤1 nm size

Nanoparticles

100's-1000's of atoms

~1-100 nm diameter

1-D

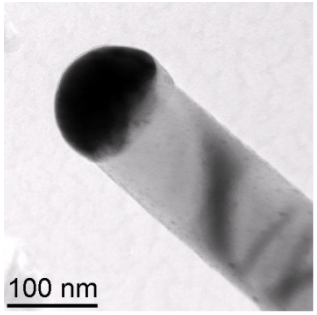

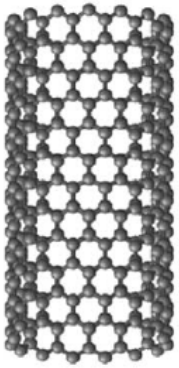

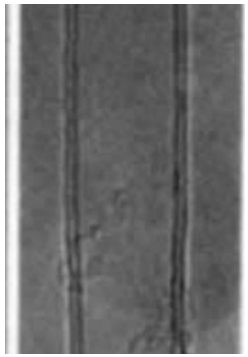

2-D

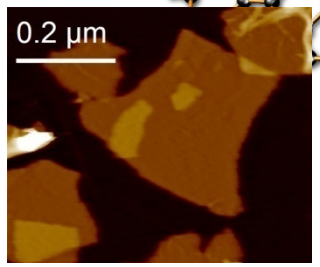

Nanowires

Filled

Nanotubes

Hollow

Nanosheets

~1 atom thick

~1-100 nm dia, up to mm long and beyond!

Ways of making ‘1D’ nanostructures

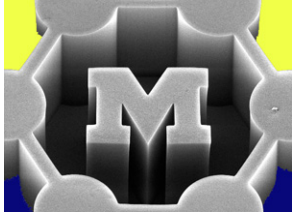

Guide along a preferred crystal direction

Confinement by liquid droplet

Template-directed (e.g., in a pore)

Kinetic control using capping reagents

Assembly of 0D structures (nanoparticles)

Size reduction

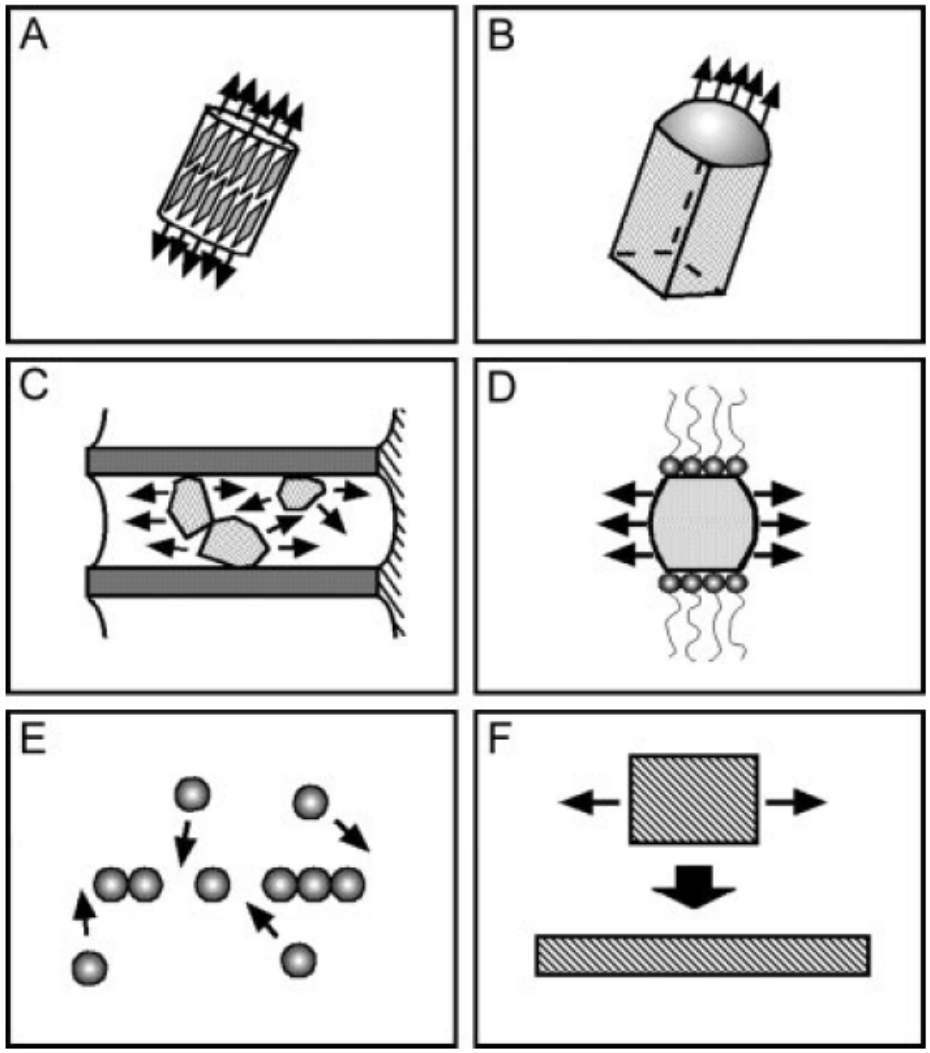

Fig. 1. Schematic illustrations of six different strategies that have been demonstrated for achieving 1D growth: a) dictation by the anisotropic crystallographic structure of a solid; B) confinement by a liquid droplet as in the vapor–liquid–solid process; C) direction through the use of a template; D) kinetic control provided by a capping reagent; E) self-assembly of 0D nanostructures; and F) size reduction of a 1D microstructure.

Ways of making ‘1D’ nanostructures

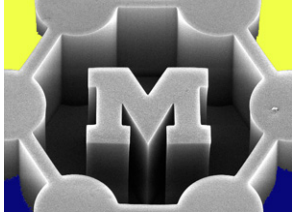

VS method

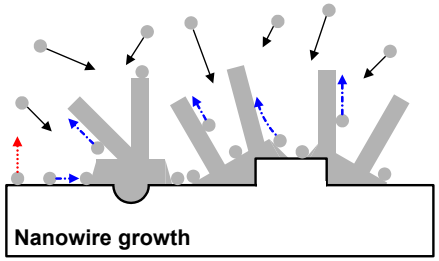

Today

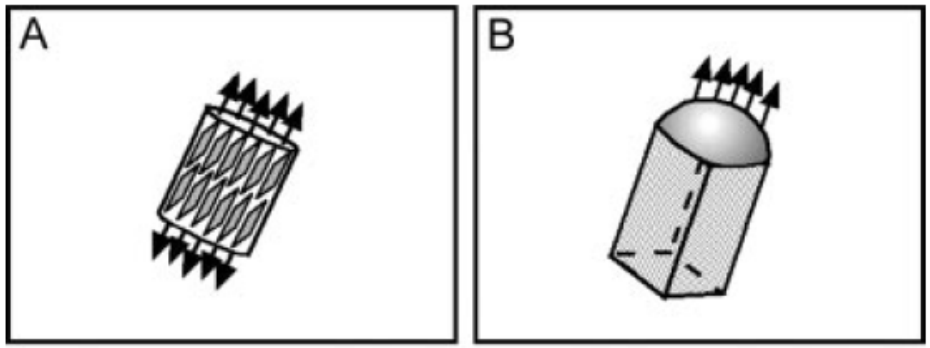

Next

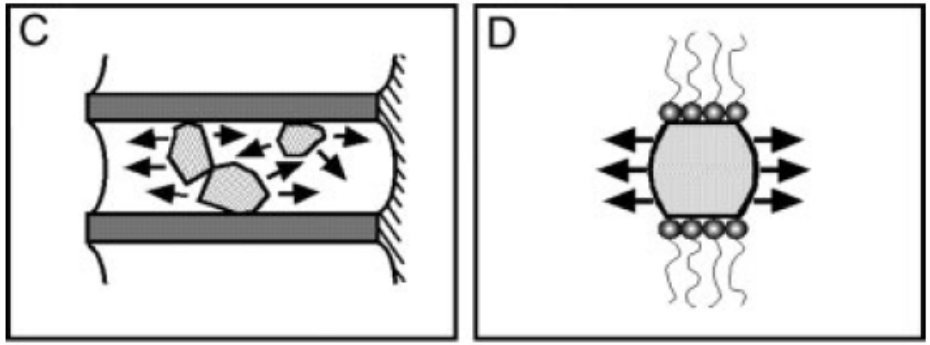

Tetrapods

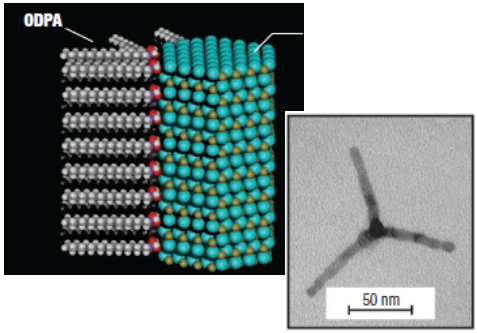

Self-assembly (later)

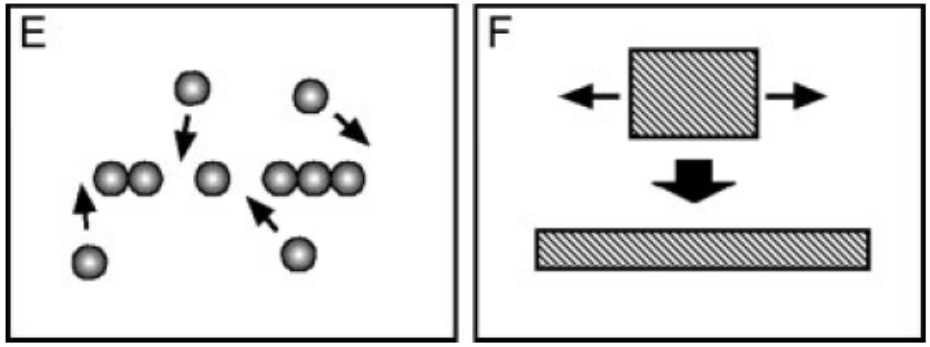

Top-down (lecture 12)

Fig. 1. Schematic illustrations of six different strategies that have been demonstrated for achieving 1D growth: a) dictation by the anisotropic crystallographic structure of a solid; B) confinement by a liquid droplet as in the vapor–liquid–solid process; C) direction through the use of a template; D) kinetic control provided by a capping reagent; E) self-assembly of 0D nanostructures; and F) size reduction of a 1D microstructure.

Templating methods

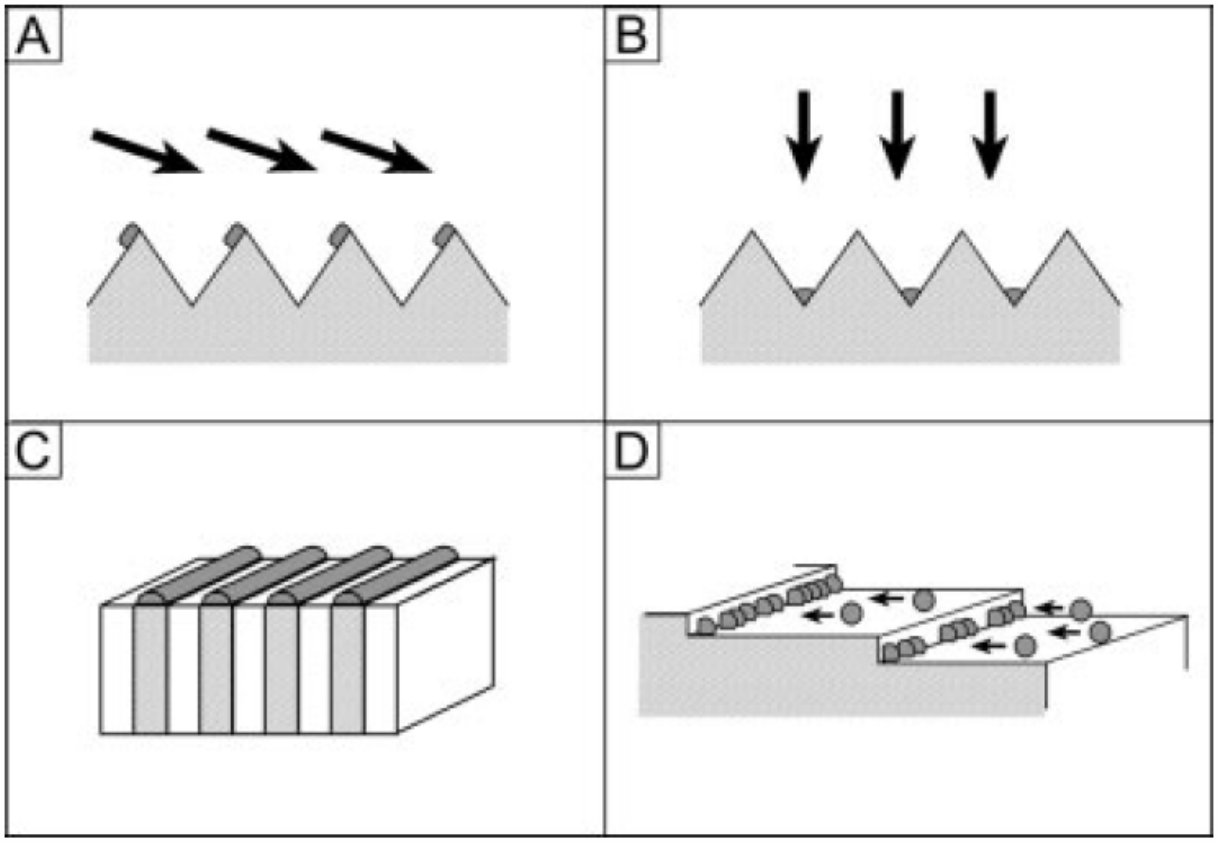

Fig. 6. Schematic illustrations of procedures that generated 1D nanostructures by A) shadow evaporation [58]; B) reconstruction at the bottom of V-grooves [60]; C) cleaved-edge overgrowth on the cross-section of a multilayer film [64]; and D) templating against step edges on the surface of a solid substrate [68].

Xia et al., *Advanced Materials* 15(5):353, 2003.

Templating methods

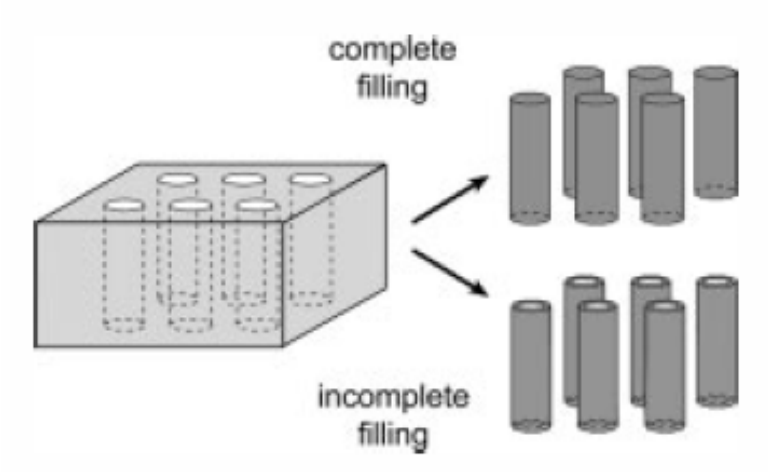

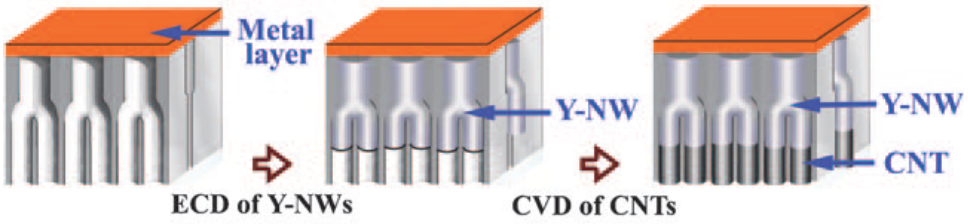

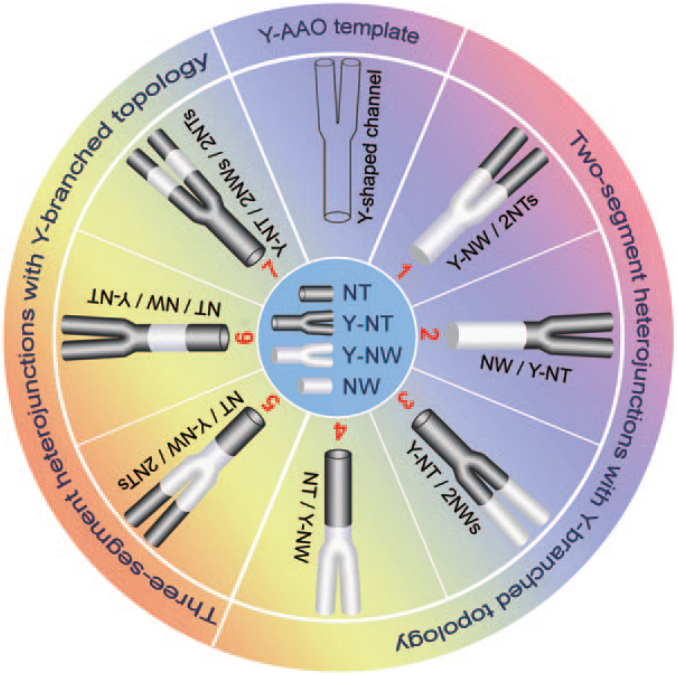

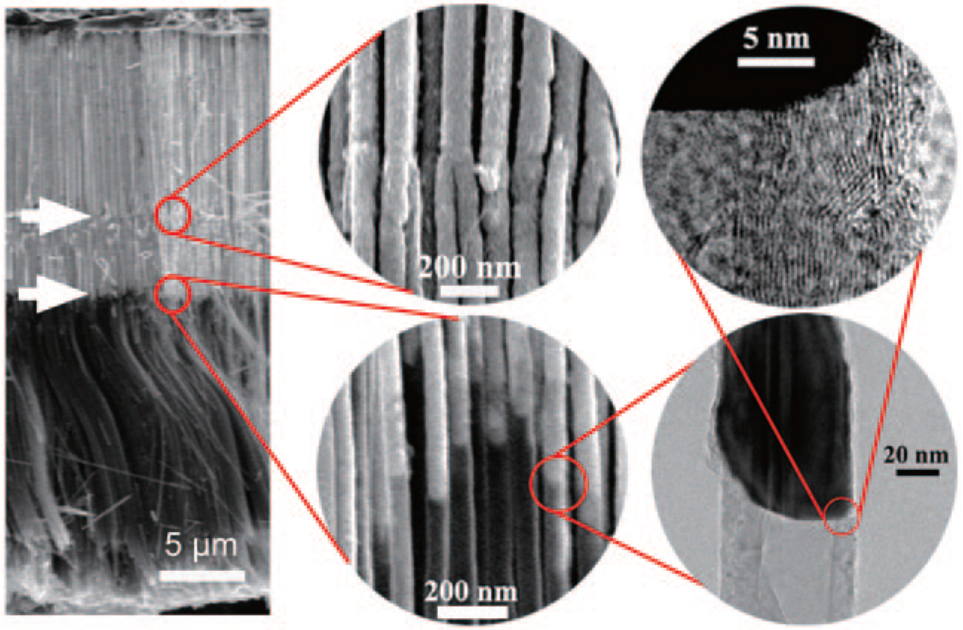

Xia et al., *Advanced Materials* 15(5):353, 2003.
Meng et al., *Angewandte Chemie* 48:1-6, 2009.

Many materials can be made into nanotubes and nanowires

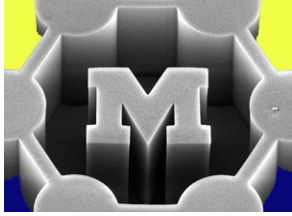

- Nanowires
  - Catalytic growth: **Si**, SiGe, CdS, CdTe, ZnO, InAs, …
  - Overall ANY 1D nanocrystal with anisotropic crystal structure, by the Vapor-Solid (VS) method
- Nanotubes
  - Catalytic growth: C, Ws_2
  - Many others by templating, e.g., TiO_2, metals
- "Catalysts"
  - have surface and/or bulk solubility for the precursor (or dissociated precursor)

2. Materials systems

Silicon was the system first investigated by Wagner and Ellis [1] and it remains one of the most intensively studied systems [7,10–14,*15,16–19]. Lieber's group [*8] has studied silicon extensively including the formation of branched Si nanowires (SiNW) [20]. Carbon nanotubes [2,21,22] and carbon nanofibers [23] are also produced by catalytic growth [24,25]. Heterojunctions between SiNW and CNT have been formed [26]. Other materials that exhibit catalytic growth of nanowires include SiO_x (a substoichiometric silicon oxide) [27]; SiO_2 [28,29]; $Si_{1-x}Ge_x$ [10,30]; Ge [31,*32]; AlN [33]; γ-Al_2O_3 [34]; oxide-coated B [*35]; CN_x [36]; CdO [37]; CdS [38]; CdSe [*9]; CdTe [*9]; α-Fe_2O_3 (hematite), ε-Fe_2O_3 and Fe_3O_4 (magnetite) [39]; GaAs [15,40,*41,42,*43,44]; GaN [18]; Ga_2O_3 [18,45]; GaP [40,*41,*46]; InAs [*41,*47]; InN (hexangular structures) [48]; InP [*9,*41,42]; In_2O_3 [45]; In_2Se_3 [49]; LiF [50]; SnO_2 [45,51,*52]; ZnO nanowires [*7,*8,53] and nanoplates [53]; ZnS [54]; ZnSe [55]; Mn doped Zn_2SO_4 [56]; and ZnTe [57]. Let us now look at the conditions under which catalytic growth has been used to create nanostructures so that we can better understand the range of growth conditions that have been used, as well as the similarities and differences in growth characteristics that have been observed so that we may generalize about some of the important mechanistic characteristics.

Kolasinski, Current Opinion in Solid State and Materials Science 10:182, 2006.

Semiconductor bandgaps → nanowire tunability

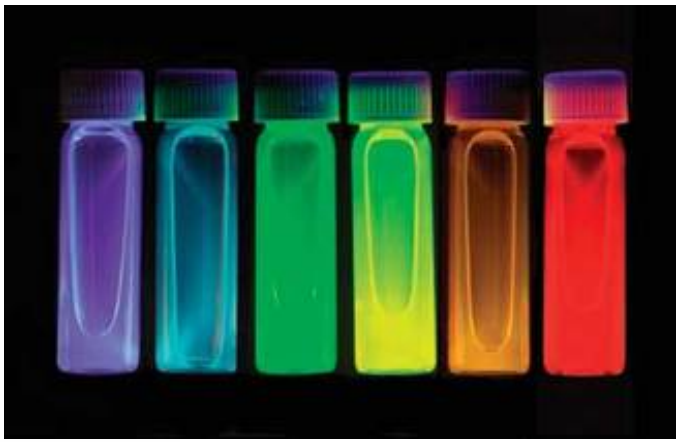

(Quantum dots) F. Frankel

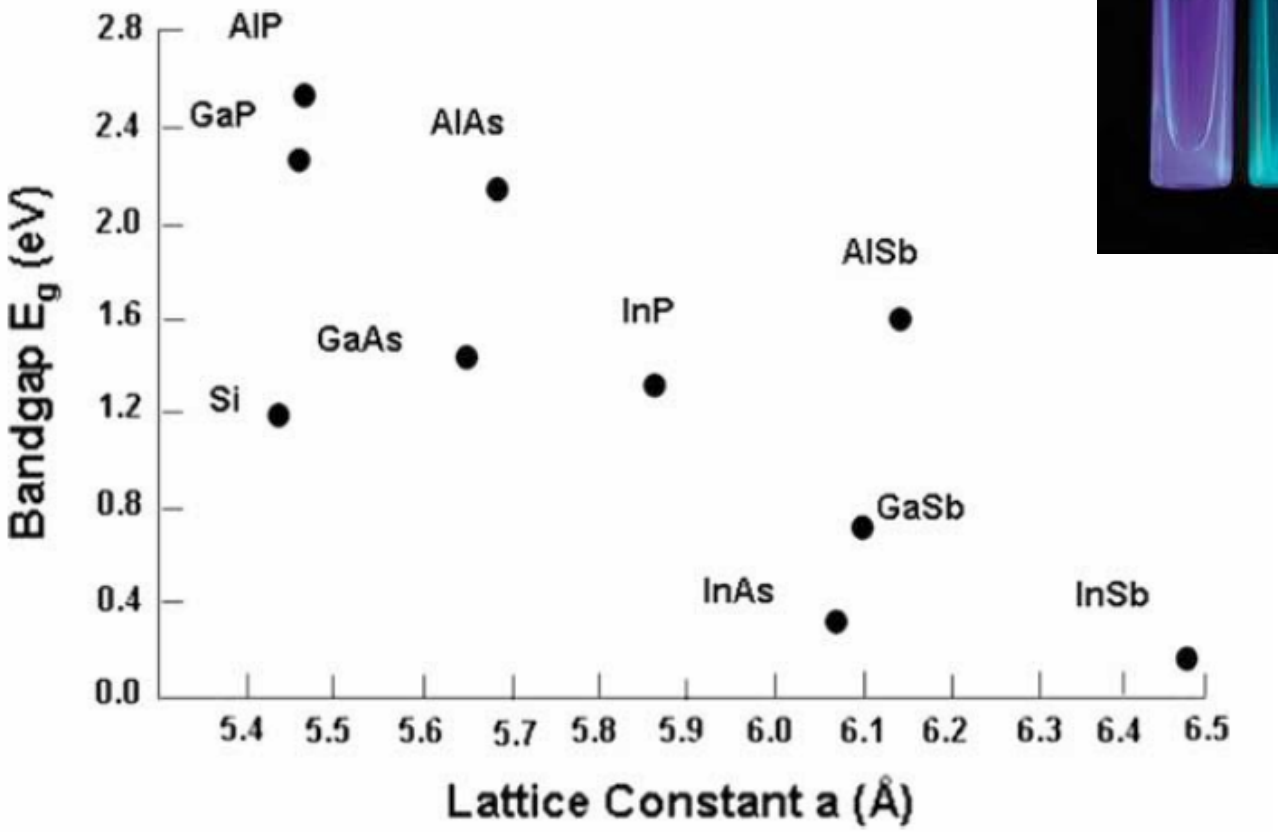

The original: vapor-liquid-solid (VLS) model

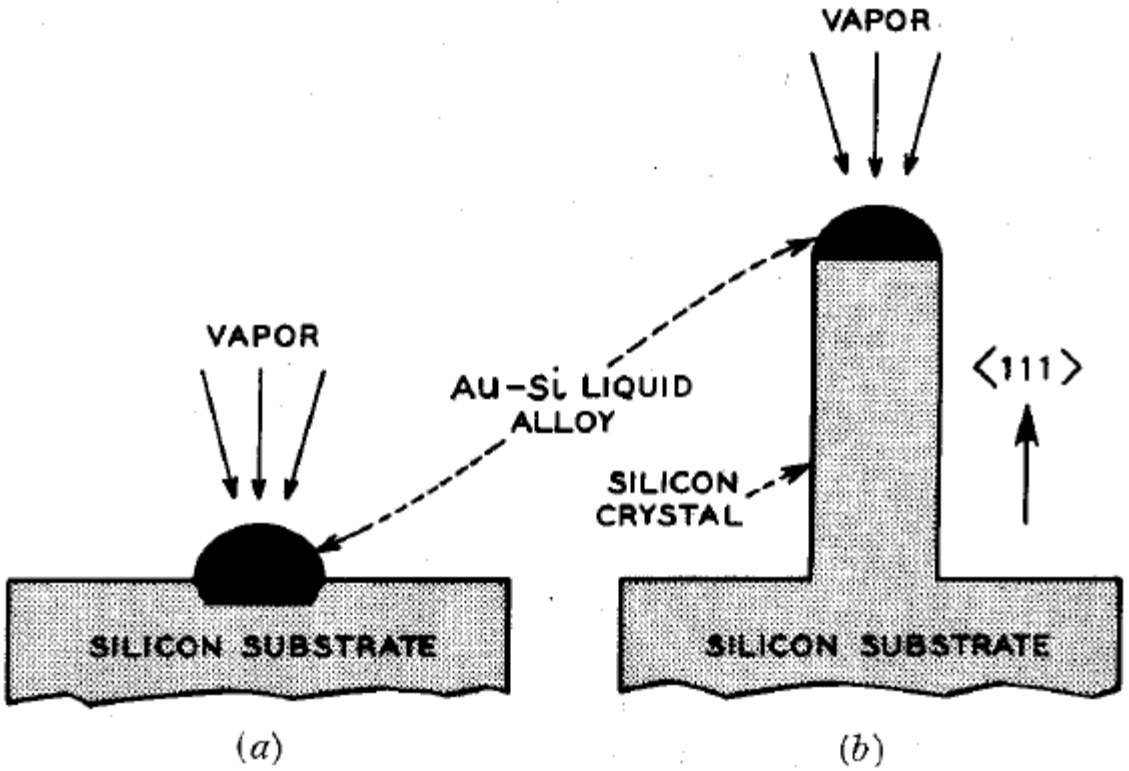

Fig. 1—Idealized drawing of VLS mechanism illustrated for growth of a silicon crystal.

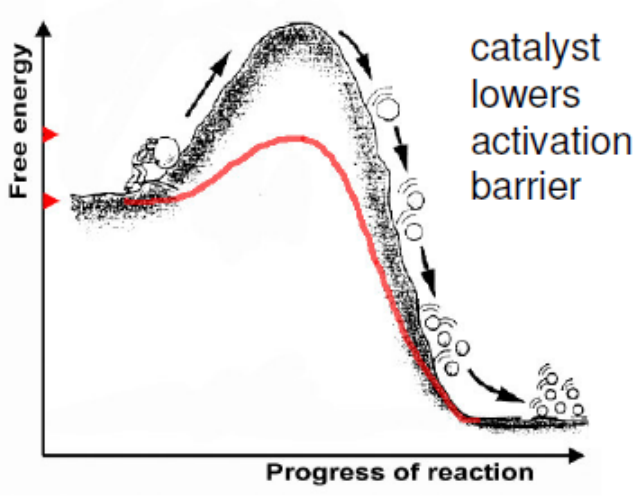

Wagner and Ellis, *Trans. AIME* 233:1053, 1965; S. Hofmann (Cambridge).

Catalytic chemical vapor deposition (C-CVD) of nanowires/nanotubes (NWs/NTs)

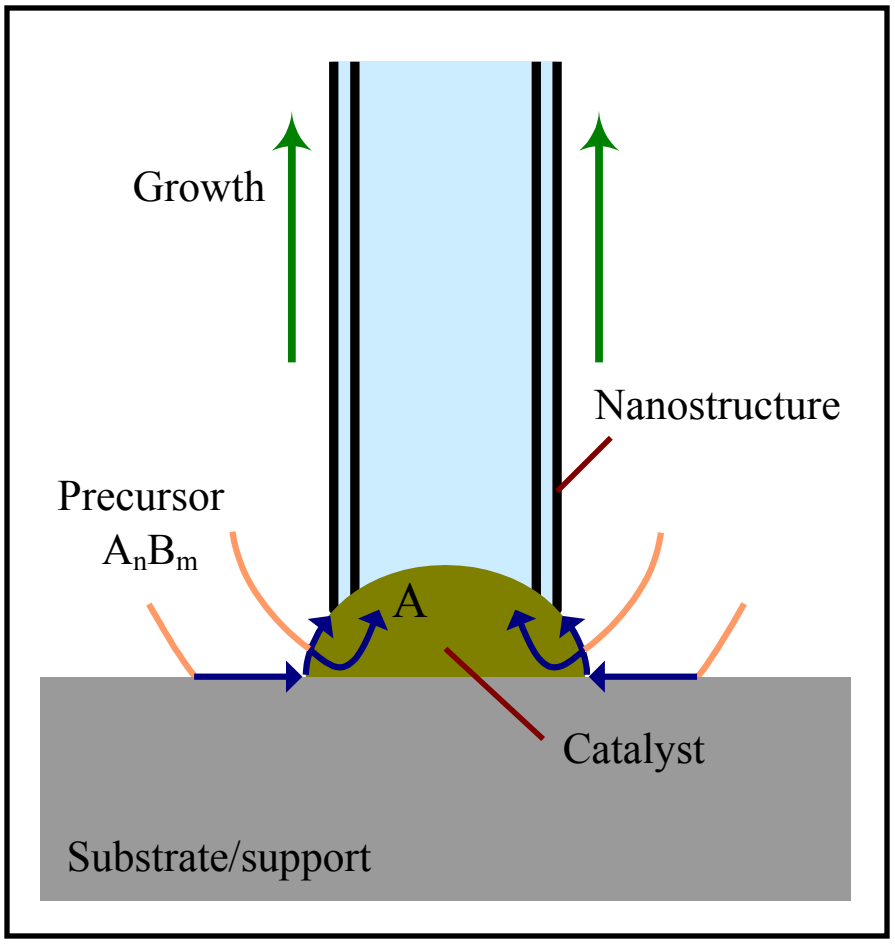

Base vs. tip growth (CNTs)

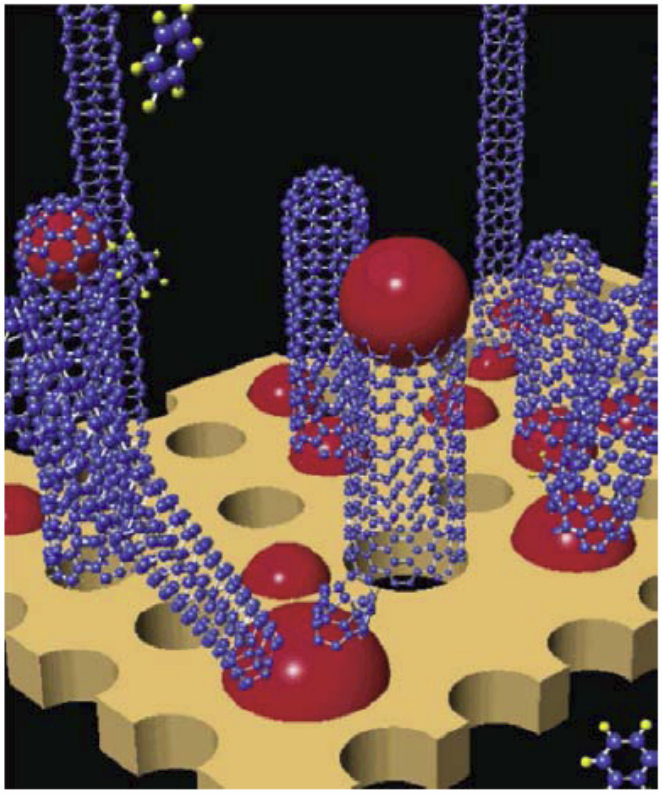

Hayashi et al., *Nano Letters* 3(7):888, 2003.

Phases and the catalyst-wire interface

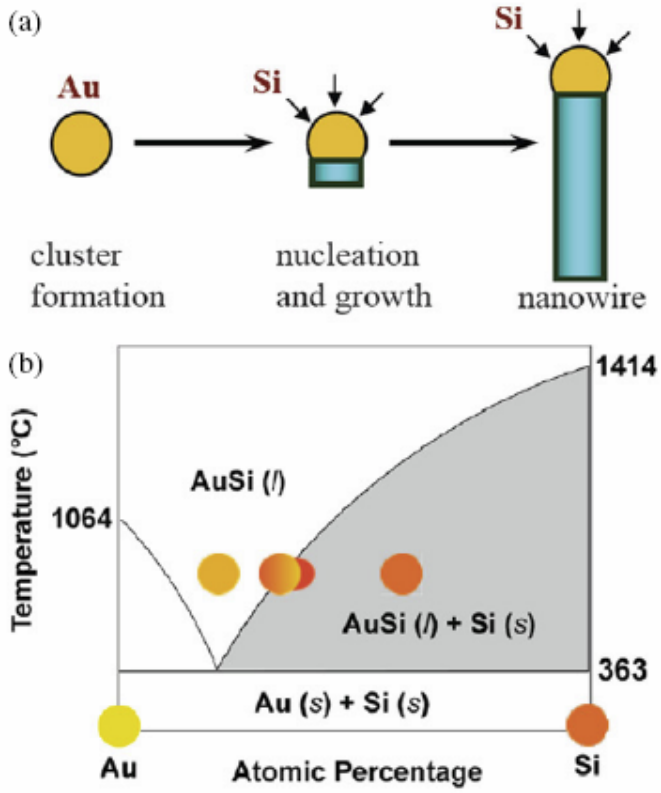

Figure 1. Schematic of VLS growth of Si nanowires (SiNWs). (*a*) A liquid alloy droplet AuSi is first formed above the eutectic temperature (363 °C) of Au and Si. The continued feeding of Si in the vapour phase into the liquid alloy causes oversaturation of the liquid alloy, resulting in nucleation and directional nanowire growth. (*b*) Binary phase diagram for Au and Si illustrating the thermodynamics of VLS growth.

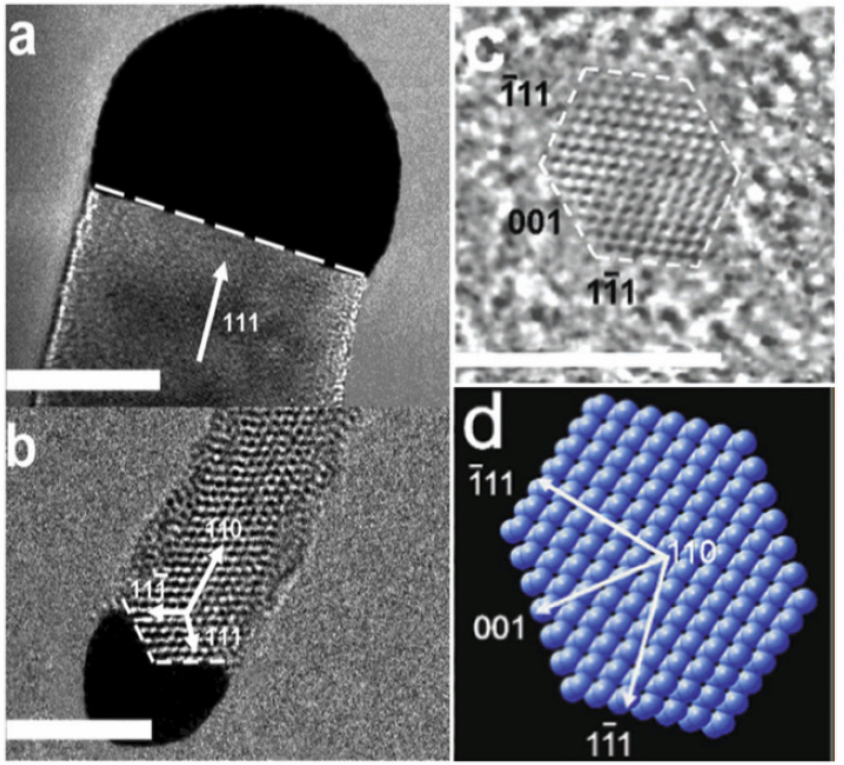

Figure 3. (*a*) HRTEM image of the catalyst alloy/NW interface of a SiNW with a ⟨111⟩ growth axis. Scale bar: 20 nm. (*b*) HRTEM image of a catalyst alloy/NW interface of a SiNW with a ⟨110⟩ growth axis. Scale bar: 5 nm. (*c*) HRTEM cross-sectional image (scale bars: 5 nm) and (*d*) equilibrium shapes for the NW cross sections predicted by Wulff construction. Adapted from [11].

Lu and Lieber, *J. Phys. D* 39:R387, 2006.

Heterostructures

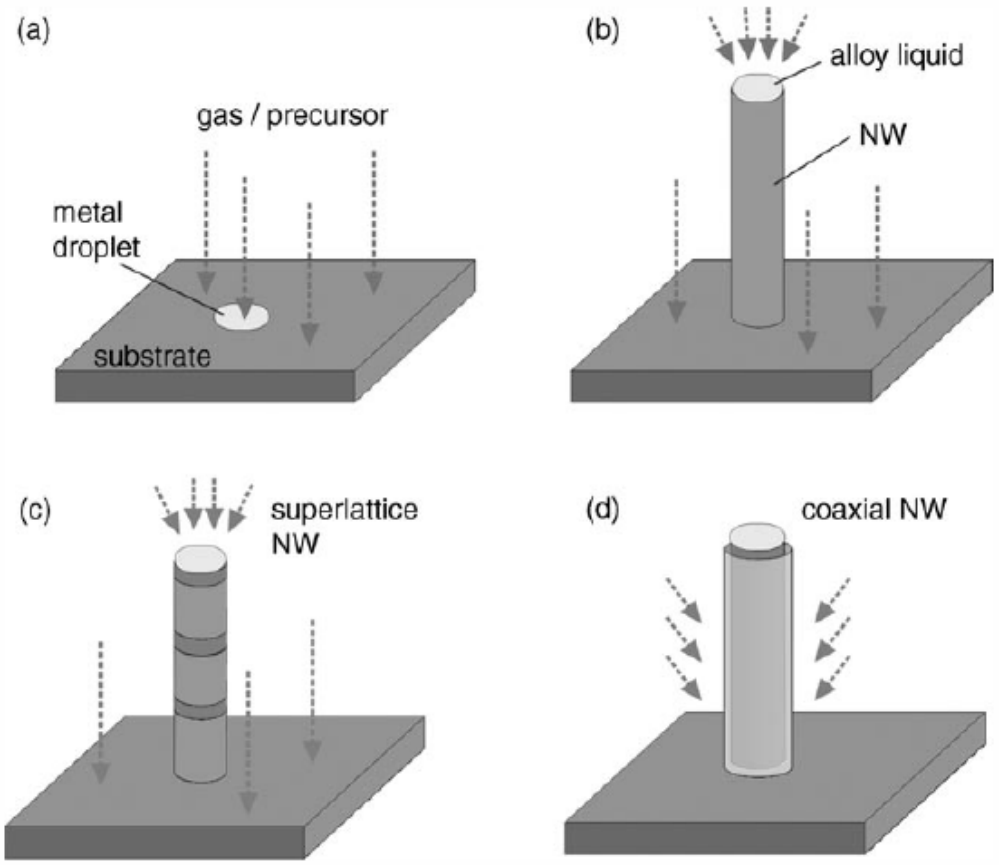

Figure 3. NWs of different structures based on the "bottom-up" growth mode: a) Exposure of a metal-droplet-coated substrate to reactant precursors; b) a monophase NW grown outwards, with the metal droplet acting as catalyst; c) a superlattice NW grown by consecutively alternating the reactant precursors; d) a coaxial NW formed by conformal coating of the preformed nanowire in (b) with a different material.

Fan et al., *Small* 6:700, 2006.

Core-shell nanowires

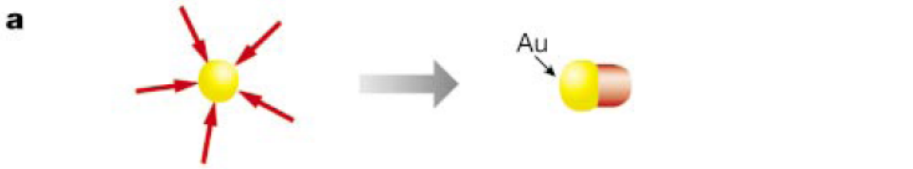

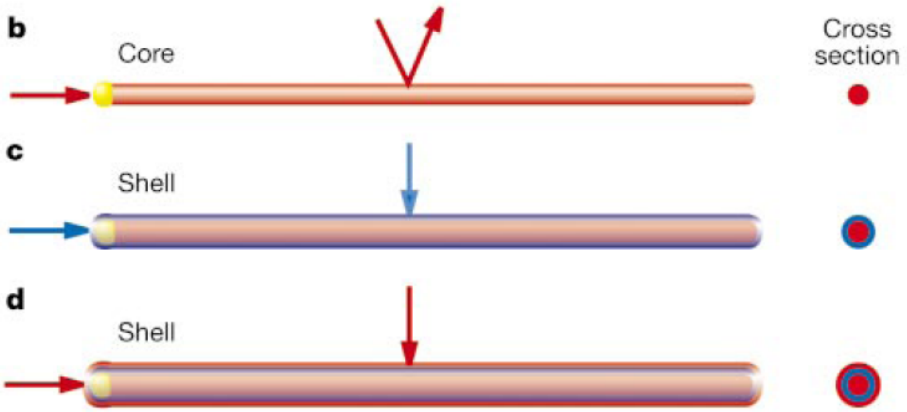

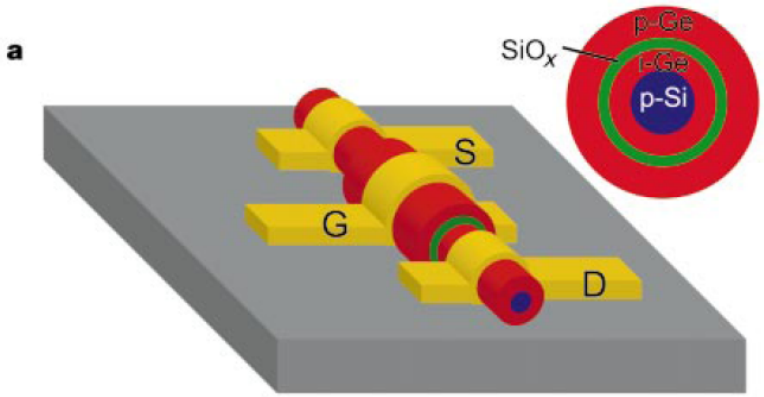

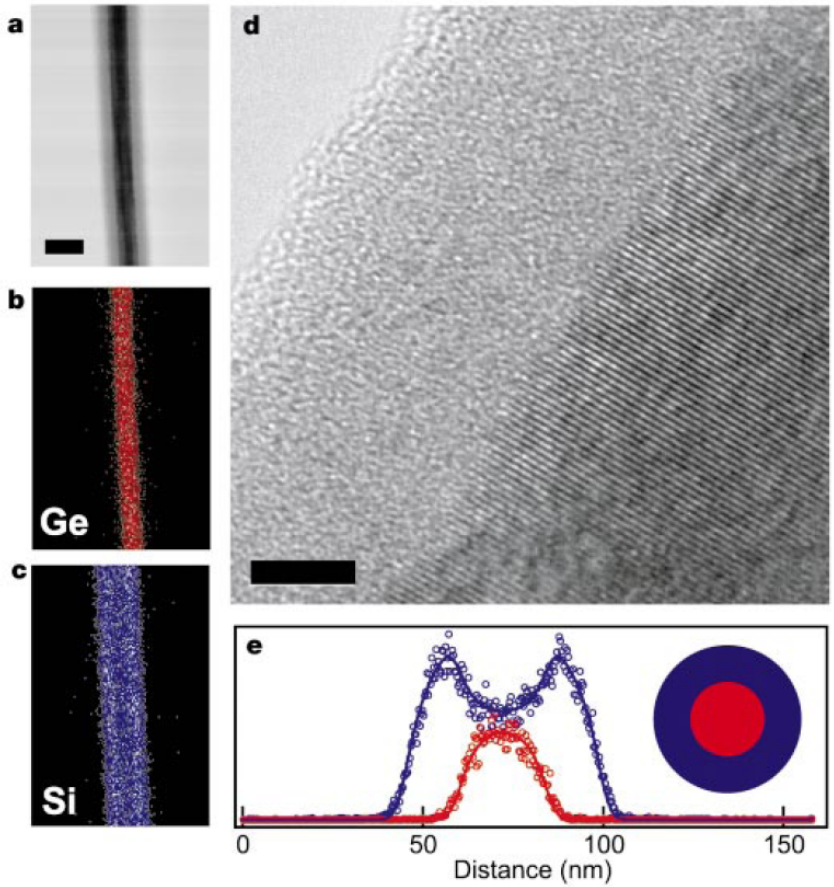

Lauhon et al, *Nature* 420, 2003.
Qian et al, *Nano Letters* 5, 2005.

Hybrids: nanowires grown on nanotubes

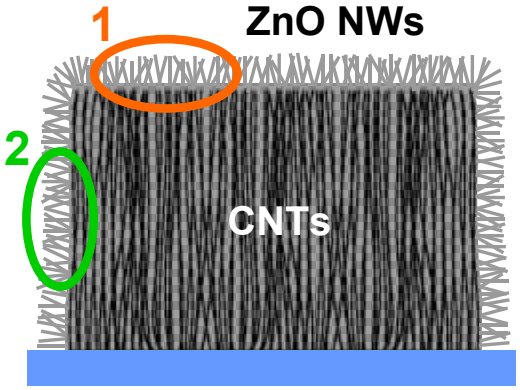

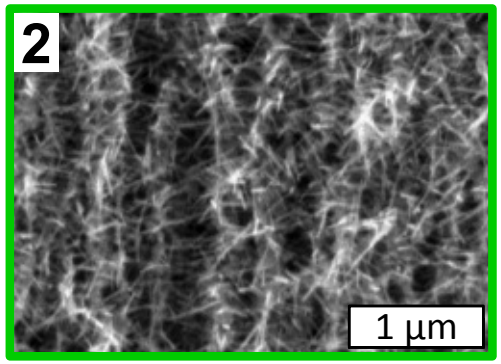

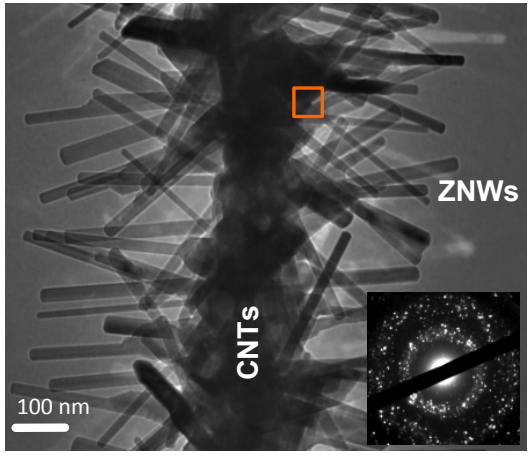

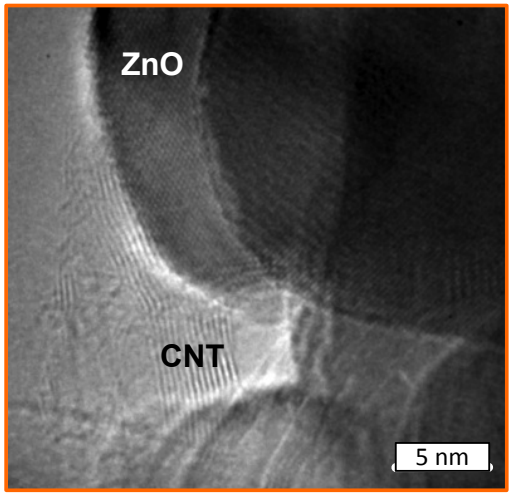

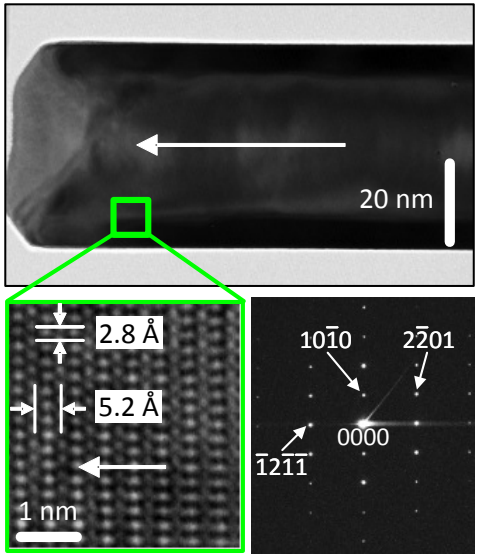

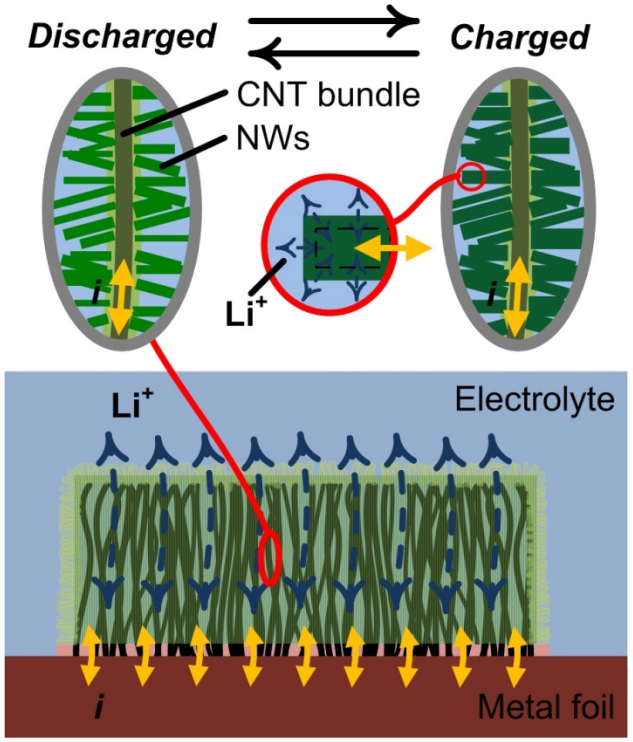

Why CVD?

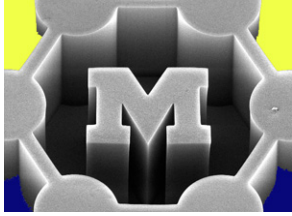

- Low temperature and low cost (relatively)
- Adaptable to a wide variety of structures (based on catalyst and reactant choice)
- Low defect density
- Rapid growth
- Direct growth on substrates
- Scalable to large areas and reactor volumes

CVD growth systems

Horizontal tube, fixed catalyst

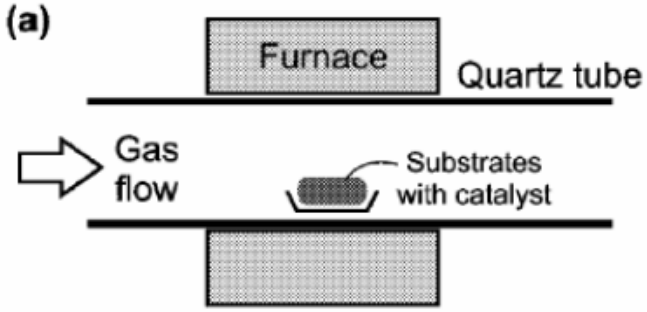

Vertical tube, floating catalyst

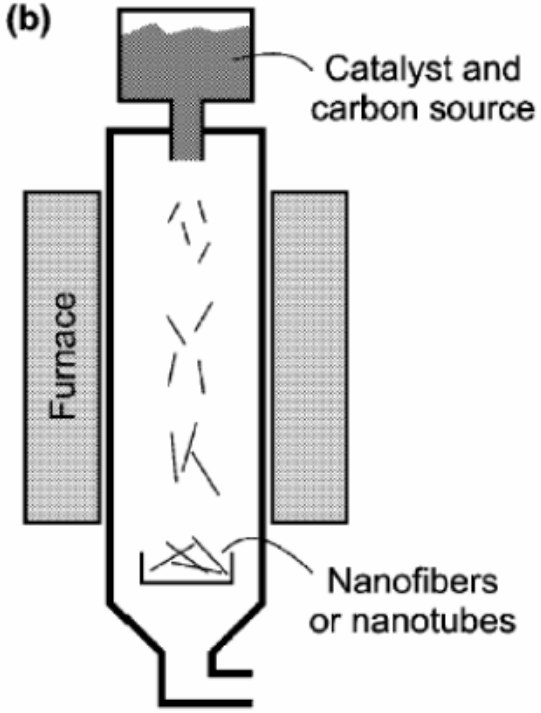

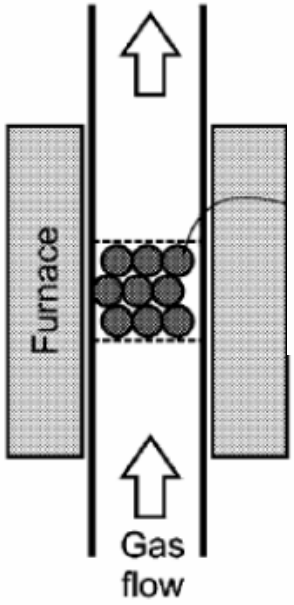

Plasma-enhanced

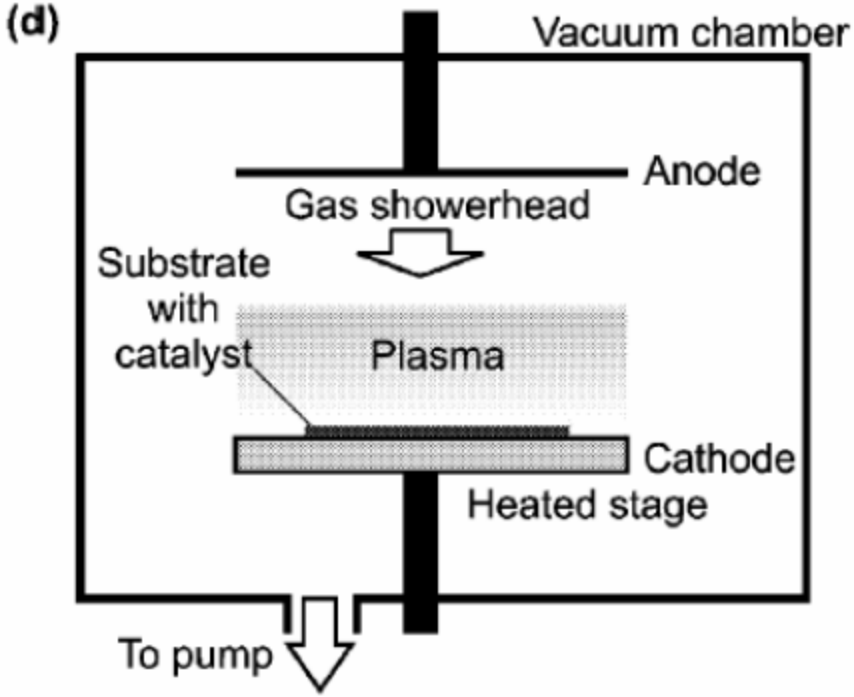

Precursor can be
- **Gas (e.g., pressurized tank)**
- **Liquid (e.g., spray, evaporate)**
- **Solid (evaporate or sublime)**

Vertical tube, fluidized bed

Teo, 2003.

CNT reactor design: tube furnace

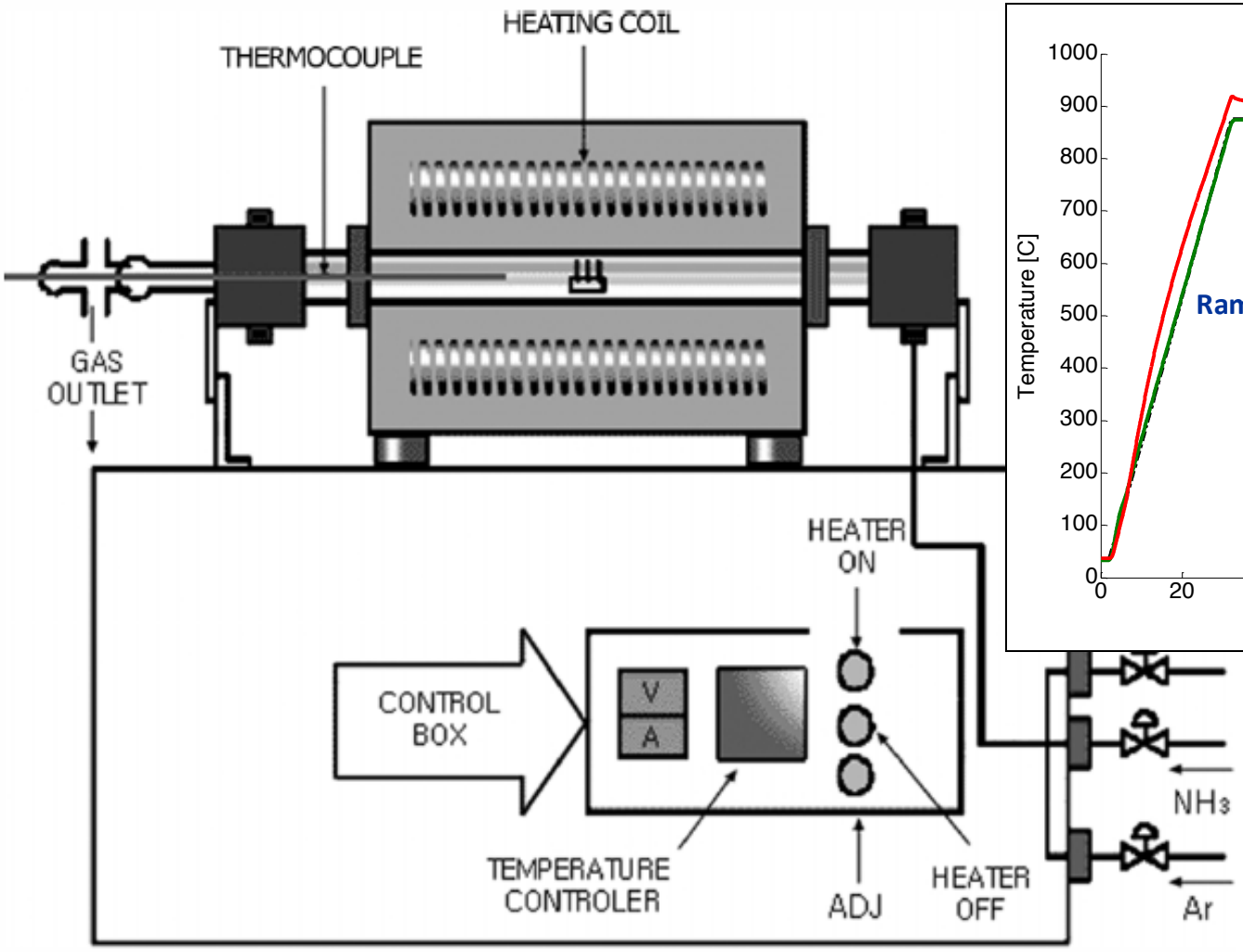

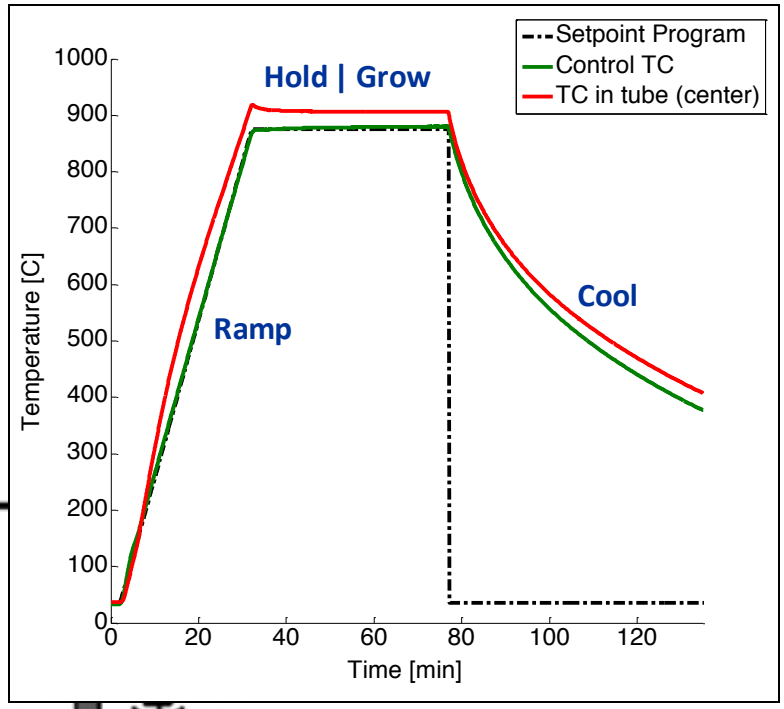

Fig. 10. Scheme of apparatus for nanotube synthesis by thermal CVD (reprinted with permission from [47], copyright 2002, Elsevier).

Terranova et al., *Chemical Vapor Deposition* 12:315, 2006.

CNT forest growth on 4” silicon wafers

VA-CNT arrays on 4” wafers
(S. Fan and K. Jiang, Tsinghua Univ)

Large rotary tube furnace

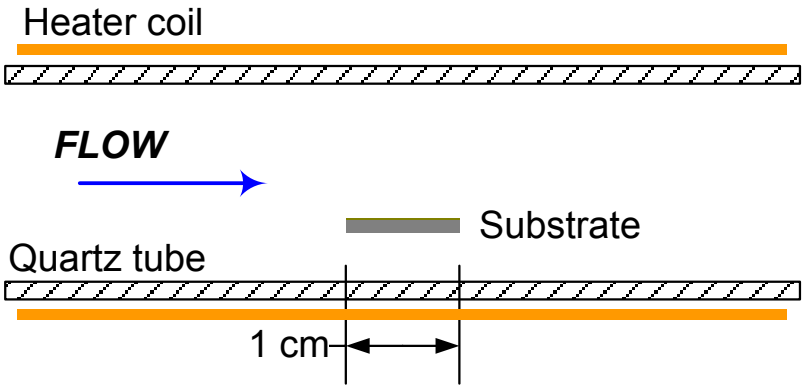

Tube OD = 400 mm, $0.9M, ~100 tons/yr @24-7
(courtesy R. Blackmon, Harper International)

Reactor design: plasma-enhanced CVD

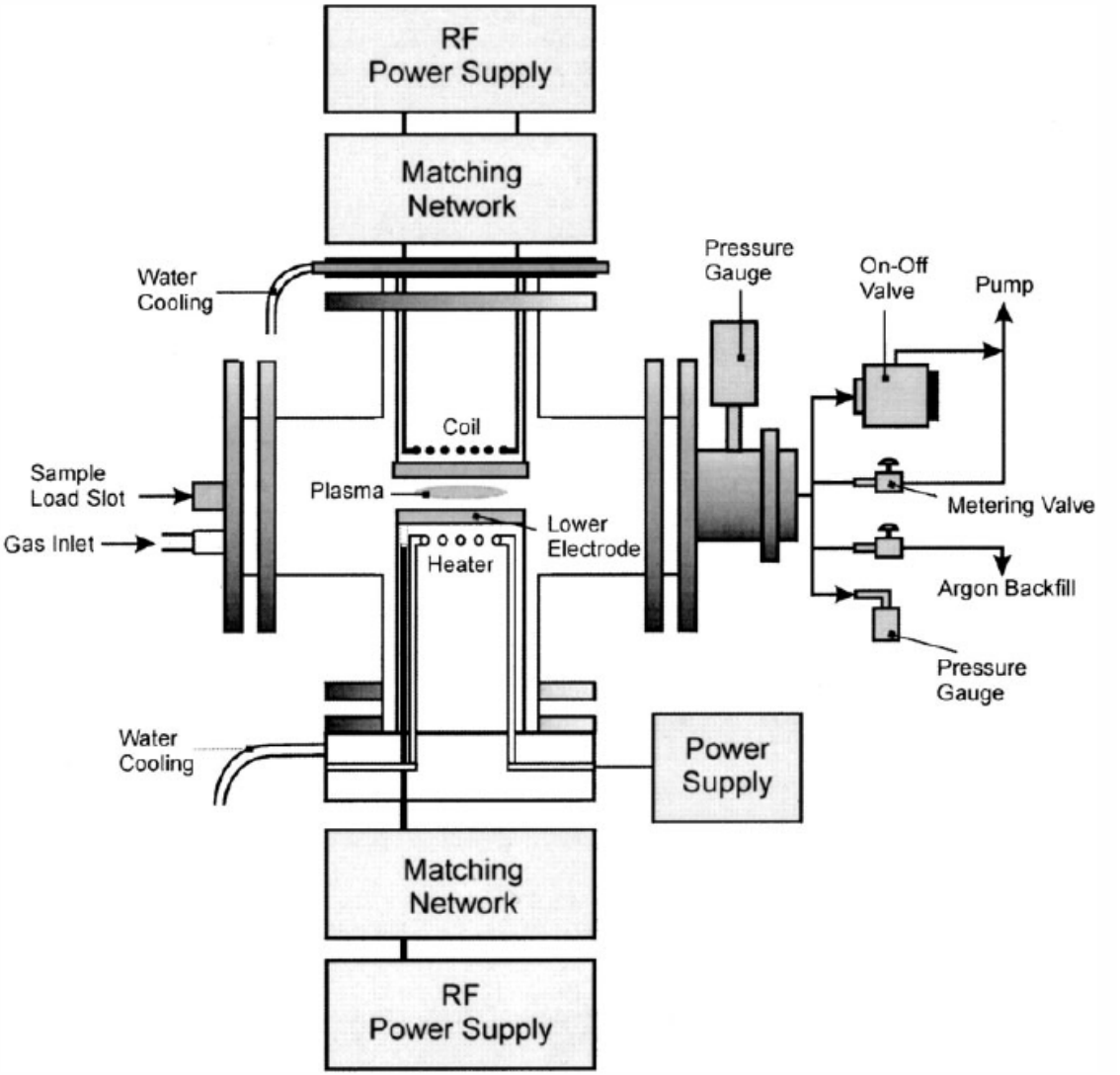

Fig. 7. Scheme of an inductively coupled plasma reactor with independent RF power CVD (reprinted with permission from [44]; copyright 2002, American Institute of Physics).

- Types of plasmas: direct, remote; inductively coupled
- Roles of electric field

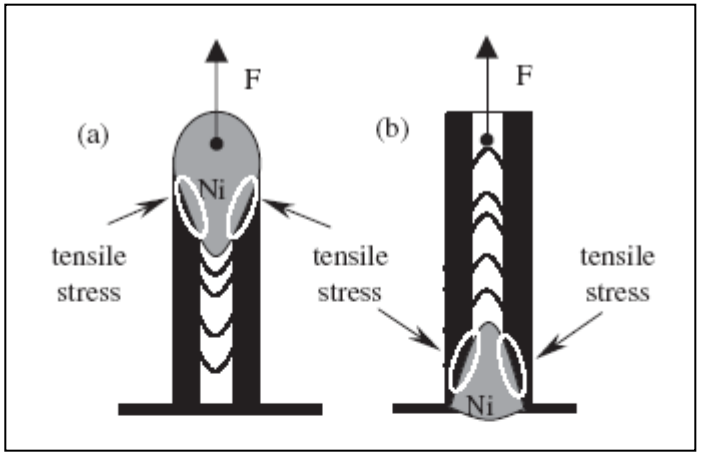

Terranova et al., *Chemical Vapor Deposition* 12:315, 2006.

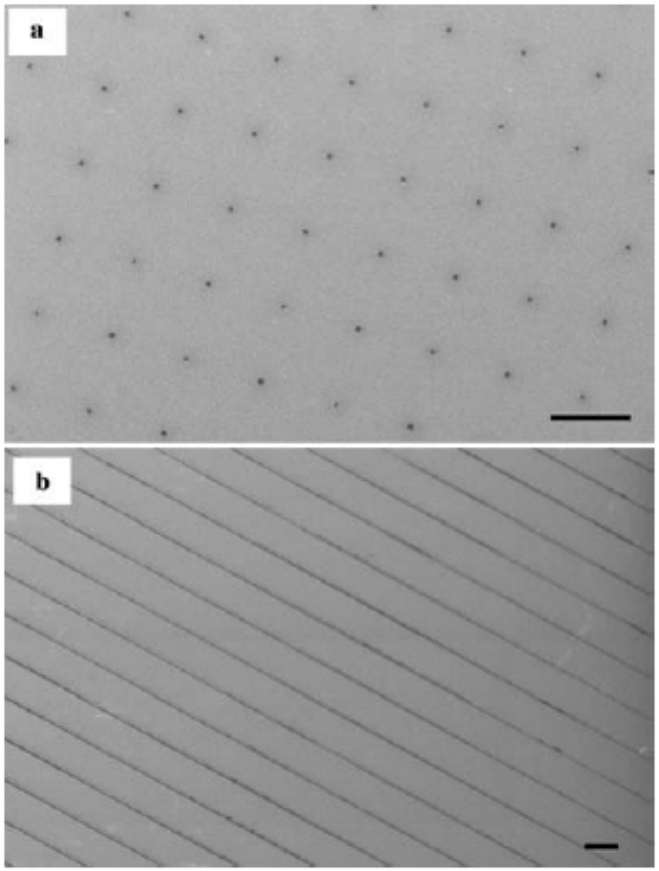

FIGURE 11 SEM images of as-printed Co colloid (a) *dot* and (b) *line patterns* (scalebars 4 μm, 3 μm, respectively)

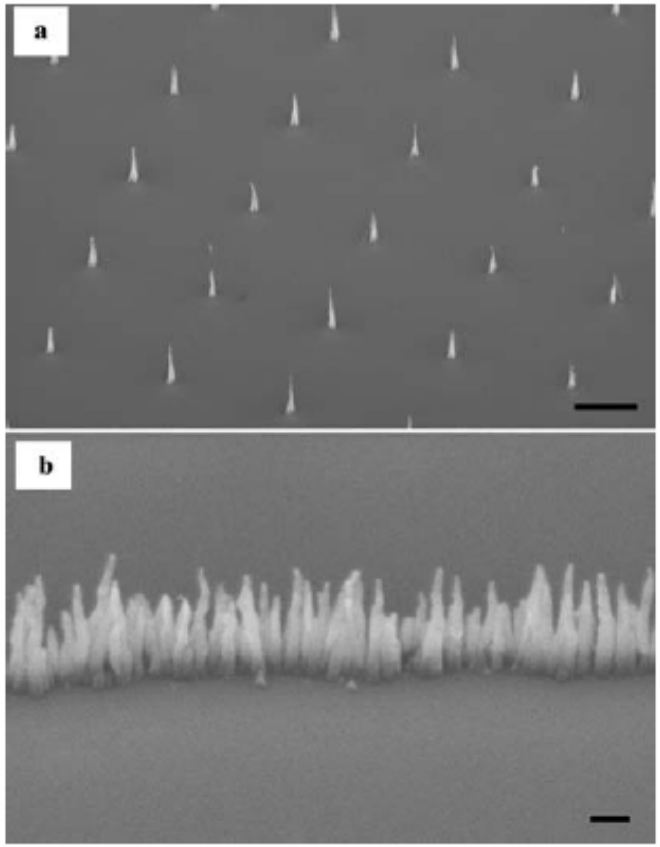

FIGURE 12 SEM images of (a) *dot* and (b) *line patterned*, aligned CNF arrays. Growth conditions: 1 : 4 C_2H_2 : NH_3 flow at 600 V DC bias, 500 °C for 15 min (scalebars 2 μm, 100 nm, respectively)

Hofmann et al., *Appl. Phys. A* 81:1559, 2005.

Reactor design: fluidized bed

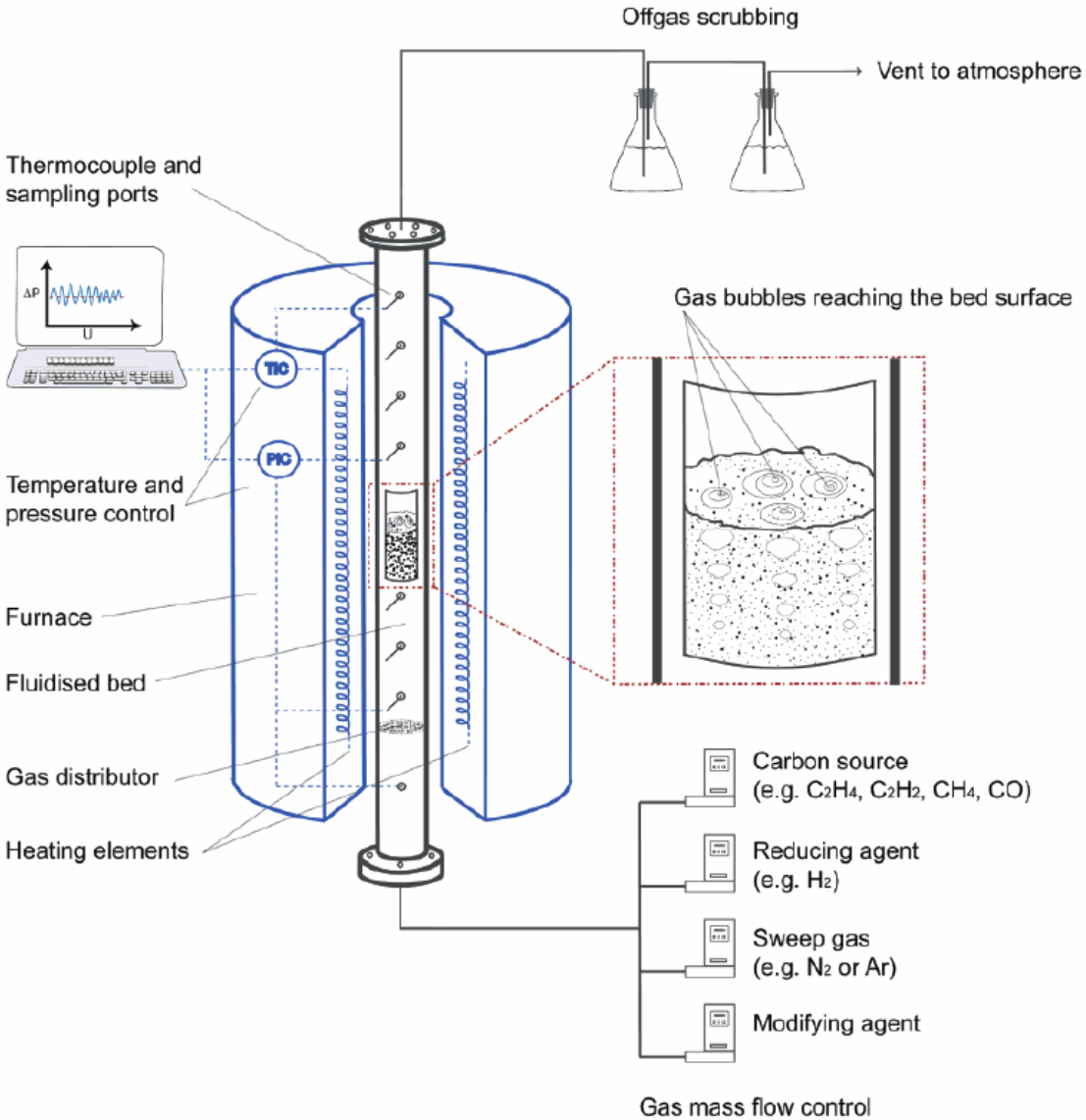

Figure 4. Sketch of a typical fluidized-bed reactor setup. A cylindrical reactor is affixed within a high-temperature furnace with appropriate temperature, pressure, and gas flow controls, connected to a data logging system. Environmental mitigation systems are incorporated to remove entrained solid particles in the off-gas before venting to atmosphere.

See et al., *Ind. Eng. Chem. Res.* 46:997, 2007.

Large fluidized bed reactor

Fluidized bed reactor: 30 kg/h MWNTs = 265 tons/yr @24-7
(F. Wei, Tsinghua Univ)

Configurations

Order = length, alignment, quality
Quantity = #/volume

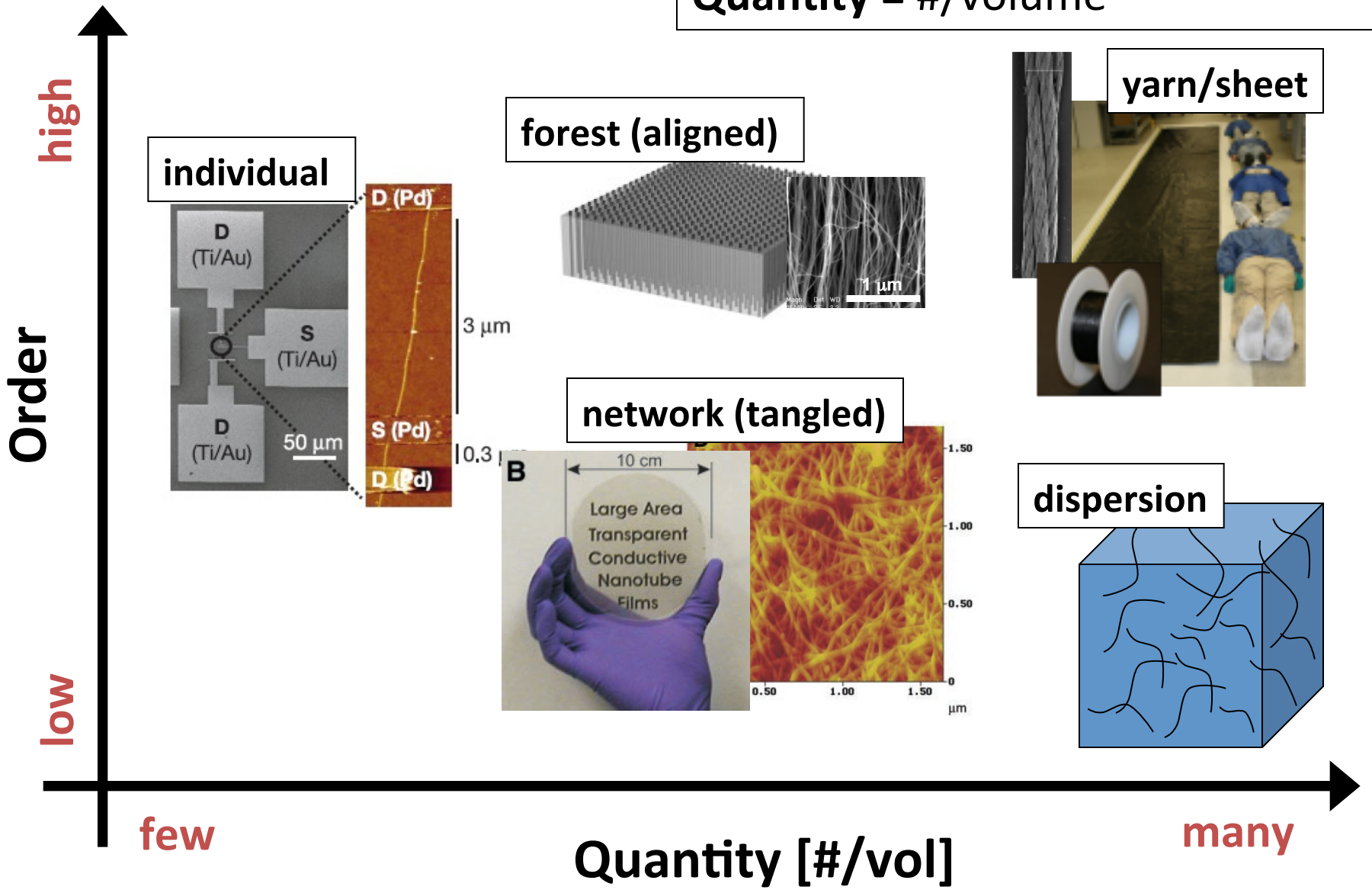

Applications

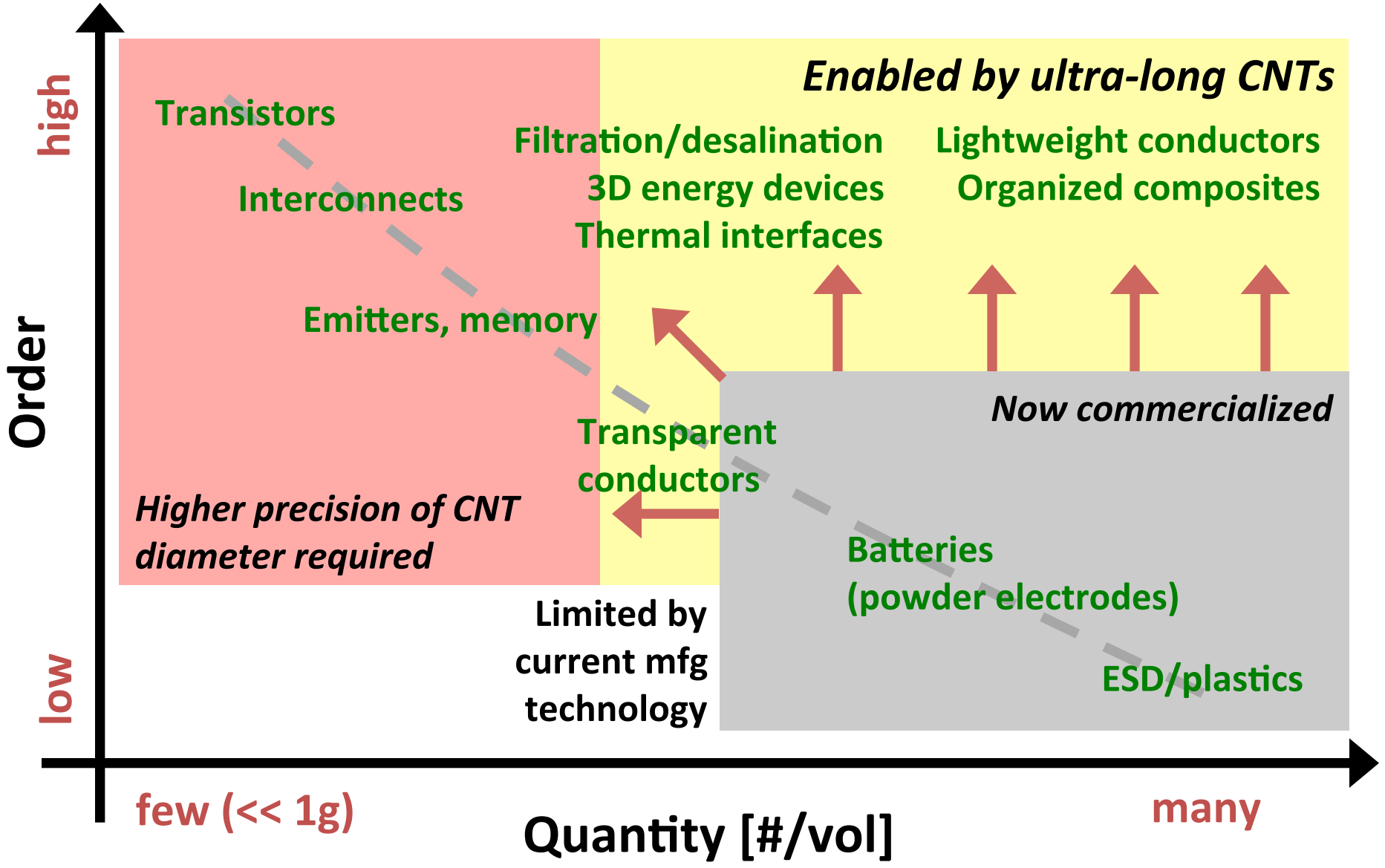

Three important stages

1. Preparation of the catalyst

- Formation and treatment (e.g., reduction of the nanoparticles)

2. Nucleation

- Organization and "liftoff" of the structure (for NTs, the cap) on the catalyst surface

3. Growth

- Steady "extrusion" of the structure from the particle
- Role of mechanical stiffness, VDW forces, thermal vibration, etc.

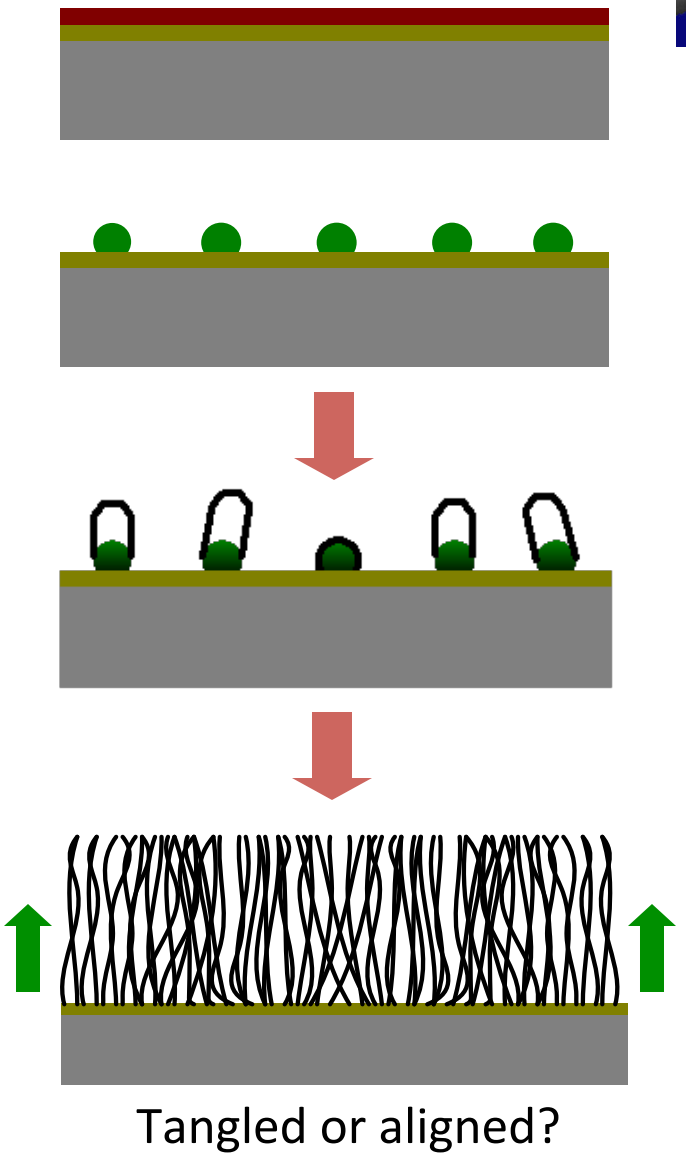

Tangled or aligned?

Key questions for understanding and controlling CVD growth of nanotubes and nanowires

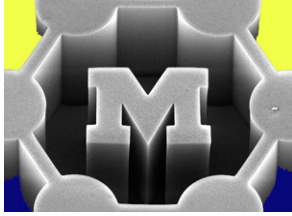

- What determines the NT/NW relationship with the catalyst? structure, and its geometry (diameter, taper) and chirality?
- Is the catalyst solid or liquid?
- What are the ideal (direct) chemical precursors? How is the precursor incorporated at the catalyst?
- How does the size distribution develop/evolve due to the nucleation and growth conditions?
- What limits catalyst lifetime, and why does the catalyst deactivate?
- What are the precise effects of oxidizing and reducing agents (sometimes impurities) on:
  - the catalyst size and structure
  - the gas-phase reaction(s)
  - the gas-catalyst reaction(s)

Inputs and outputs

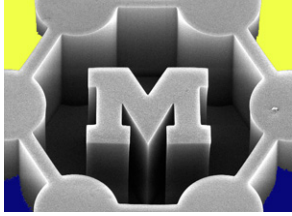

INPUTS

Catalyst and support:

- Material and composition
- Particle size
- Chemical state (annealing)
- Surface roughness

Reaction conditions:

- Substrate temperature
- Pressure
- Reactant composition
- Buffer/etchant composition
- Reactant pre-treatment
- Supply rates
- Flow profiles/dynamics
- Time and temporal adjustment
- Forces acting during growth

OUTPUTS

- Diameter and structure
- Length, growth rate, lifetime
- Defect density
- Properties: electrical, mechanical, thermal, optical, etc…

Simulating nucleation

Limitations:
- substrate (free vs. supported)
- precursor (C vs. hydrocarbon)
- model size
- time

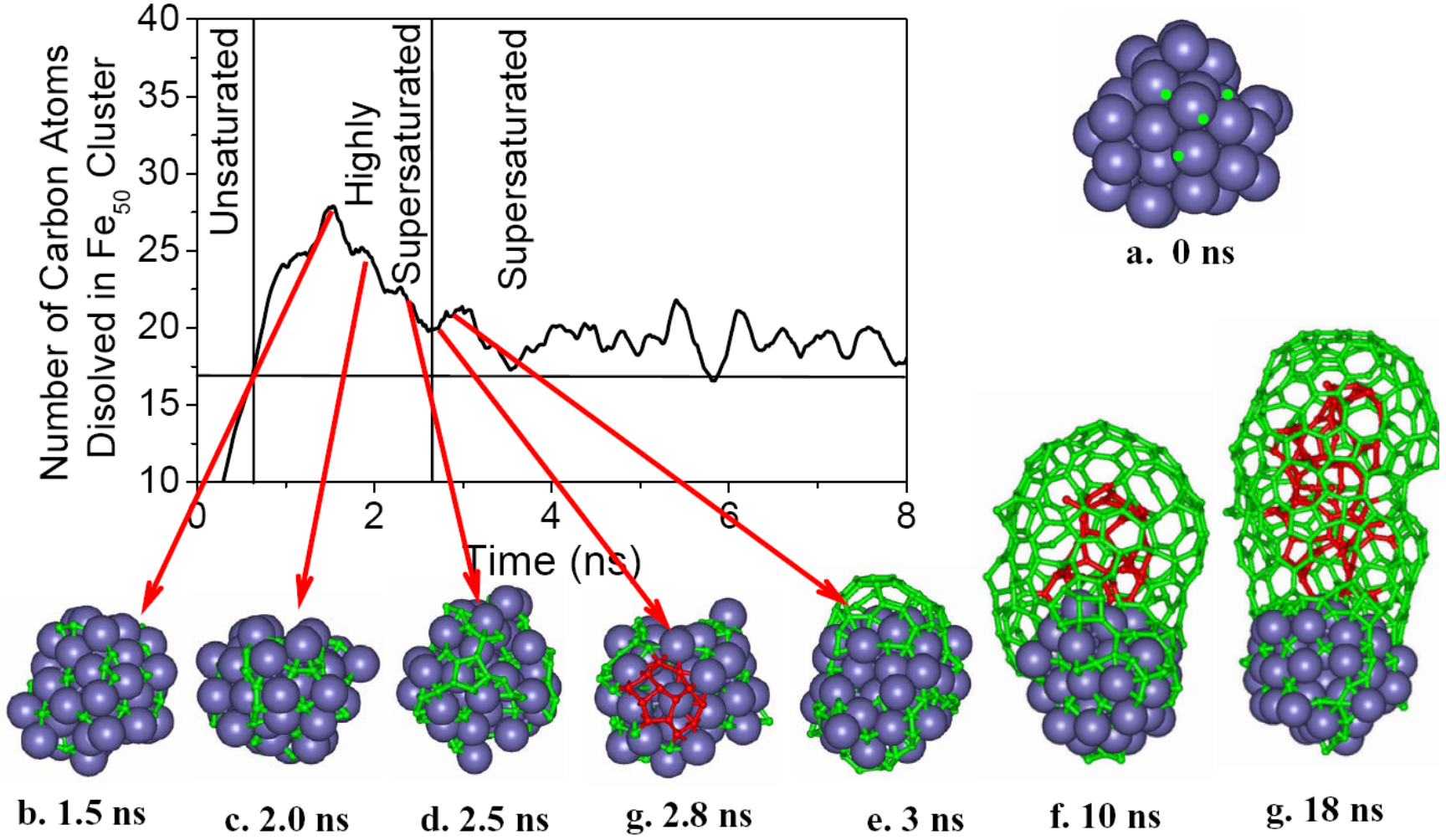

Zhu et al., *Small* 1(12):1180, 2005.

Snapshots of SWNT nucleation

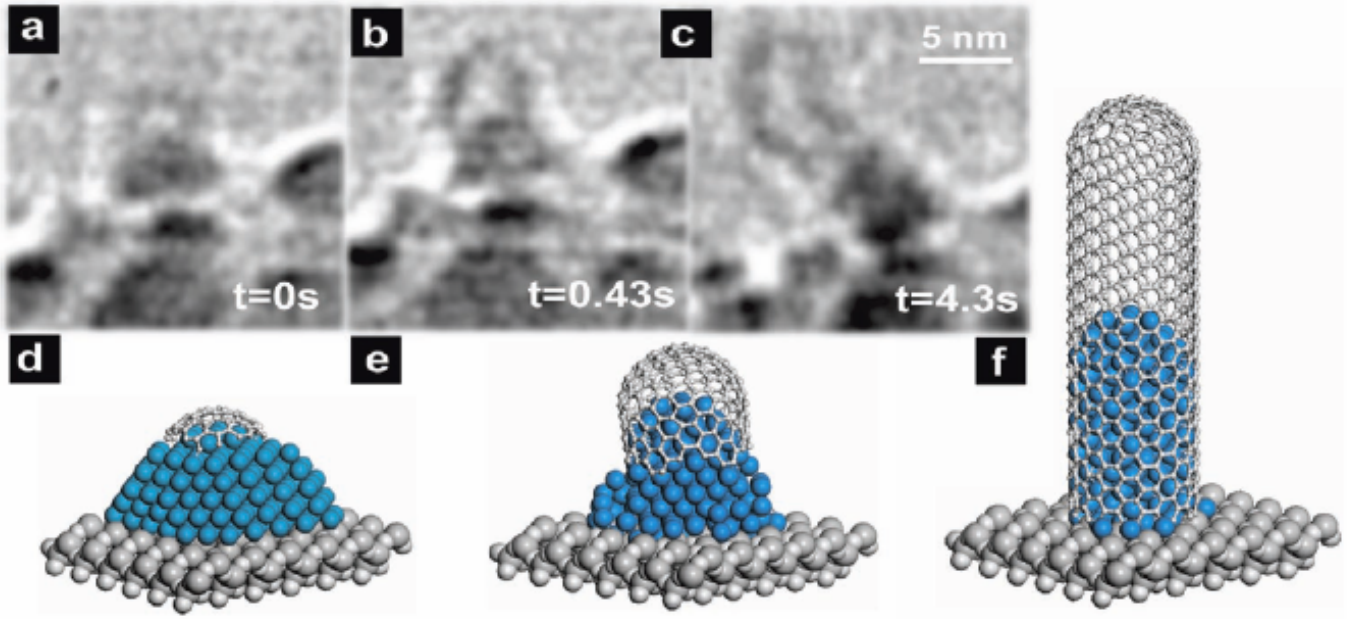

Figure 7. (a–c) ETEM image sequence of Ni-catalyzed CNT root growth recorded in 8×10^{-3} mbar C_2H_2 at 615 °C (extracted from Supporting Information video S2). The time of the respective stills is indicated. (d–f) Schematic ball-and-stick model of different SWNT growth stages.

Hofmann et al., *Nano Letters* 7(3):602-608, 2007.

Watching nucleation of a CNT by tip growth

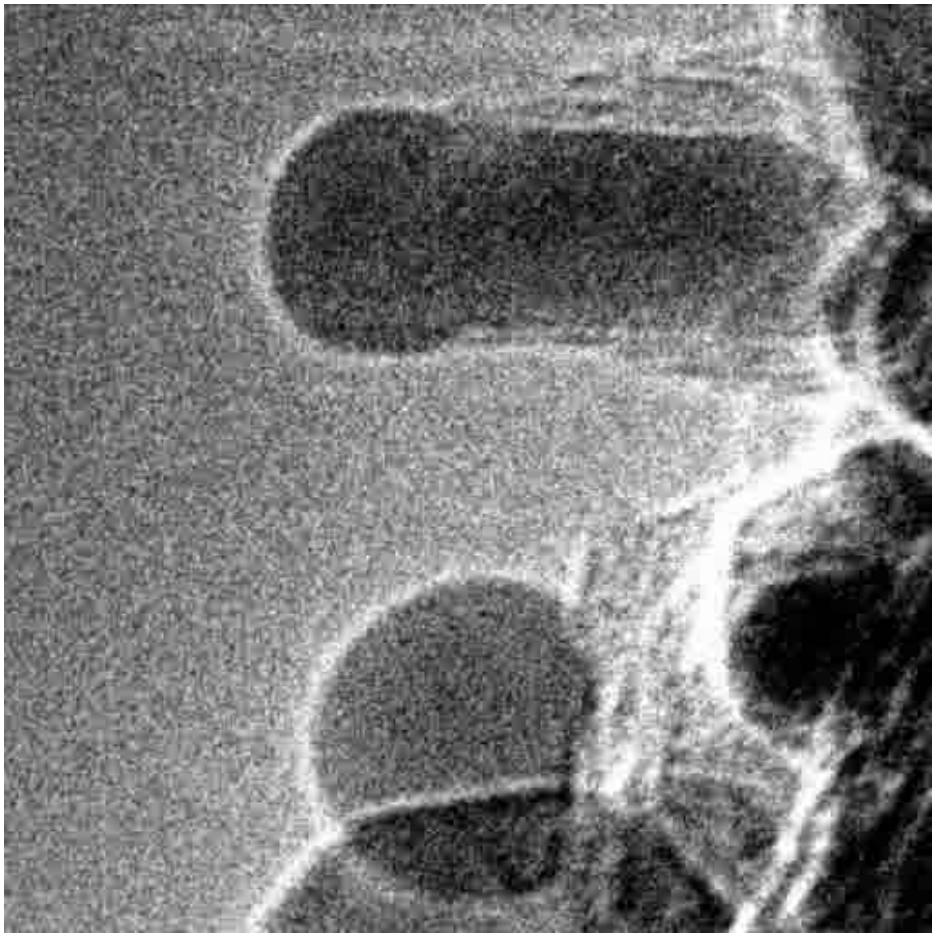

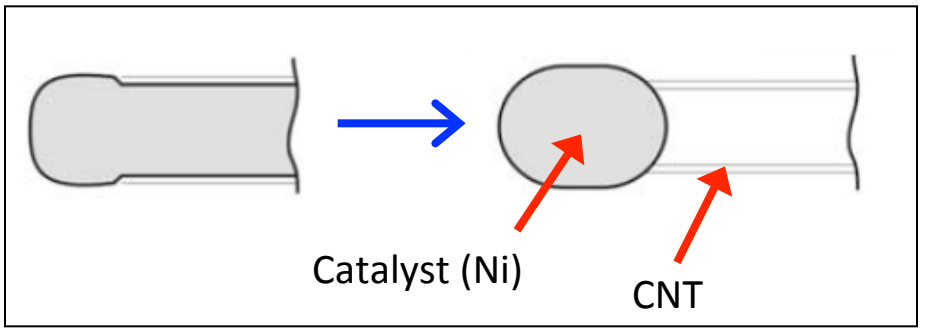

Helveg et al, *Nature,* 427:426-429, 2004

Nucleation of SiNWs by phase separation (liquid Au catalyst in Si_2H_6)

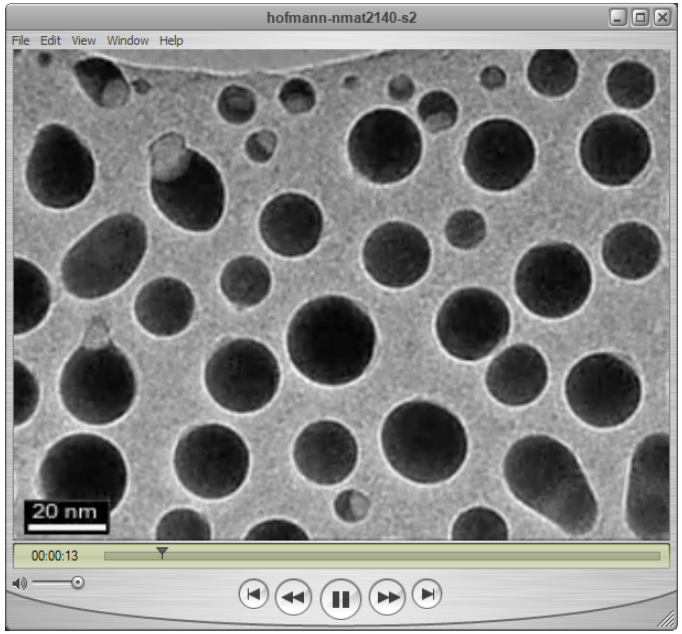

Video S1 on journal website

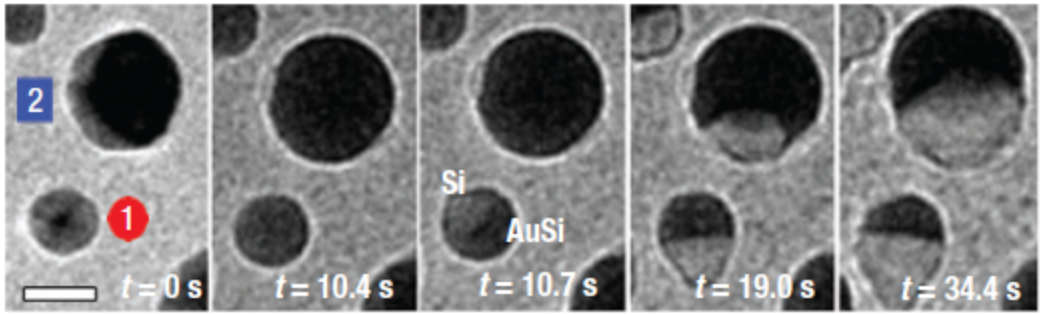

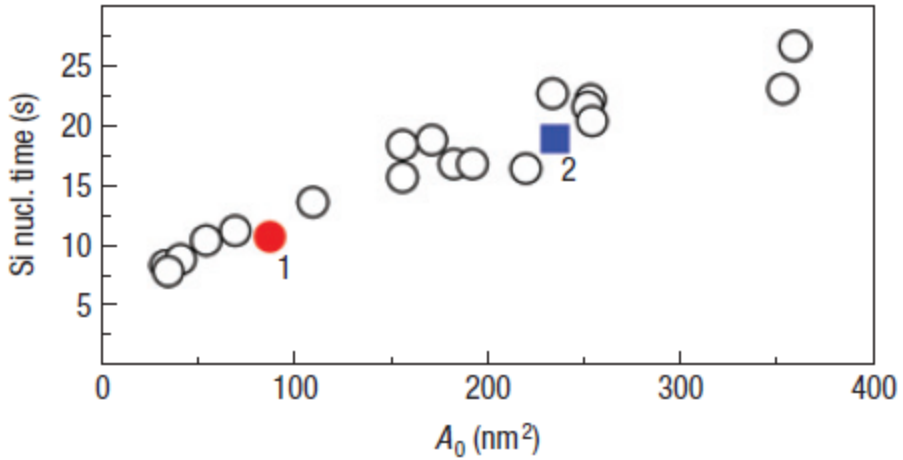

- Rate of Si inclusion ~R^2
- Si concentration ~$1/R^3$
- Thus, rate of supersaturation ~$1/R$

Hofmann et al., *Nature Materials* 7:372-375, 2008.

Ledge flow during SiNW growth from Pd catalyst (solid Pd_xSi)

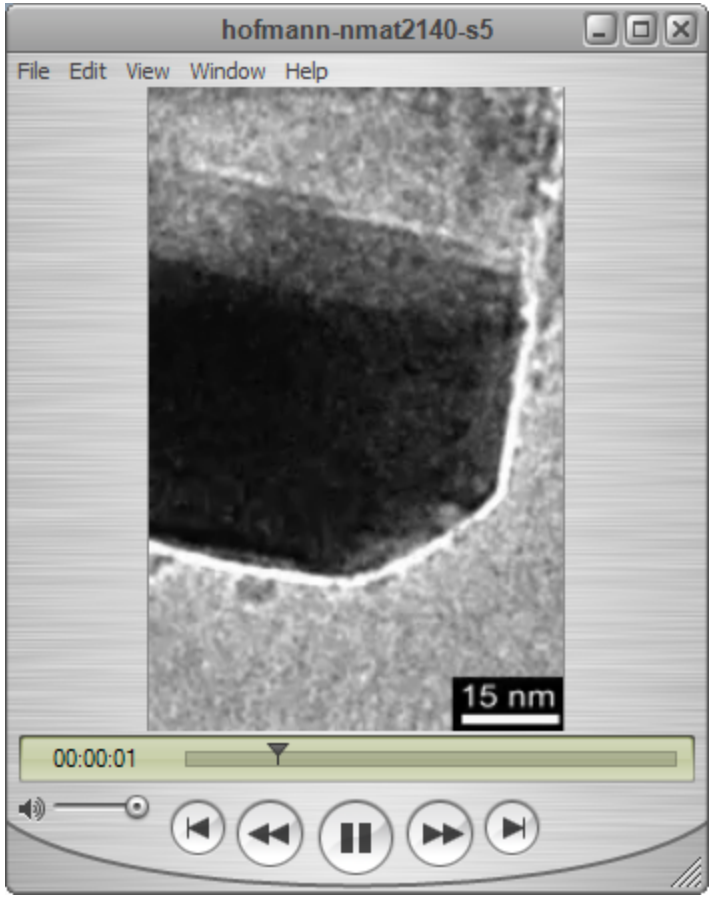

Video S4 on journal website

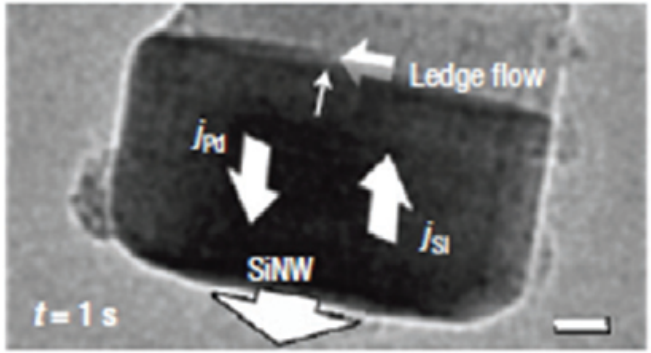

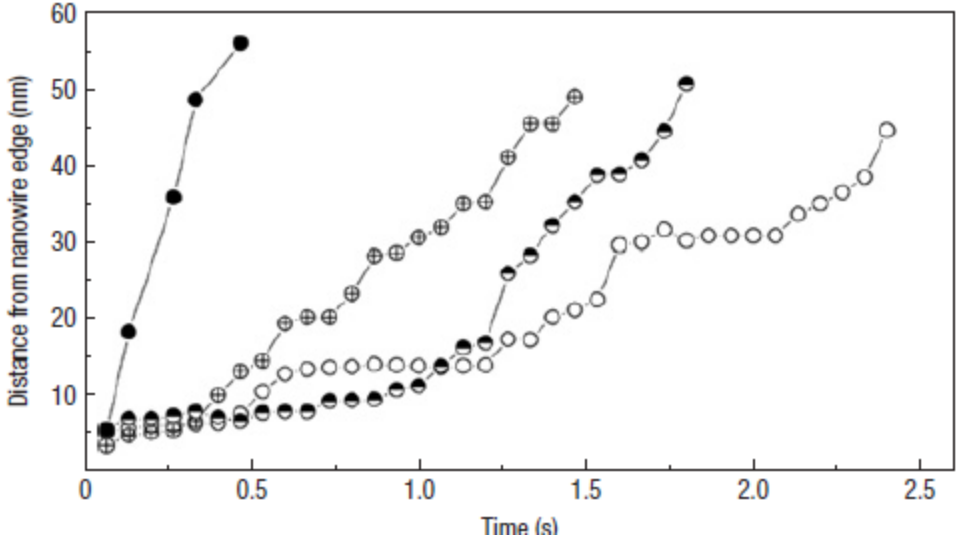

Hofmann et al., *Nature Materials* 7:372-375, 2008.

Is the catalyst solid or liquid?

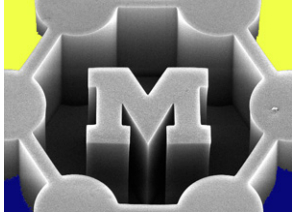

Growth temp:

Bulk diffusion

Surface diffusion

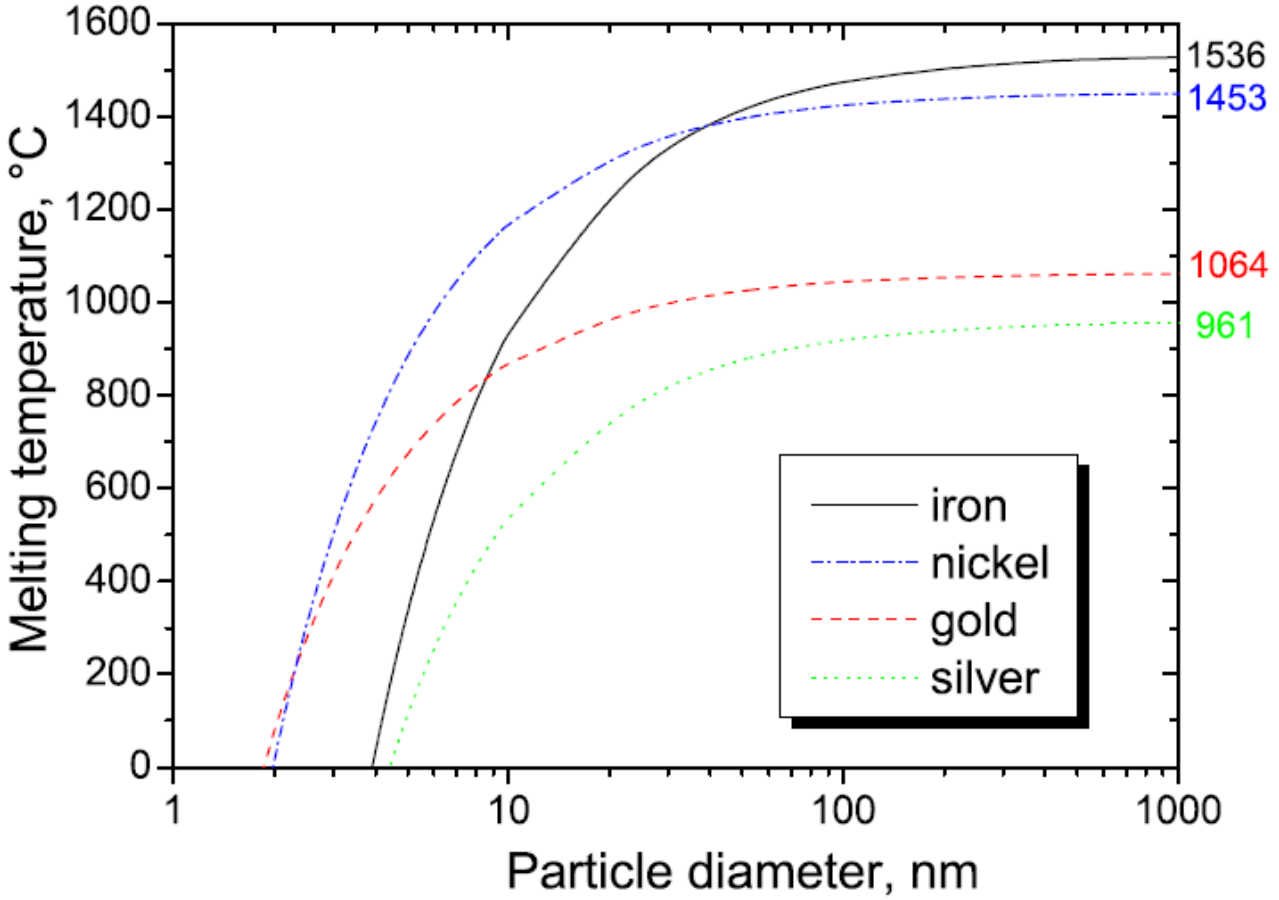

Figure 3. Melting temperature of selected metals as a function of particle diameter.

Moisala et al., *J. Phys. Cond. Matt.* 15:S3011, 2003.

Catalyst can be solid (VSS) or liquid (VLS), but VLS growth is much faster

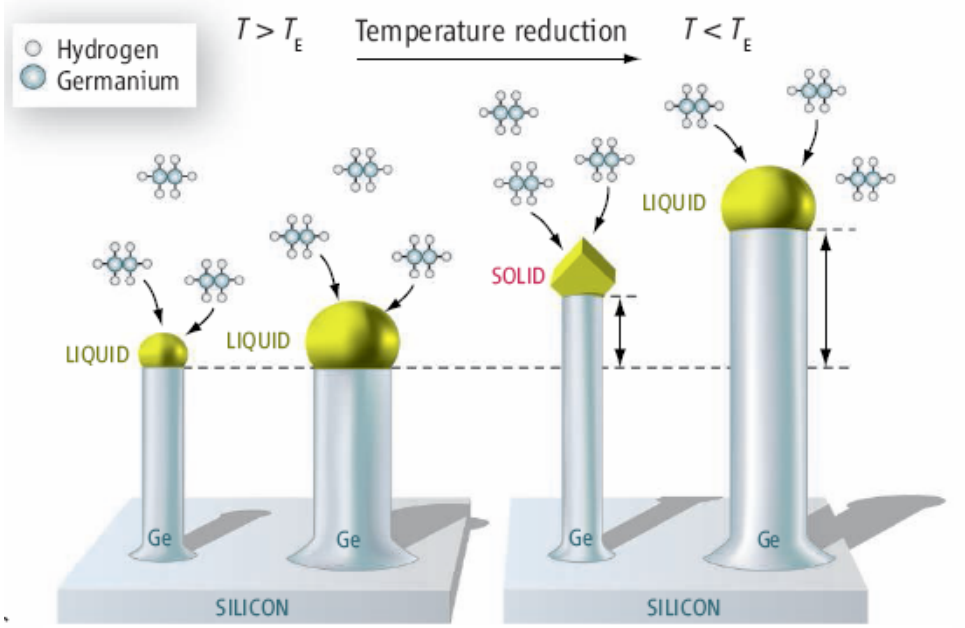

Germanium nanowires. The mechanism by which Ge nanowires grow may depend not only on the temperature but also on the diameter of the nanowire, as shown by Kodambaka *et al.* Above T_E (**left**), the nanowires have a liquid gold cap and grow via VLS growth. Below T_E (**right**), the cap of relatively thick nanowires is liquid, whereas the cap of relatively thin nanowires becomes a crystalline solid. The latter nanowires grow via a different mechanism that is slower than VLS growth.

Liquid, 340°C

Solid

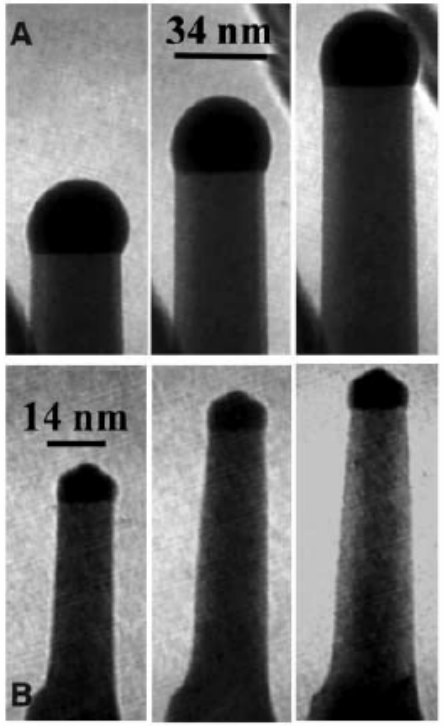

Fig. 2. (**A**) Series of images of a single Ge wire acquired at times t = 0, 309, and 618 s (from left to right, respectively) during growth by the VLS mechanism at 340°C and 4.6×10^{-6} Torr Ge_2H_6. The background features act as markers, showing a growth rate of 9.9×10^{-2} nm/s. (**B**) Another image series for a second wire growing at the same temperature and pressure but with a solid catalyst at t = 0, 1340, and 1824 s (from left to right, respectively). The growth rate for this VSS mode is 1.3×10^{-2} nm/s.

Verification that the catalyst can be solid during growth

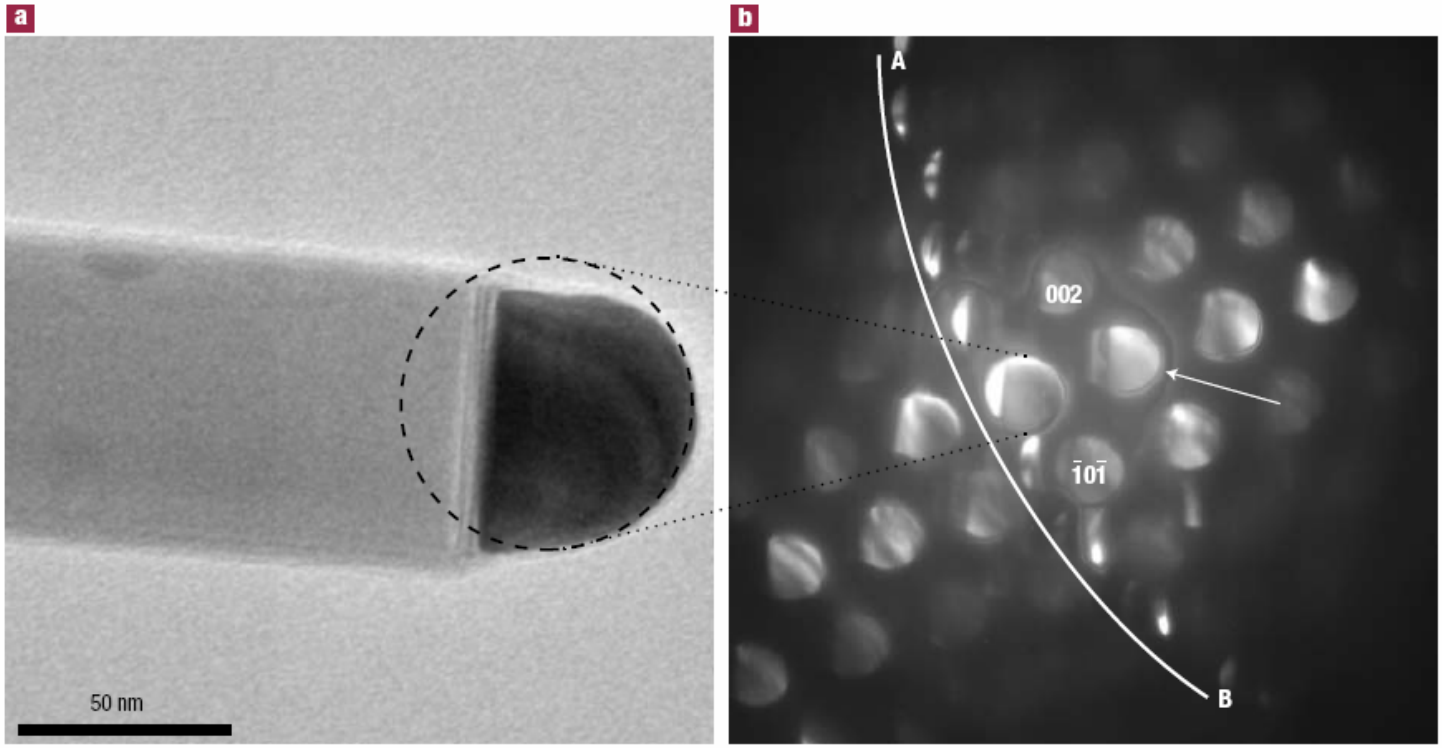

Figure 3 TEM image and electron diffraction of a GaAs nanowire at high temperature. a, A wire with a solid gold particle, imaged at 540 °C (equivalent to the growth temperature). **b**, Defocused diffraction pattern of the whisker at 540 °C proving the crystallinity. The encircled area in **a** is the central spot of the diffraction pattern. The set of defocused diffracted beams originating from the gold–gallium alloy lattice, one marked with an arrow, contains a bright diffraction image of the seed particle. The projection of the seed particle is close to [110] of a face-centred-cubic lattice. The off-axis diffraction spots originating from the GaAs part of the wire can be seen along the arc A–B. The contrast in the direct beam at the centre has been reduced in brightness to enhance visibility.

Persson et al., *Nature Materials* 3:677, 2004.

What elements are CNT growth catalysts?

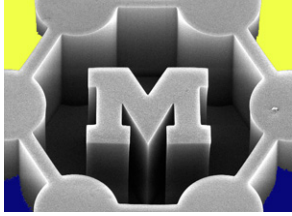

- SWNTs
- MWNTs
- As primary part of a two-component catalyst, SWNTs
- Oxide

1												13	14	15	16	17	18
1 H hydrogen 1.007 94(7)	2																2 He helium 4.002 602(2)
3 Li lithium 6.941(2)	4 Be beryllium 9.012 182(3)											5 B boron 10.811(7)	6 C carbon 12.0107(8)	7 N nitrogen 14.0067(2)	8 O oxygen 15.9994(3)	9 F fluorine 18.998 4032(5)	10 Ne neon 20.1797(6)
11 Na sodium 22.989 769 28(2)	12 Mg magnesium 24.3050(6)	3	4	5	6	7	8	9	10	11	12	13 Al aluminium 26.981 538 6(8)	14 Si silicon 28.0855(3)	15 P phosphorus 30.973 762(2)	16 S sulfur 32.065(5)	17 Cl chlorine 35.453(2)	18 Ar argon 39.948(1)
19 K potassium 39.0983(1)	20 Ca calcium 40.078(4)	21 Sc scandium 44.955 912(6)	22 Ti titanium 47.867(1)	23 V vanadium 50.9415(1)	24 Cr chromium 51.9961(6)	25 Mn manganese 54.938 045(5)	26 Fe iron 55.845(2)	27 Co cobalt 58.933 195(5)	28 Ni nickel 58.6934(2)	29 Cu copper 63.546(3)	30 Zn zinc 65.409(4)	31 Ga gallium 69.723(1)	32 Ge germanium 72.64(1)	33 As arsenic 74.921 60(2)	34 Se selenium 78.96(3)	35 Br bromine 79.904(1)	36 Kr krypton 83.798(2)
37 Rb rubidium 85.4678(3)	38 Sr strontium 87.62(1)	39 Y yttrium 88.905 85(2)	40 Zr zirconium 91.224(2)	41 Nb niobium 92.906 38(2)	42 Mo molybdenum 95.94(2)	43 Tc technetium [97.9072]	44 Ru ruthenium 101.07(2)	45 Rh rhodium 102.905 50(2)	46 Pd palladium 106.42(1)	47 Ag silver 107.8682(2)	48 Cd cadmium 112.411(8)	49 In indium 114.818(3)	50 Sn tin 118.710(7)	51 Sb antimony 121.760(1)	52 Te tellurium 127.60(3)	53 I iodine 126.904 47(3)	54 Xe xenon 131.293(6)
55 Cs caesium 132.905 451 9(2)	56 Ba barium 137.327(7)	57-71 lanthanoids	72 Hf hafnium 178.49(2)	73 Ta tantalum 180.947 88(2)	74 W tungsten 183.84(1)	75 Re rhenium 186.207(1)	76 Os osmium 190.23(3)	77 Ir iridium 192.217(3)	78 Pt platinum 195.084(9)	79 Au gold 196.966 569(4)	80 Hg mercury 200.59(2)	81 Tl thallium 204.3833(2)	82 Pb lead 207.2(1)	83 Bi bismuth 208.980 40(1)	84 Po polonium [208.9824]	85 At astatine [209.9871]	86 Rn radon [222.0176]
87 Fr francium [223]	88 Ra radium [226]	89-103 actinoids	104 Rf rutherfordium [261]	105 Db dubnium [262]	106 Sg seaborgium [266]	107 Bh bohrium [264]	108 Hs hassium [277]	109 Mt meitnerium [268]	110 Ds darmstadtium [271]	111 Rg roentgenium [272]							

Key: atomic number **Symbol** name standard atomic weight

57 La lanthanum 138.905 47(7)	58 Ce cerium 140.116(1)	59 Pr praseodymium 140.907 65(2)	60 Nd neodymium 144.242(3)	61 Pm promethium [145]	62 Sm samarium 150.36(2)	63 Eu europium 151.964(1)	64 Gd gadolinium 157.25(3)	65 Tb terbium 158.925 35(2)	66 Dy dysprosium 162.500(1)	67 Ho holmium 164.930 32(2)	68 Er erbium 167.259(3)	69 Tm thulium 168.934 21(2)	70 Yb ytterbium 173.04(3)	71 Lu lutetium 174.967(1)
89 Ac actinium [227]	90 Th thorium 232.038 06(2)	91 Pa protactinium 231.035 88(2)	92 U uranium 238.028 91(3)	93 Np neptunium [237]	94 Pu plutonium [244]	95 Am americium [243]	96 Cm curium [247]	97 Bk berkelium [247]	98 Cf californium [251]	99 Es einsteinium [252]	100 Fm fermium [257]	101 Md mendelevium [258]	102 No nobelium [259]	103 Lr lawrencium [262]

Catalyst deposition on a substrate: dip-coating or annealing a thin-film

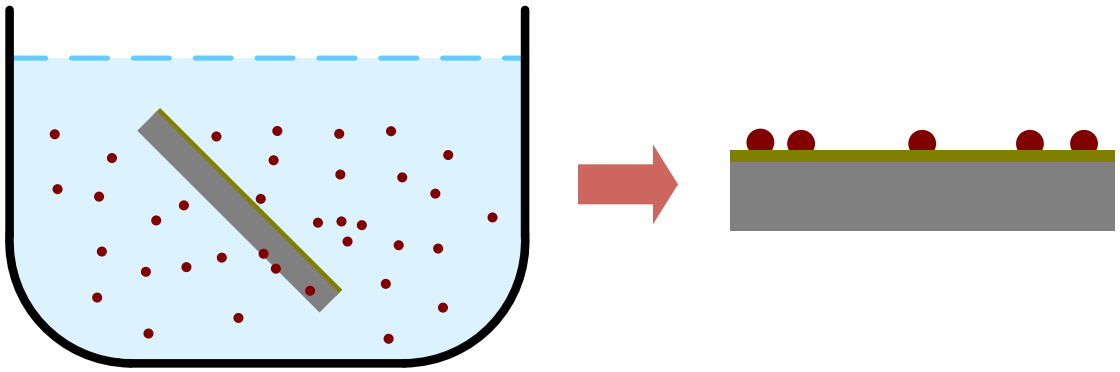

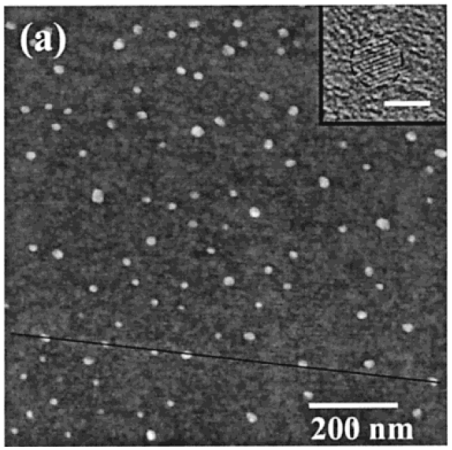

Li et al., *J. Phys. Chem. B* 105(46):11424-31, 2001

Deposit a thin film → **Anneal to form particles**

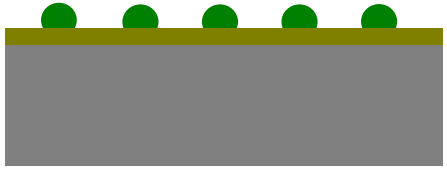

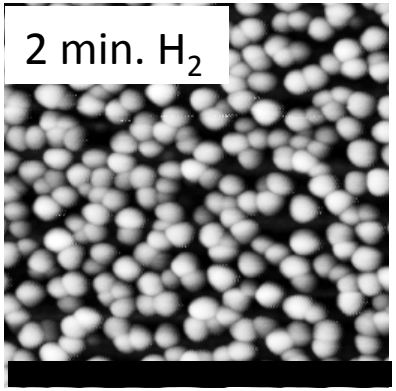

500 nm

CNT diameter control by size of nanoparticles made by chemical methods

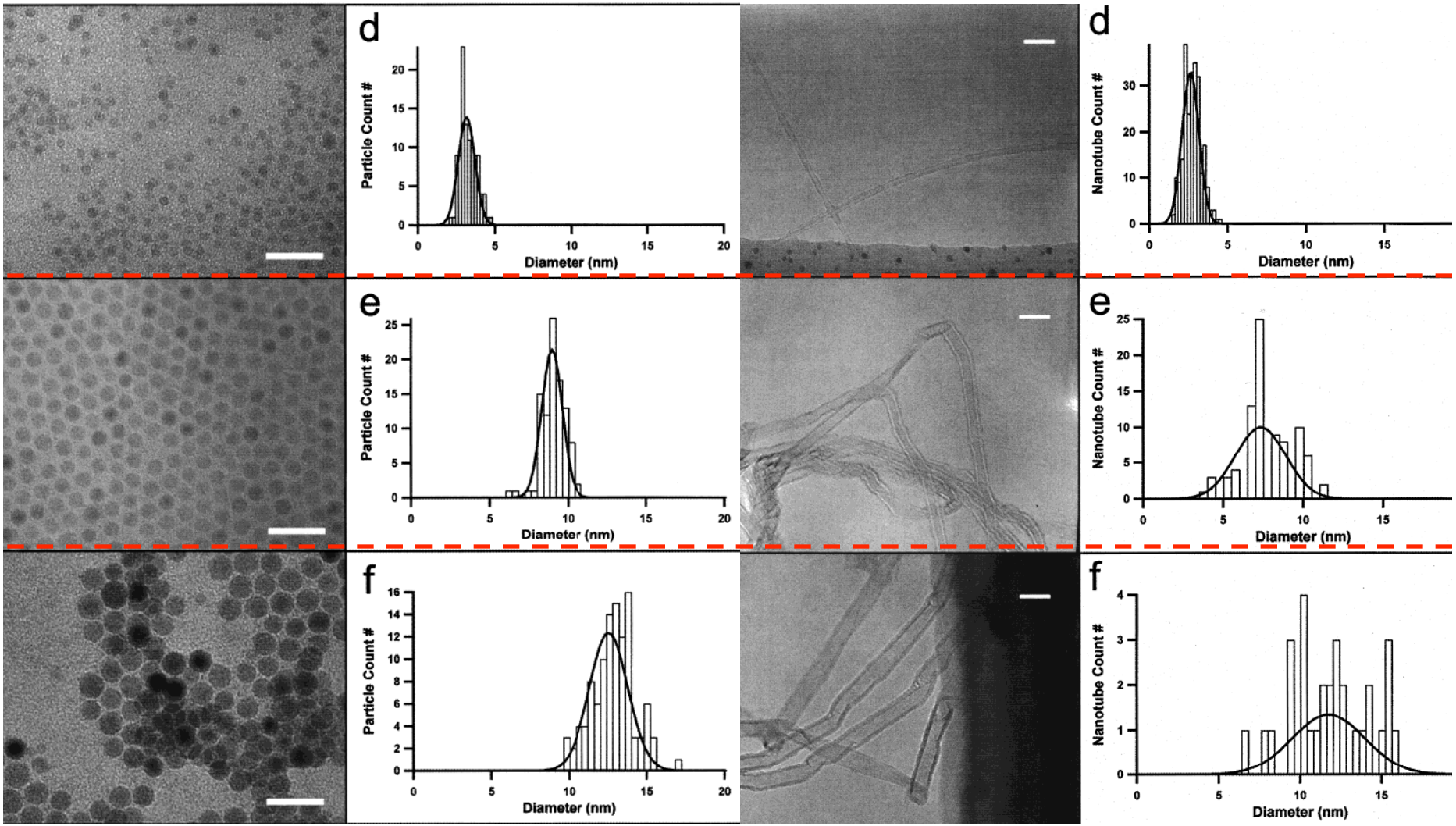

Cheung et al, *JPCB* 106:2429-33, 2002.

Size-driven structure transitions

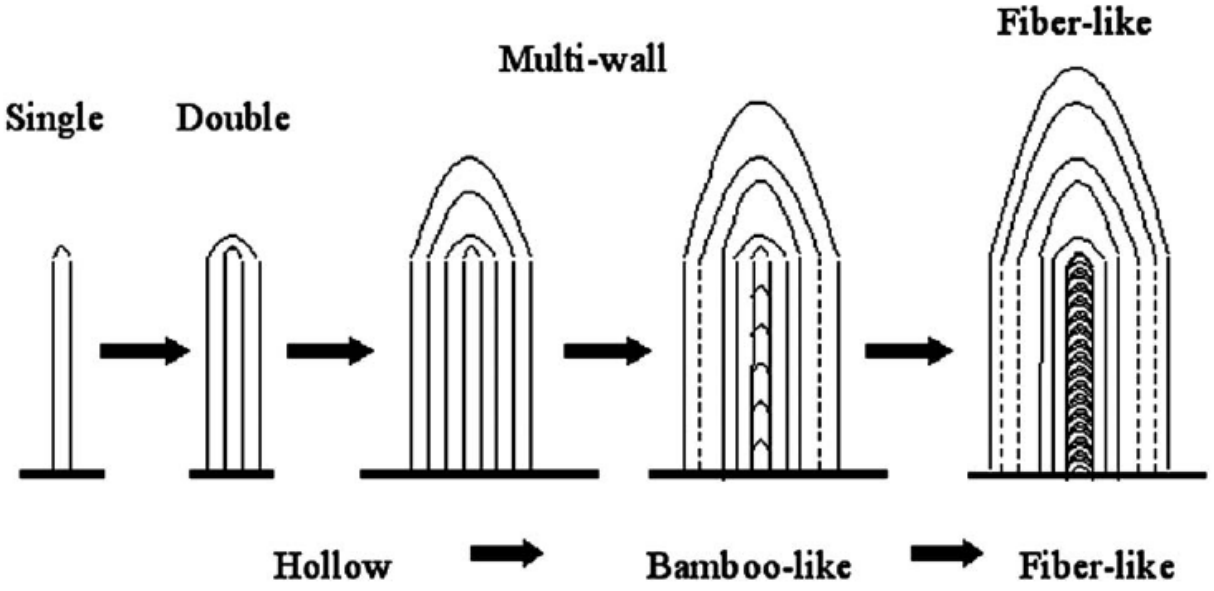

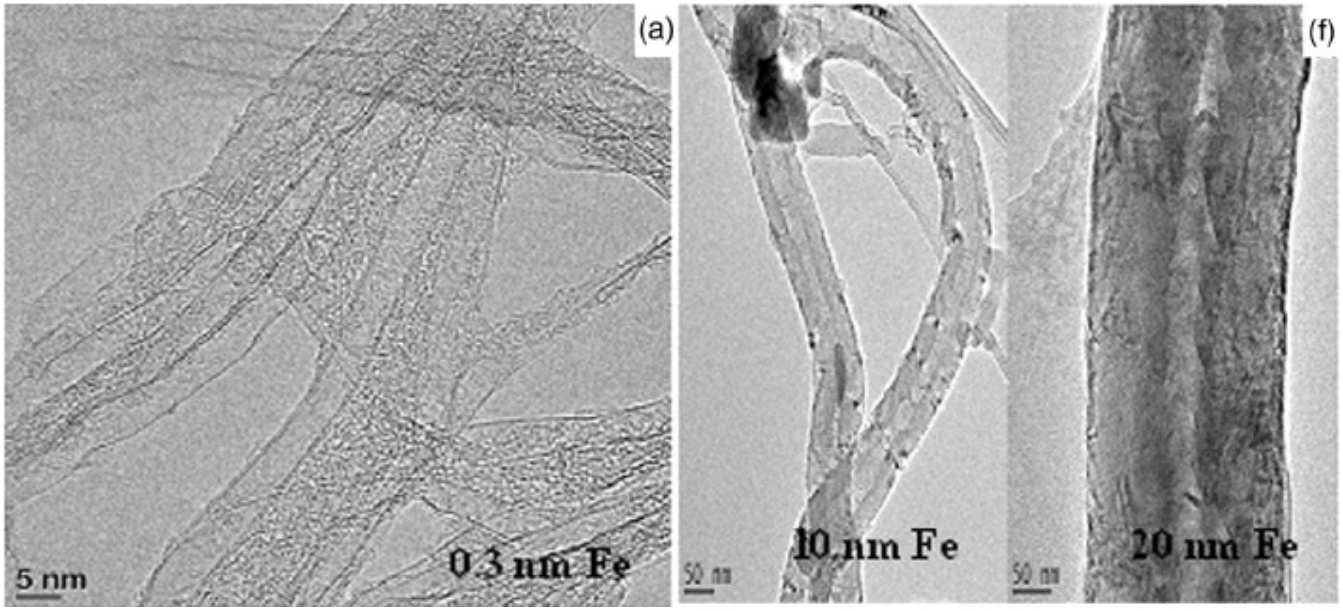

Wang et al., *Journal of Applied Physics* 98:014312, 2005.

CoMoCat process

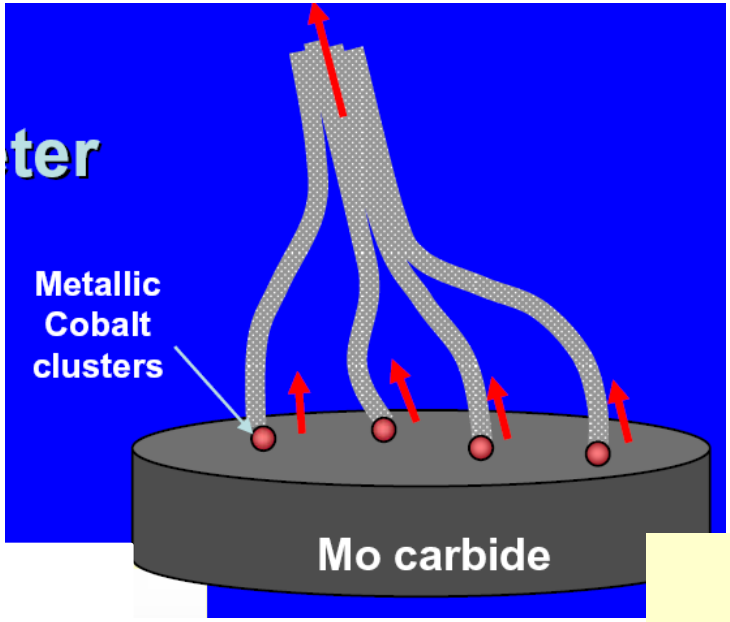

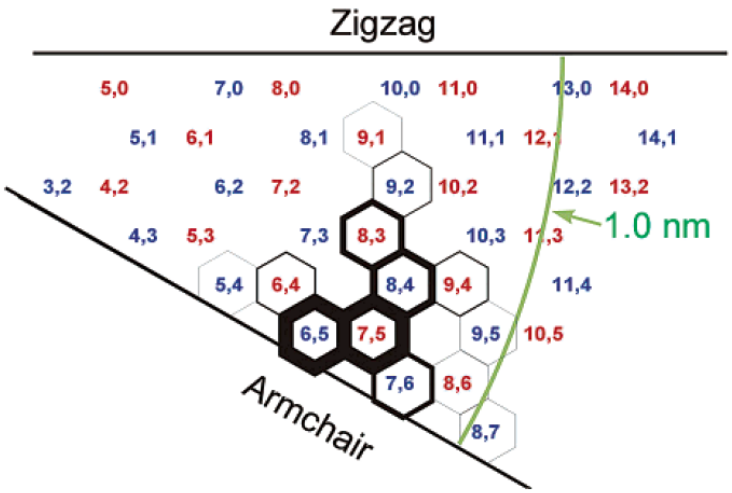

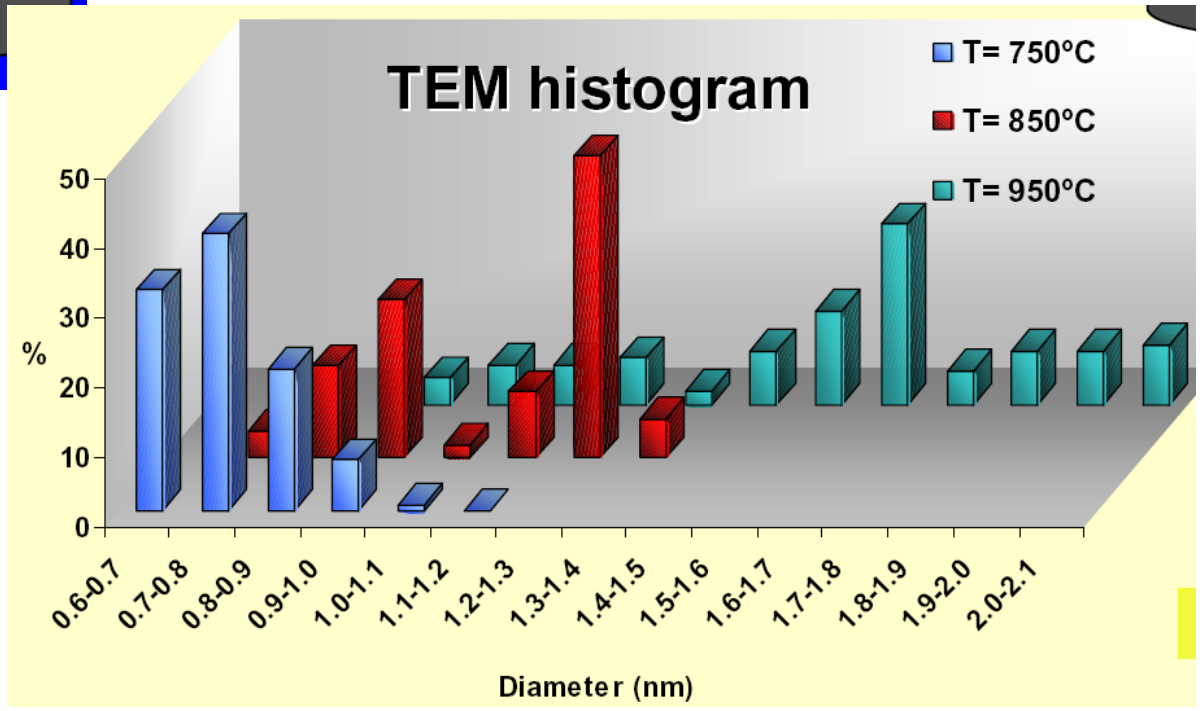

CNT diameter increases with reaction temperature

Resasco et al., University of Oklahoma

CNT diameter control by carbon supply rate

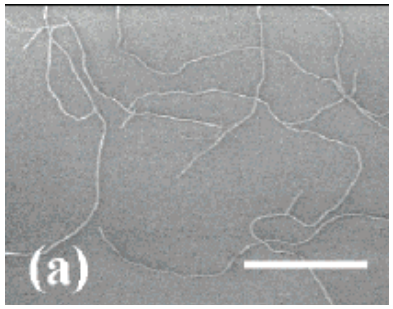

140 ppm C_2H_6

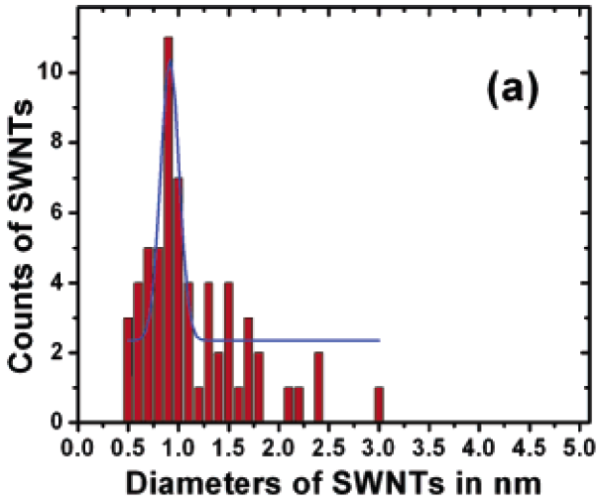

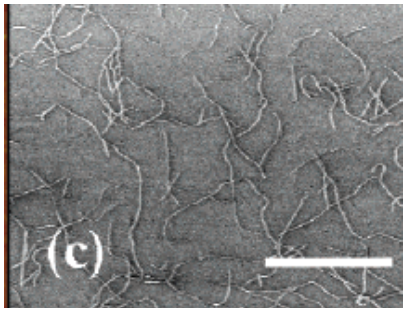

1600 ppm C_2H_6

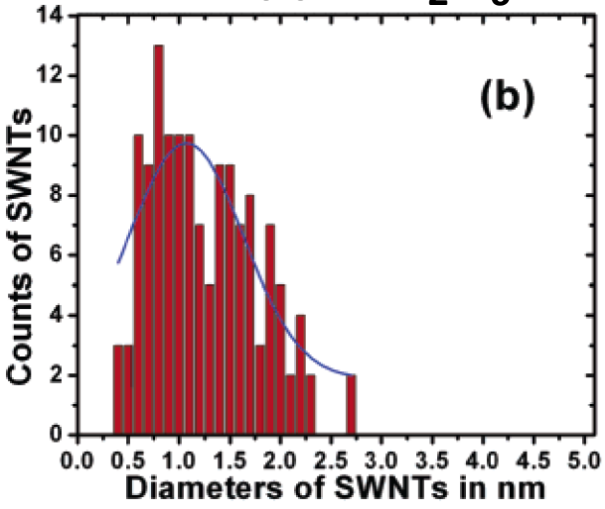

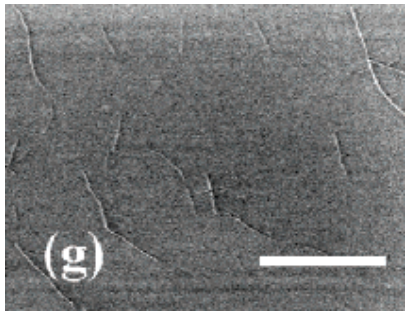

14400 ppm C_2H_6

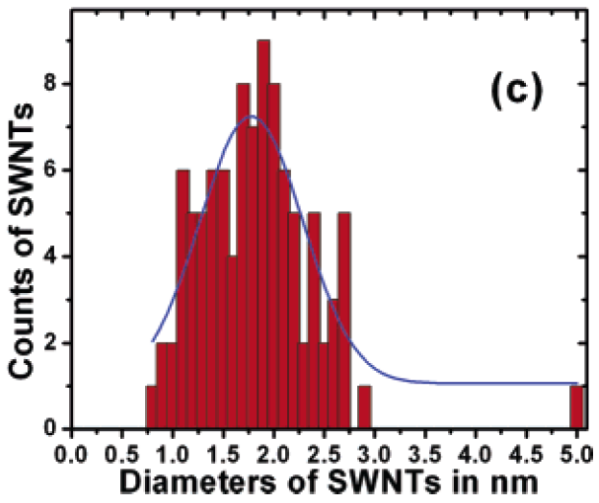

Lu and Liu, *Journal of Physical Chemistry B* 110:20254-7, 2006.

Limiting cases of carbon deposition

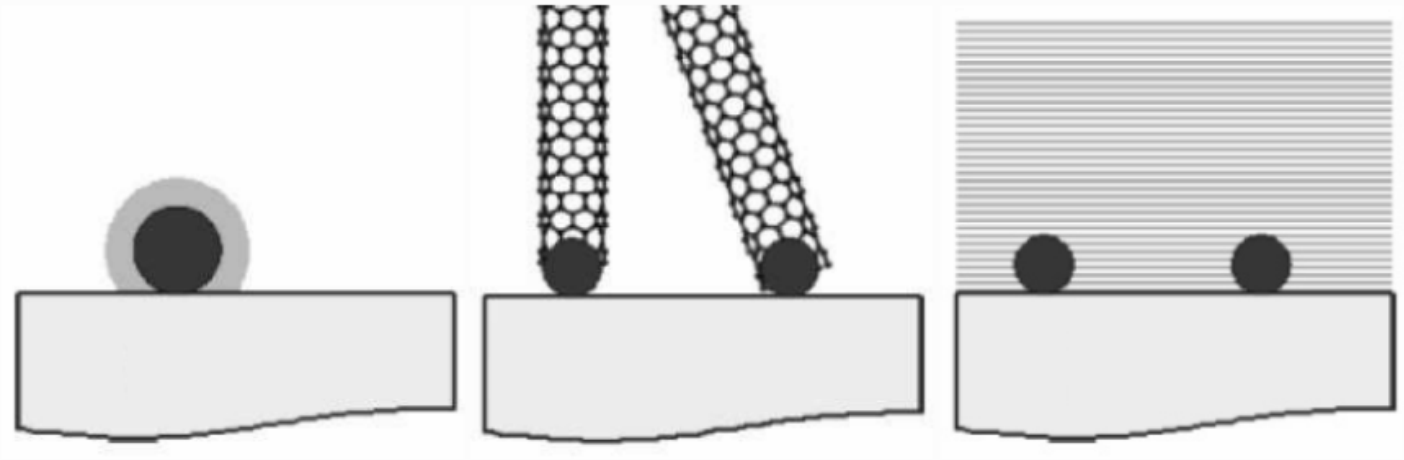

→ graphene

Figure 2-11. Limiting scenarios of carbon deposition, diffusion, and precipitation under CVD reaction conditions (from [177]): (b) rate of carbon supply or conversion is too low, and the catalyst particle is encapsulated by graphitic layers; (c) nucleation and growth conditions are appropriate and CNTs grow normally; (d) rate of carbon supply is too high and carbon coats the catalyst and substrate before nucleation occurs.

Seidel et al., *Journal of Physical Chemistry B*, 108:1888 2004.

Gas-phase reactions

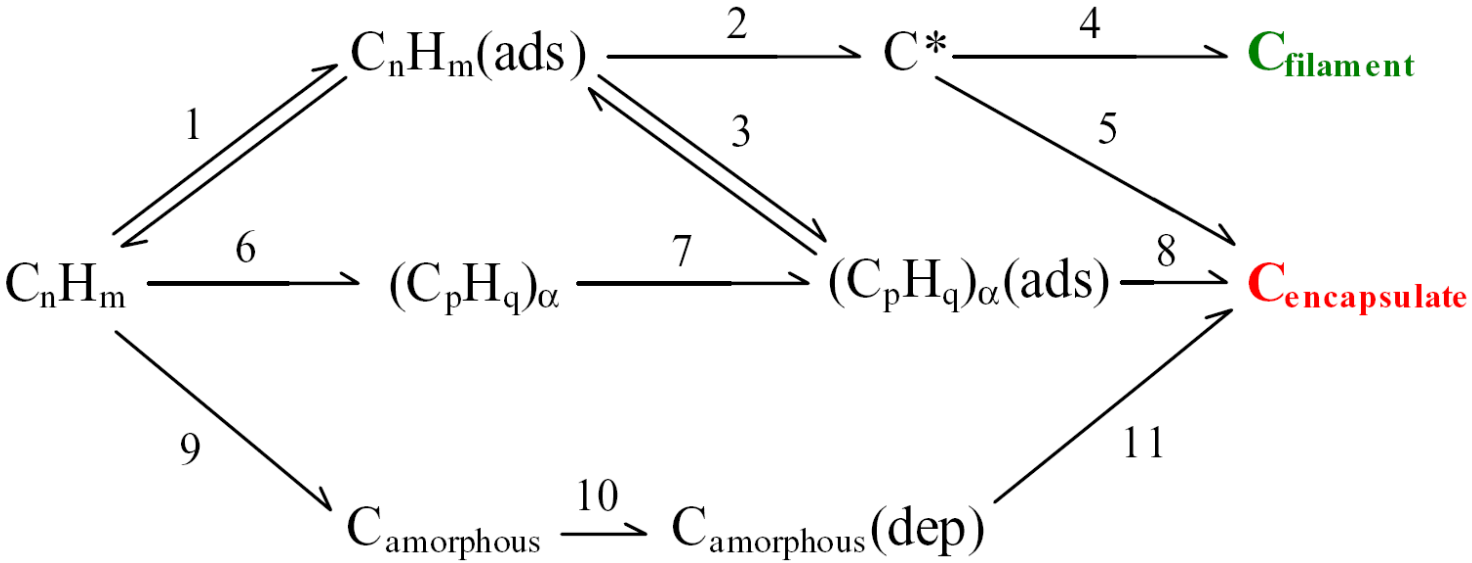

1→2→4: Adsorption of hydrocarbon, dissociation of carbon, incorporation to filament

1→2→5: Adsorption, dissociation, encapsulation

6→7→8: Gas-phase polymerization, encapsulation

Effects of O_2 and H_2 are also important

C_2H_4/H_2 forms a polydisperse ambient

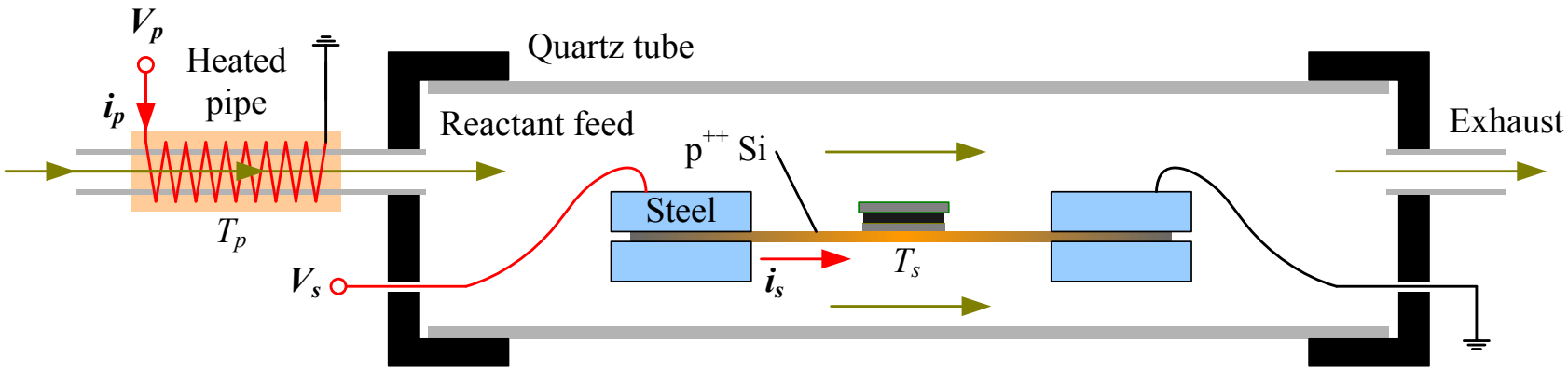

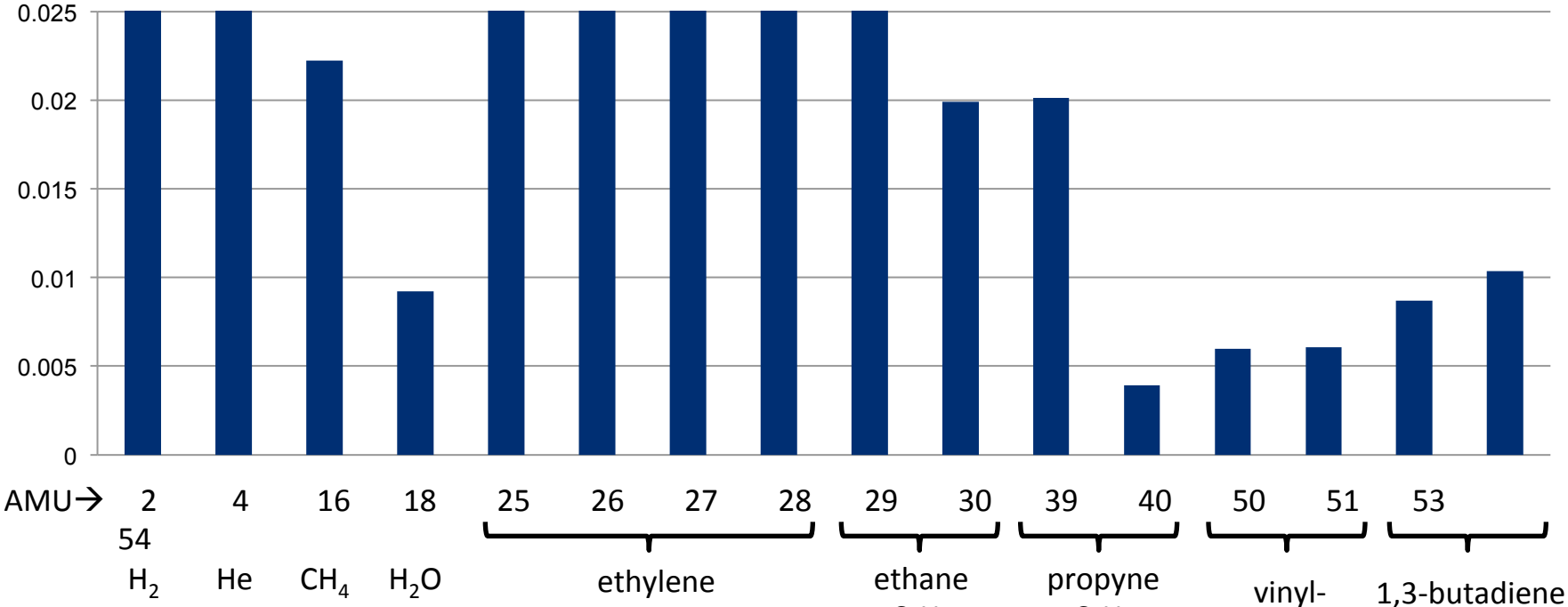

*Normalized to C_2H_4 signal

Plata, Hart, Reddy, Gschwend. *Environmental Science and Technology*, 2009.
Meshot, Plata, Tawfick, Zhang, Verploegen, Hart. *ACS Nano*, 2009.

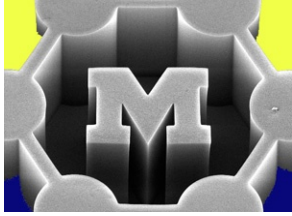

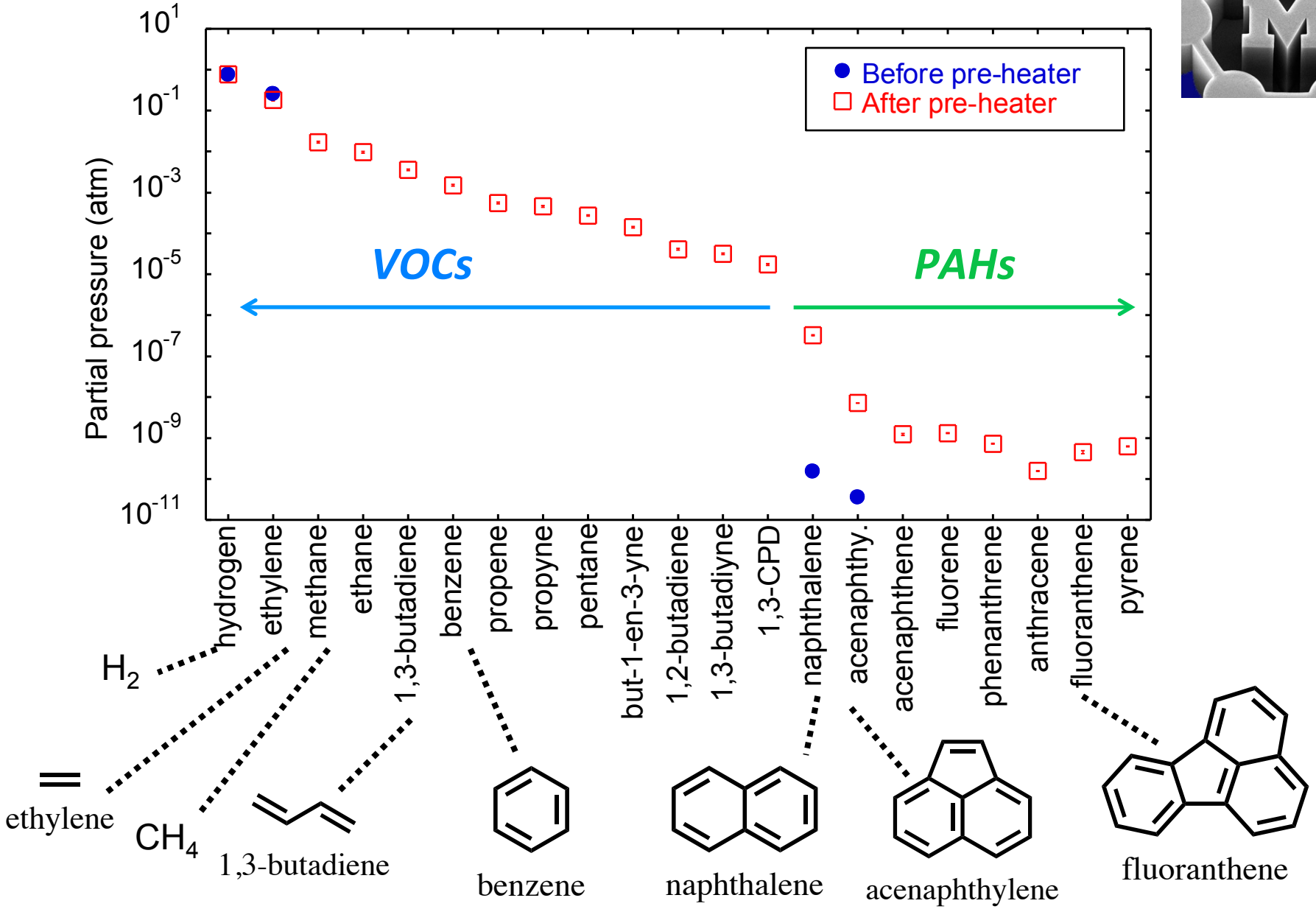

Plata, Hart, Reddy, Gschwend. *Environmental Science and Technology*, 2009.
Meshot, Plata, Tawfick, Zhang, Verploegen, Hart. *ACS Nano*, 2009.

CNT films: tangled vs. aligned

(1) $Mo/Fe/Al_2O_3$ in CH_4/H_2, 875 °C

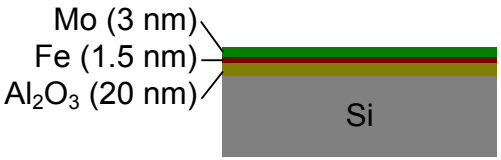

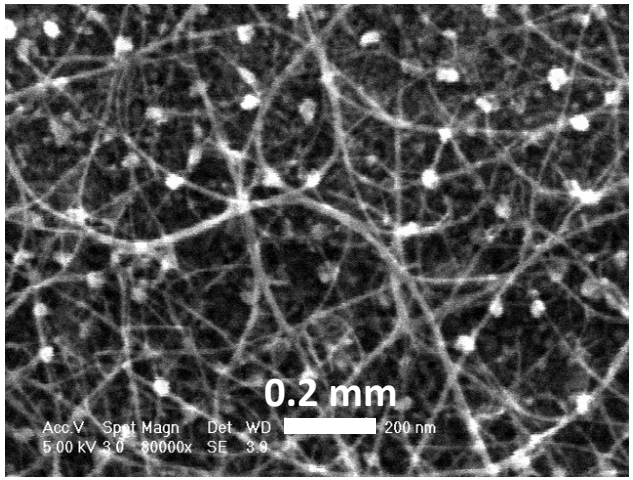

SWNT selectivity

Mo mediates CH_4 decomposition to give SWNTs

Fewer active catalyst particles
Low activity carbon source

(2) Fe/Al_2O_3 in C_2H_4/H_2, 750 °C

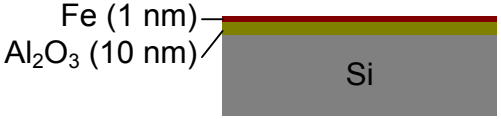

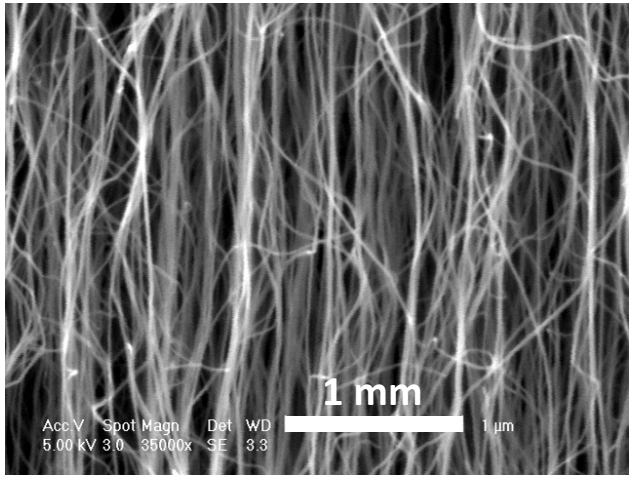

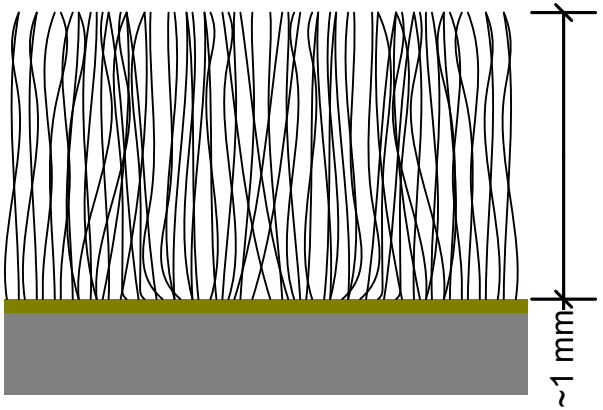

More active catalyst particles
High activity carbon source

Hart, Slocum, Royer, *Carbon* 44:348-59, 2006.

Physically making ~2 nm nanoparticles: e-beam lithography and angled deposition

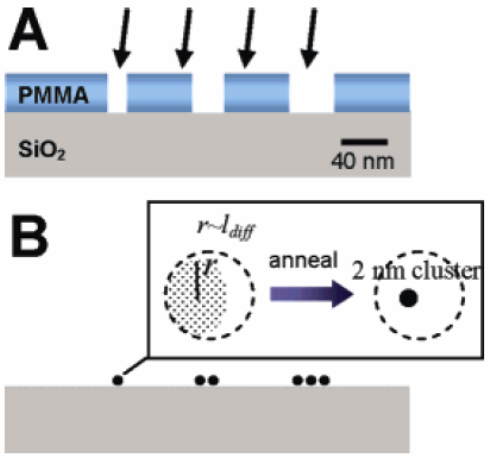

Figure 1. Formation of regular arrays of metal clusters down to 2 nm in diameter. (A) Arrays of 20−50 nm wells are patterned in ~100 nm thick PMMA on Si/SiO_2 (10 nm) substrates by electron-beam lithography. Thin metal films (0.2−2 nm) are then deposited by an electron-beam evaporator at a 5−10° angle with respect to the substrate normal. (B) After lift-off and annealing, one or multiple particles per well are formed depending on the well size. Inset: formation of a ~2 nm particle when the radius of metal-deposited area (dotted region) r is less than or equal to the metal atom diffusion length, l_{diff}. Angle evaporation reduces r by shadowing of the vertical PMMA wall. Dashed circles: bottom of the PMMA wells.

Or just e-beam lithography to achieve ~20-200 nm dots and lines

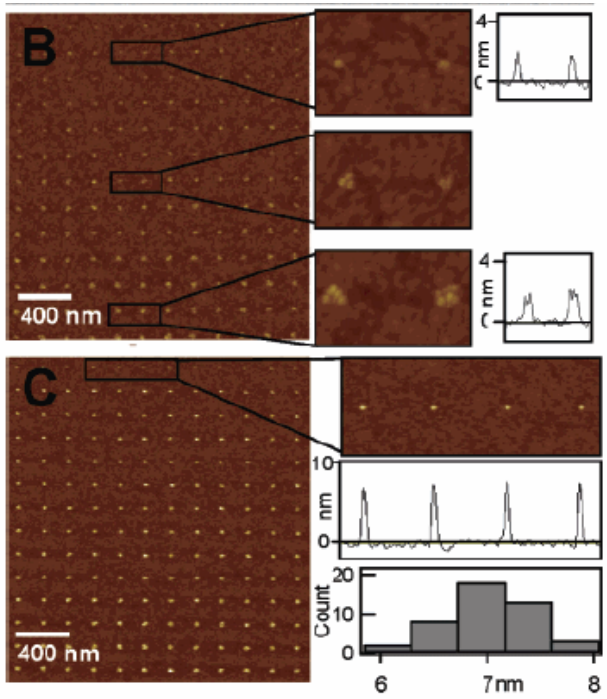

Figure 2. Patterning of monodispersed ~2 and ~7 nm Co nanoclusters. (A) Scanning electron microscopy image of patterned wells (holes) in a PMMA-coated Si/SiO_2 substrate. Diameter of wells in each row increases by ~5% and ranges from ~20 nm on top to ~30 nm at the bottom. (B) AFM image of rows of single (top right) and multiple (bottom right) ~2.2 nm Co particles and topographic line scans. The particle diameter is on the order of the measured height of ~2.2 nm as the apparent width is due to AFM tip effect. (C) AFM image of rows of single (top right, topography in middle; histogram at bottom) and multiple ~7 nm Co particles.

Javey et al., *JACS* 127:11942, 2005.

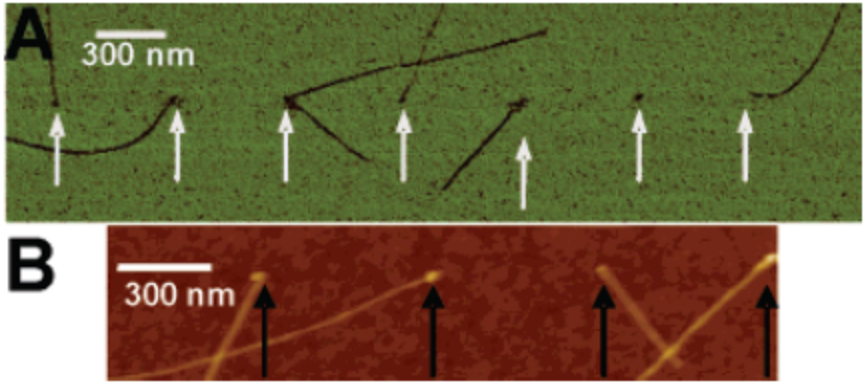

Figure 4. Deterministic growth of SWNTs from patterned discrete Co nanoparticles. (A and B): AFM images of nanotubes grown from arrays of 1−2 nm Co particles (pointed by arrows) with nearly one-particle to one-nanotube correspondence. The four SWNTs in (B) have a mean diameter of ~1.7 nm. The nanotube diameter is known to be determined by the diameter of the catalyst dot.

Javey et al., *JACS* 127:11942, 2005.

Isolated CNTs: bridging

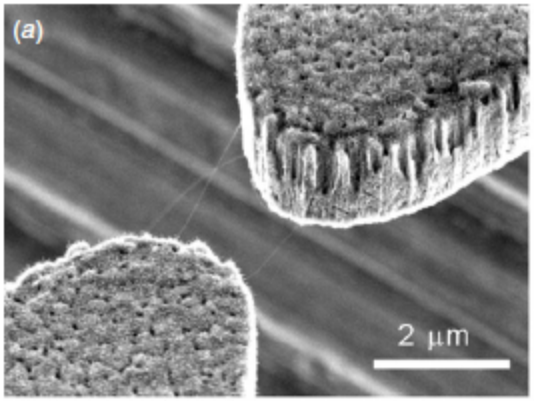

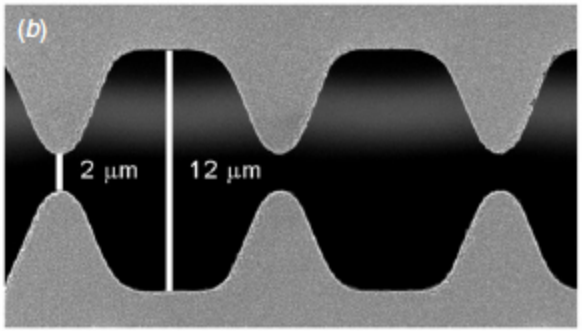

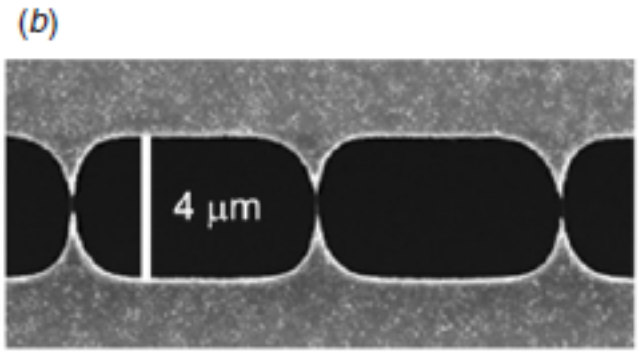

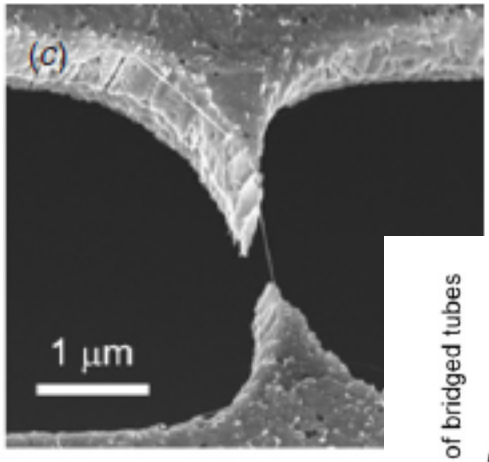

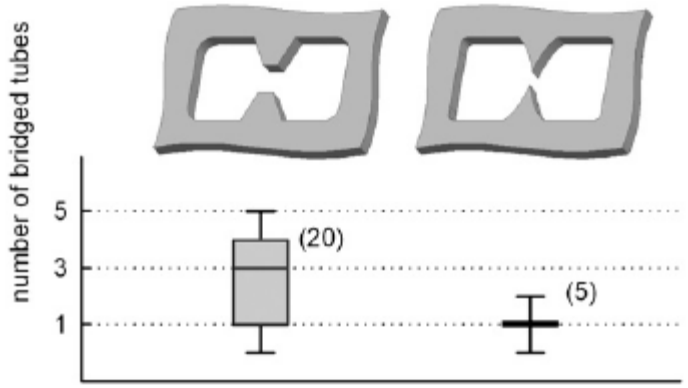

Figure 6. Box plot of two different tip apex geometries. Figures in parenthesis indicate the number of measured tip pairs. The ultra-sharp tips have a mean number of spanned SWNT of 1 tube per tip pair.

Jungen et al., *J. Micromech Microeng.*, 17:603-608, 2007.

Controlling film morphology by varying catalyst particle number density

Q: What is the critical catalyst density for vertically aligned growth?

Before Growth

Particle diameter 16±2 nm

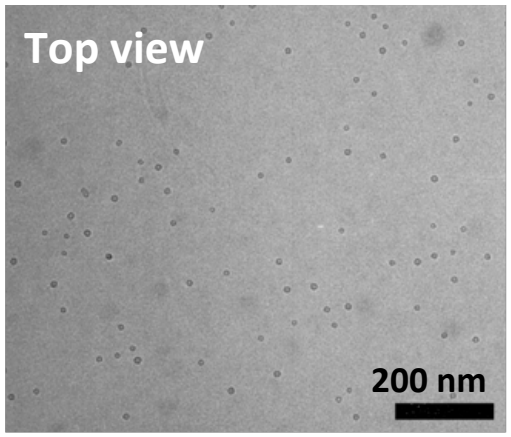

6×10^9 particles/cm^2

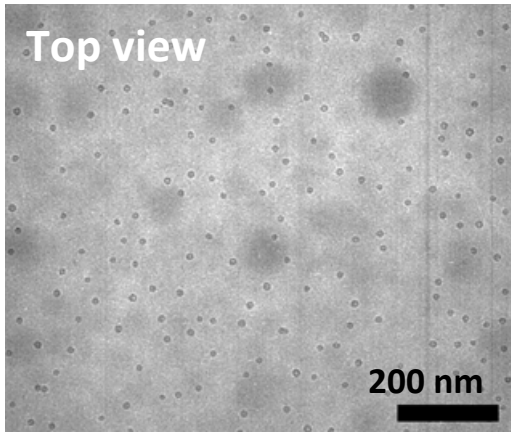

2.5×10^{10} particles/cm^2

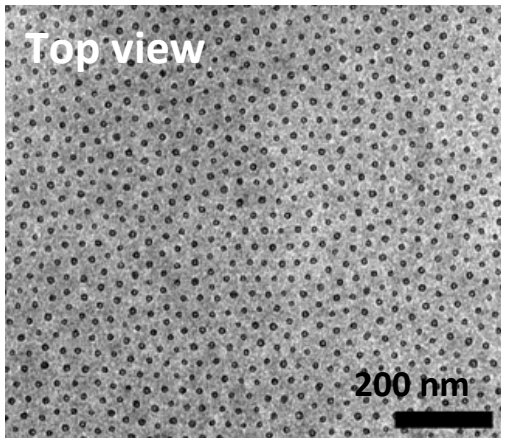

6×10^{10} particles/cm^2

After Growth

CNT diameter 12±2 nm, 8 walls

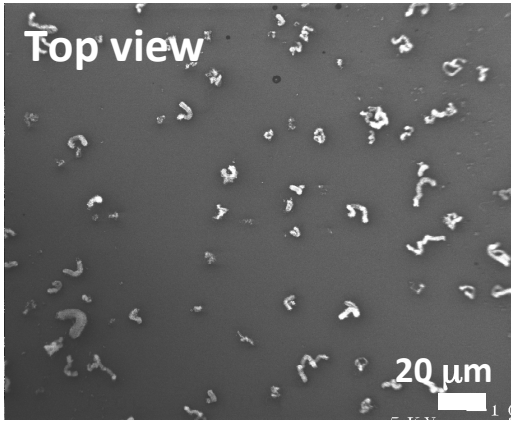

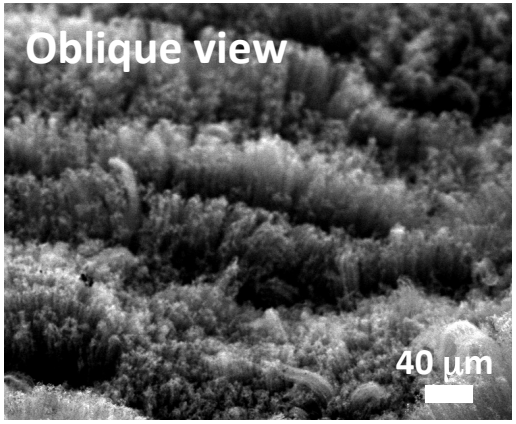

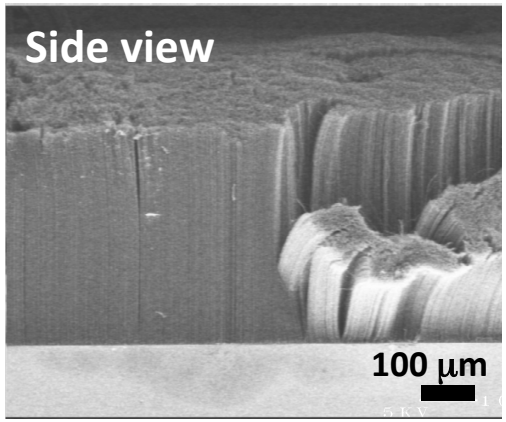

but only ≈5% activity!

Morphology control: Bennett, Hart, Cohen, *Advanced Materials* 18:2274-9, 2006.
Micro-contact printing: Bennett, Hart, et al., *Langmuir* 22:8273-8276, 2006.

CNT growth on microstructures and microstructures made of CNTs

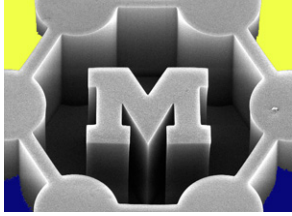

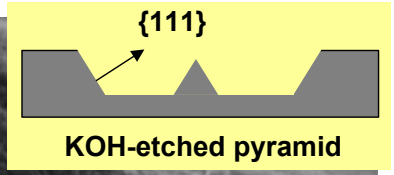

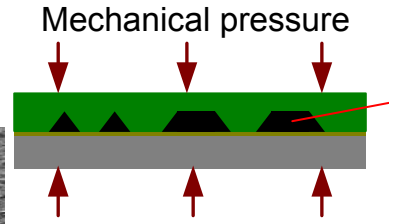

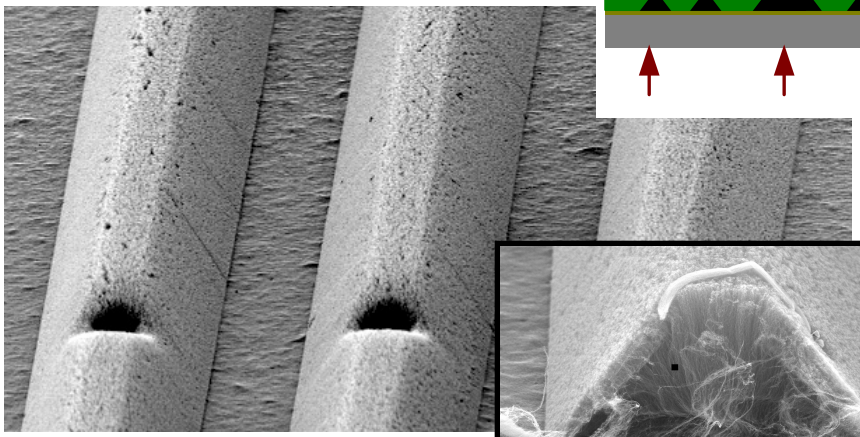

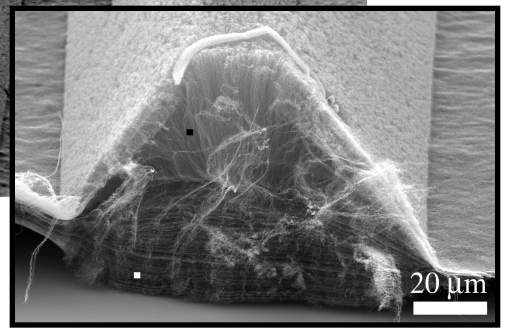

Hart, Slocum, et al., *Carbon* 44:348-59, 2006; *Nanotechnology* 17:1397-1403, 2006; *J. Phys. Chem. B* 110:8250-7, 2006; *Nano Letters* 6:1254-60, 2006.

CNT forest microstructures

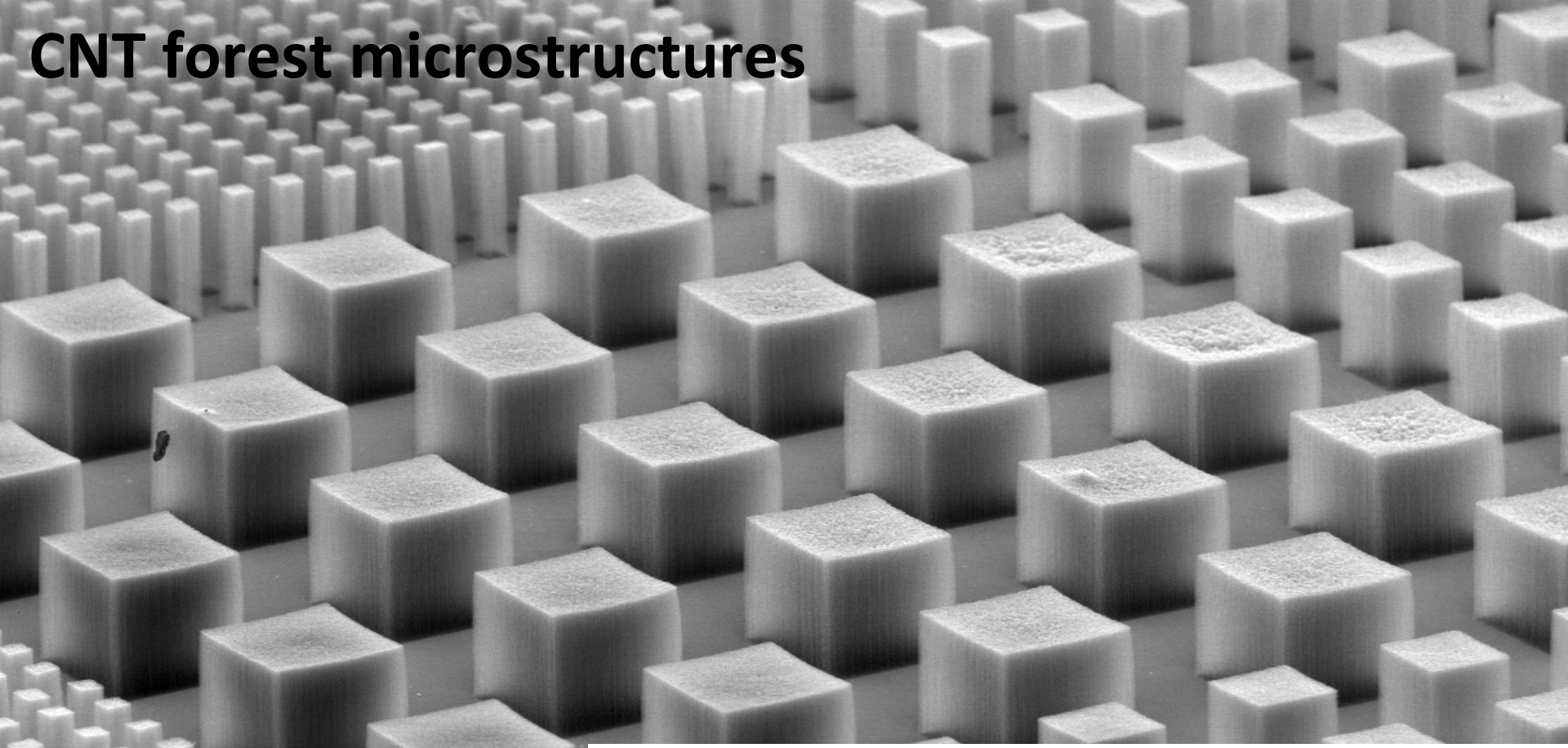

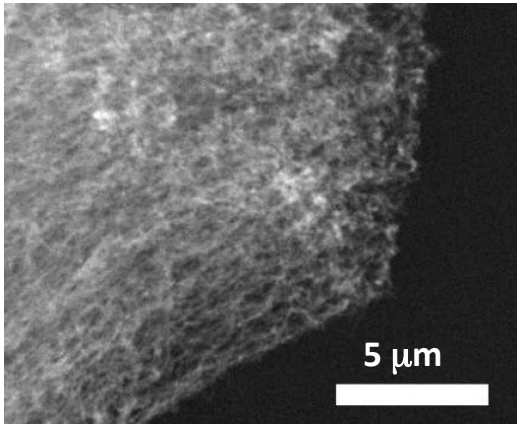

Sharp corner

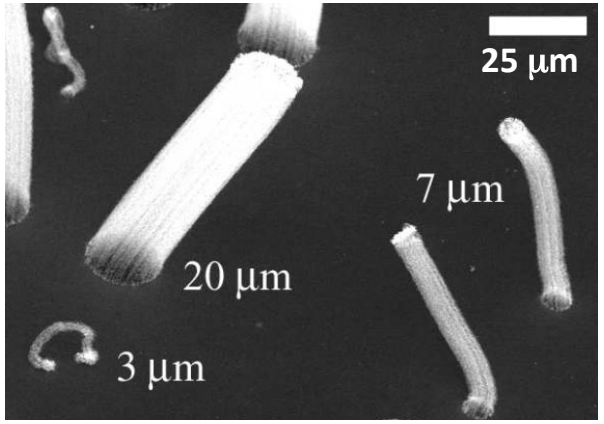

Loss of self-stability

3D substrates: growth on woven microfibers

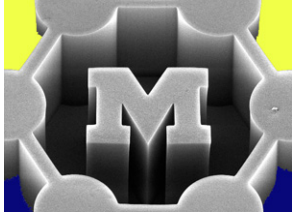

On alumina/glass fiber hose

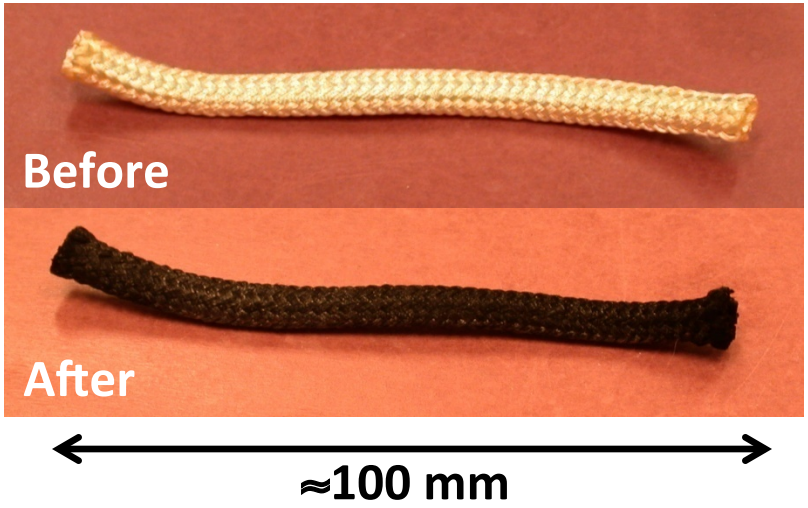

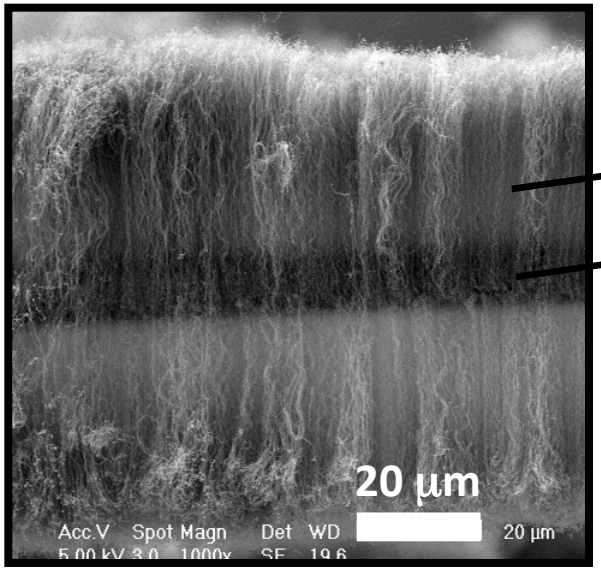

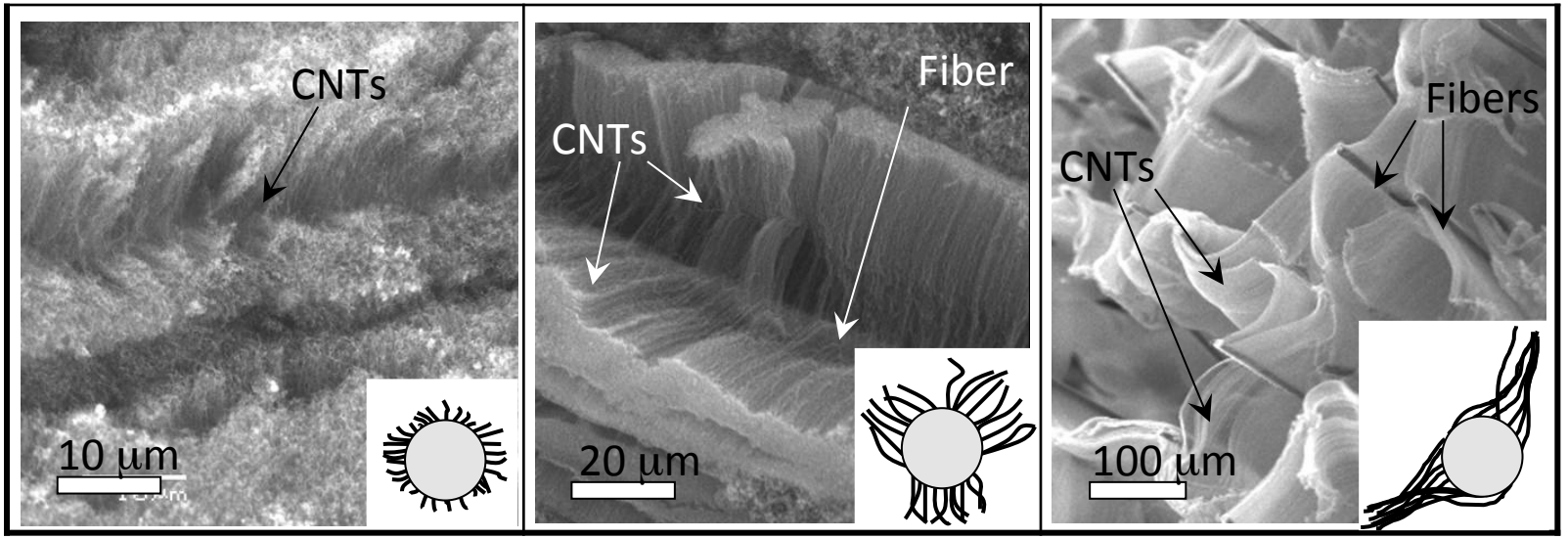

Yamamoto, Hart, et al., *Carbon* 47(3):551-560, 2009.

Vertical nanowire arrays

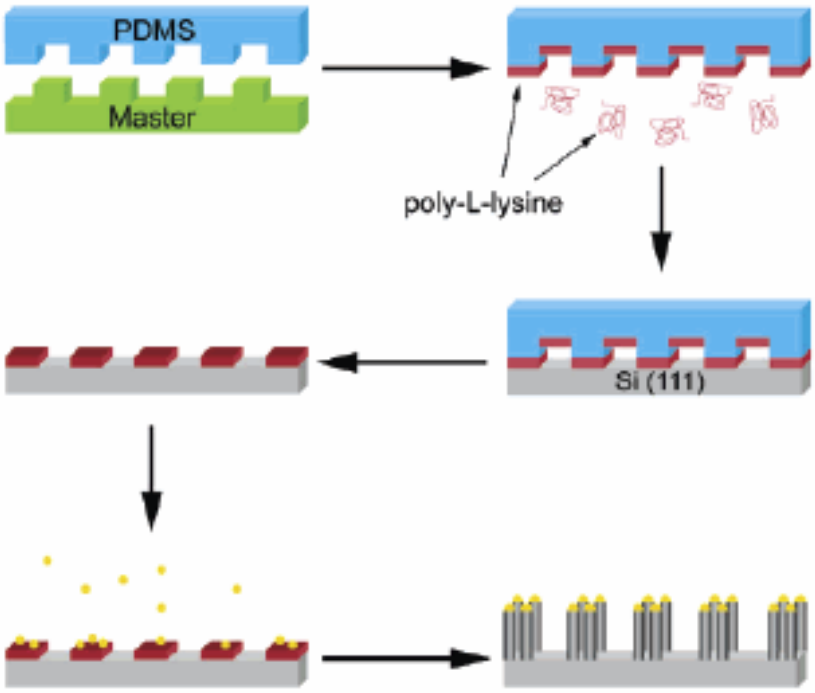

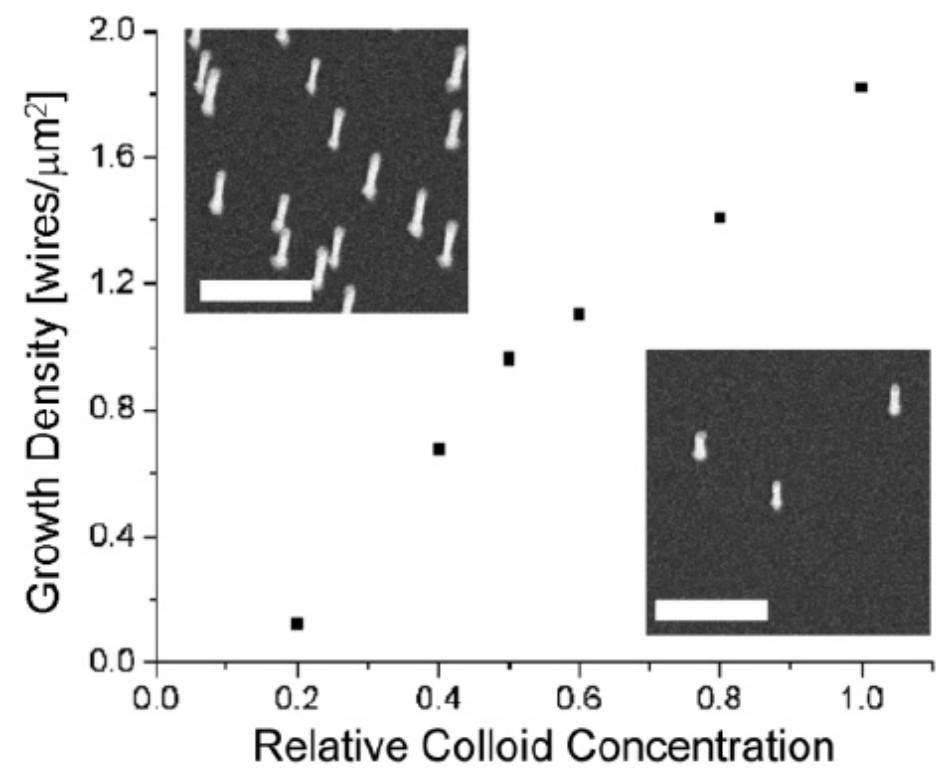

Hochbaum et al., *Nano Letters* 5(3):457, 2005.

Vertical nanowire arrays

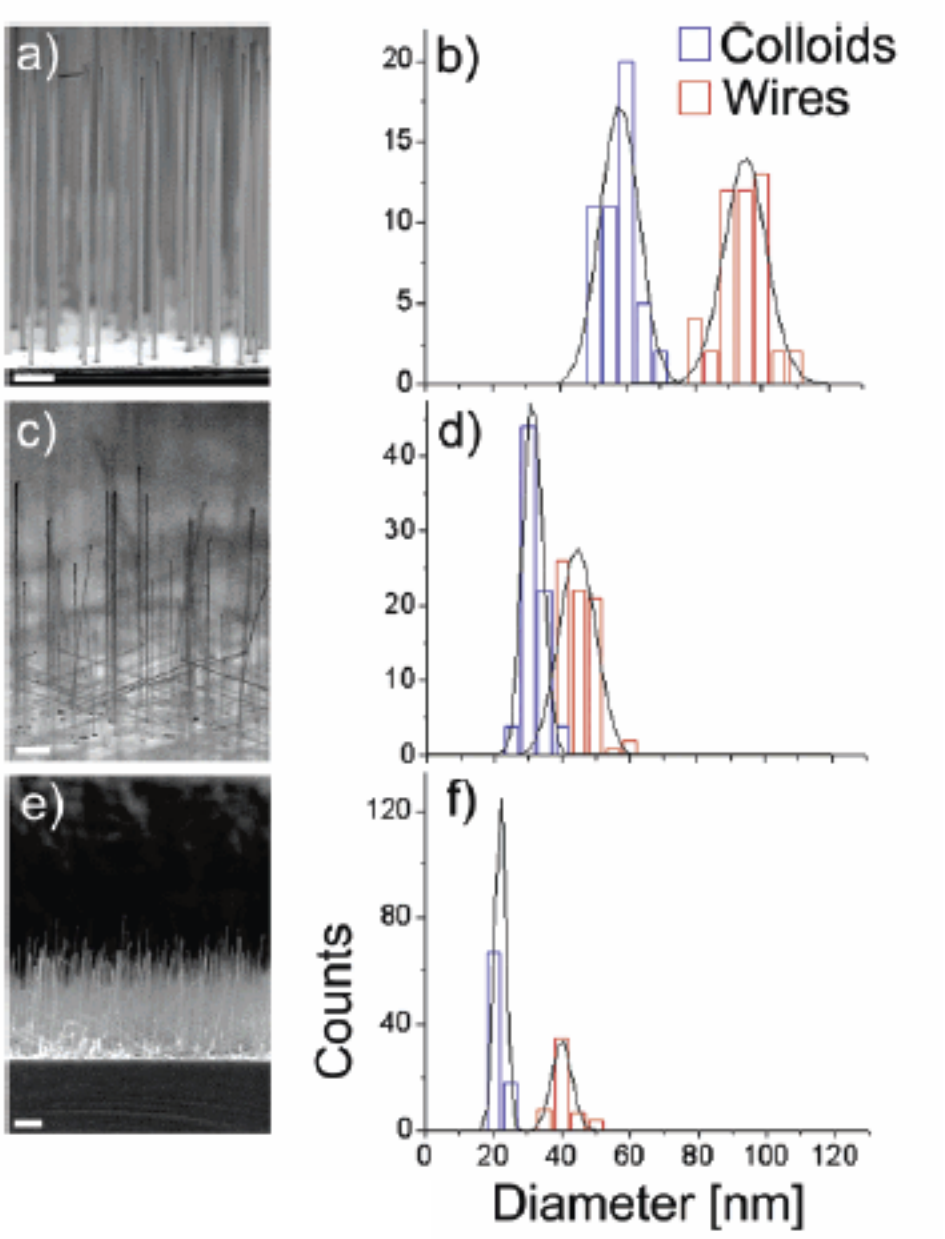

Hochbaum et al., *Nano Letters* 5(3):457, 2005.

Catalyst ripening (size broadening) causes NW diameters to change during growth

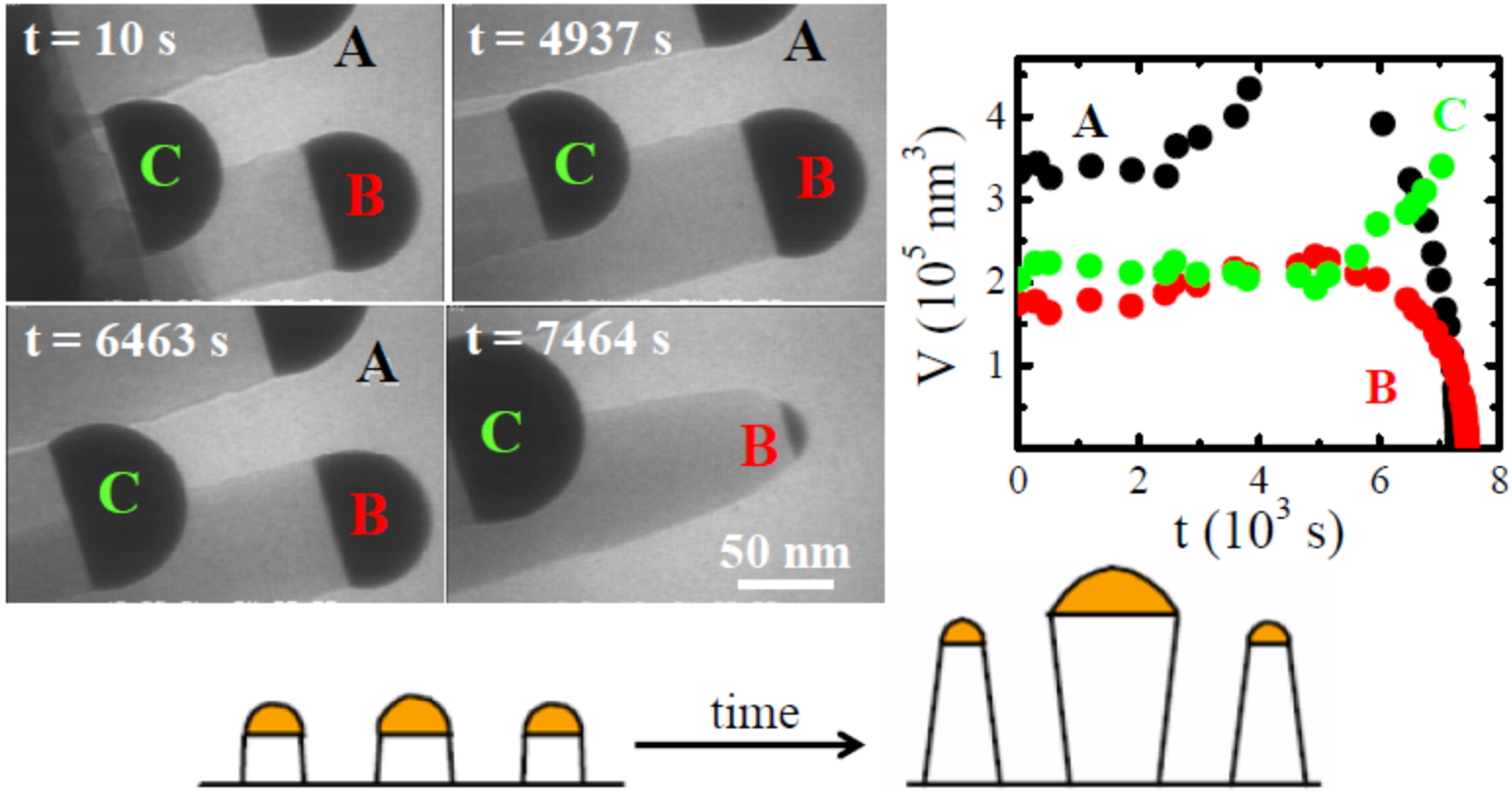

Figure 5. Upper panel shows TEM images of three Si wires labeled A, B, and C acquired at four successive times t (indicated on the images) and a plot of their droplet volumes V vs. t during wire growth at T = 655 °C and disilane pressure of 1×10^{-6} Torr. Lower panel is a schematic illustration of the wire tapering that occurs as a result of catalyst droplet coarsening. [Adapted from Ref. 57]

Kodambaka et al., *Proc. of SPIE* Vol. 7224 72240C-1, 2009.

Oxygen can be used to stop the Au catalyst from shrinking

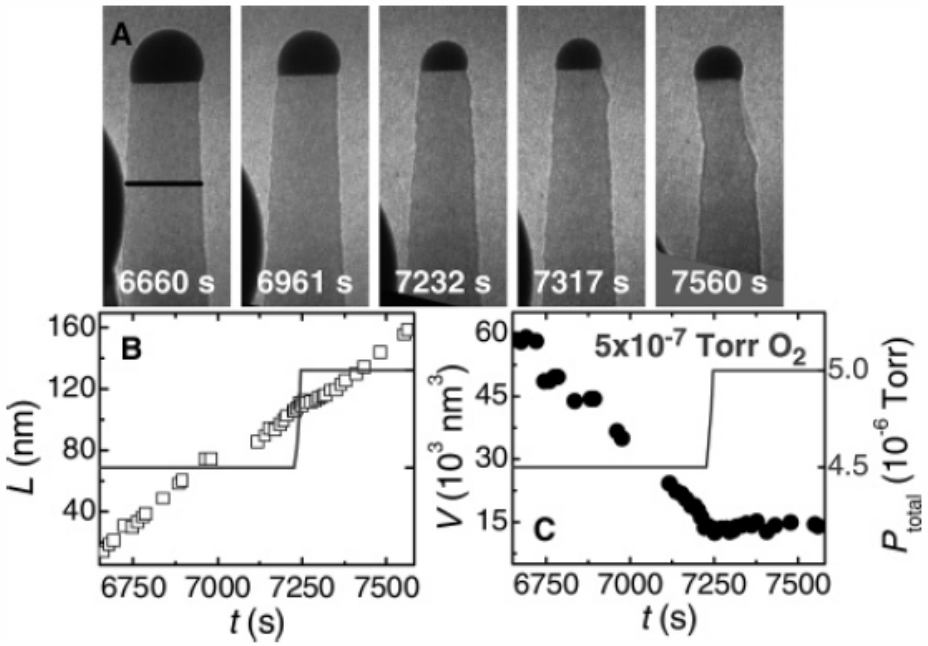

Figure 3. Effect of increasing oxygen pressure on Si wire growth kinetics. (A) Series of images extracted from a video sequence showing the effect of introducing oxygen to a wire that was previously growing in disilane. The growth was carried out in 4.5 $\times$ 10^{-6} Torr disilane at 610 °C for 111 minutes. At this point a wire was chosen that was tapering rapidly due to migration of Au from its droplet, and 5 $\times$ 10^{-7} Torr oxygen was introduced while maintaining the disilane pressure constant. The scale bar is 50 nm. (B) Length L of the wire as a function of time t, showing that growth continues at the same rate in the presence of oxygen. The oxygen pressure is superimposed. (C) Volume V of the droplet as a function of time t.

Oxygen passivates the Si surface (no Au migration), so catalyst stops shrinking!

Kodambaka et al., *Nano Letters* 6(6):1292-1296, 2006

Material can also be supplied by surface diffusion on the substrate

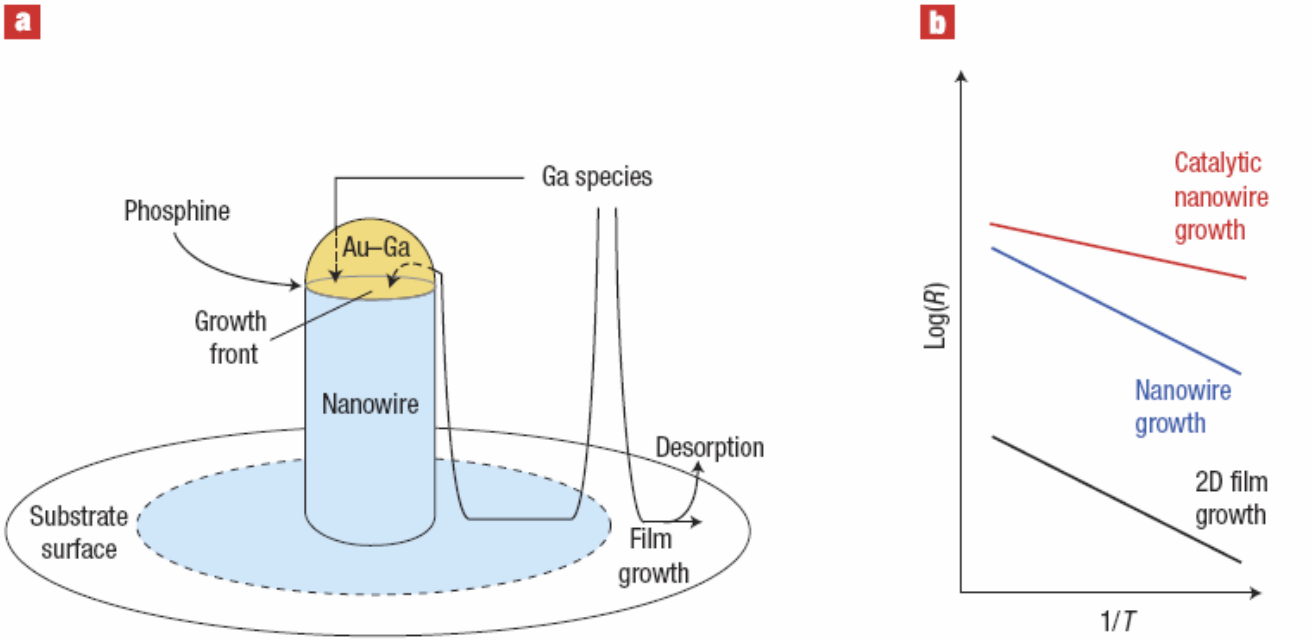

Figure 1. How gallium phosphide (GaP) nanowires grow. **a**, Gallium species that hit the substrate within one diffusion length of the growth interface between the seed particle (gold) and the nanowire contribute to nanowire growth by diffusing to the growth front. Gallium species that hit the substrate outside this region (which is shown in blue) either desorb or contribute to film growth on the substrate. Phosphorus is almost insoluble in gold and must reach the growth interface from the side. **b**, A schematic showing the logarithm of the rate of growth versus the reciprocal temperature (in Kelvin) for two-dimensional (2D) epitaxial film growth (black line), gold-seeded nanowire growth (blue line), and catalytic gold-seeded nanowire growth (red line). The gold-seeded nanowire growth rate is orders of magnitude higher than the two-dimensional film growth rate, even though the activation energies are the same. The rate for catalytic gold-seeded nanowire growth is even higher.

Borgstrom et al., *Nature Nanotechnology* 2:541, 2007.

Catalyst density affects kinetics by competition for precursor supply (GaNWs)

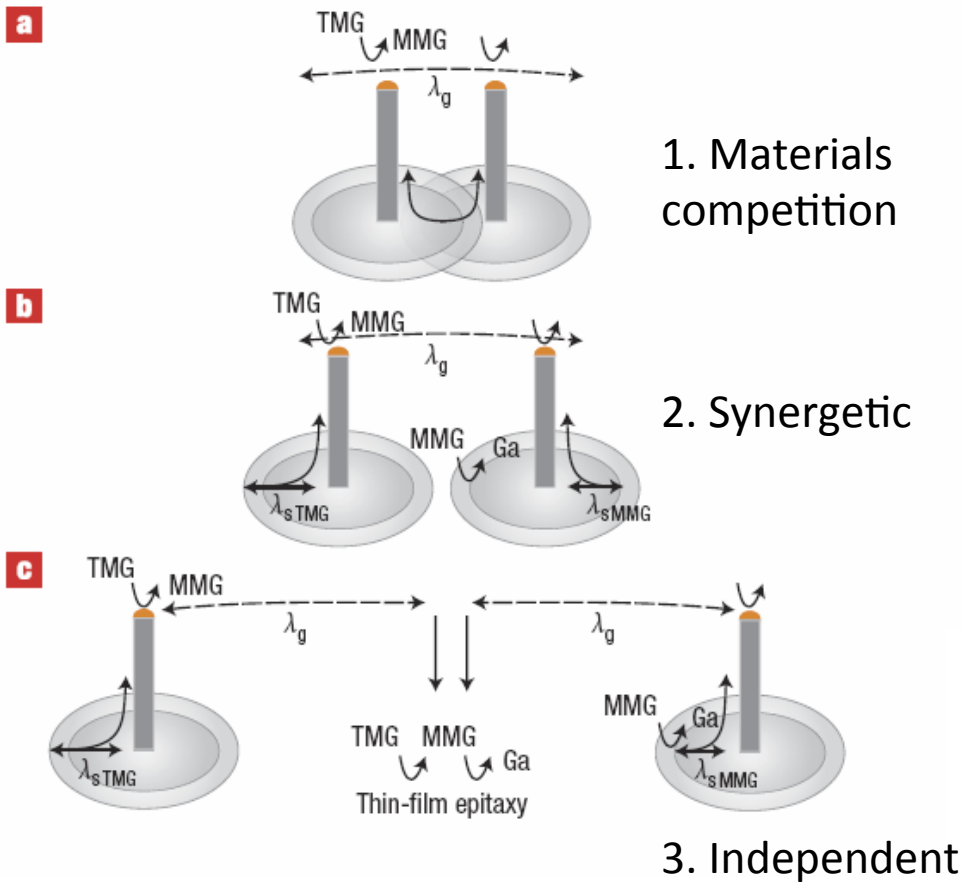

1. Materials competition

2. Synergetic

3. Independent

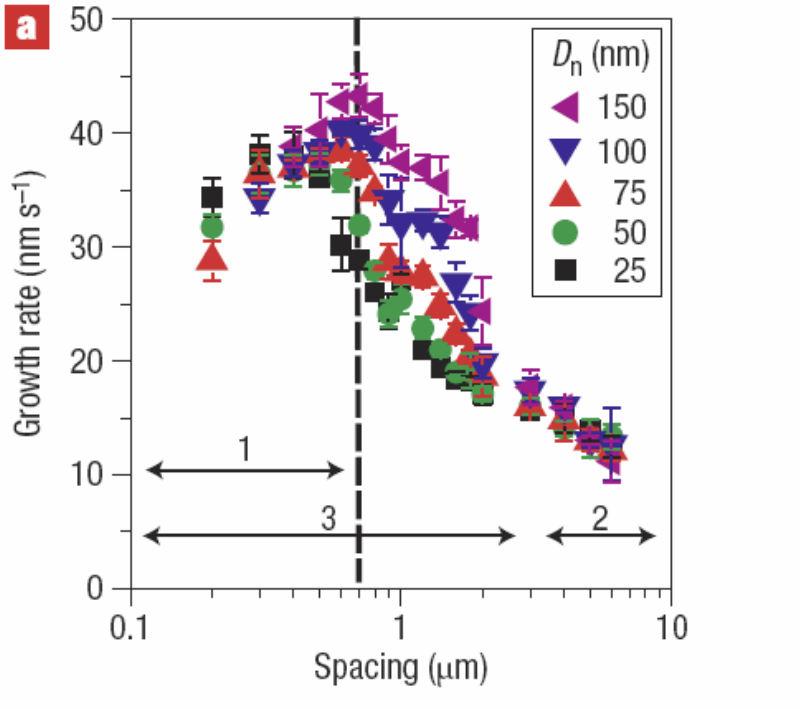

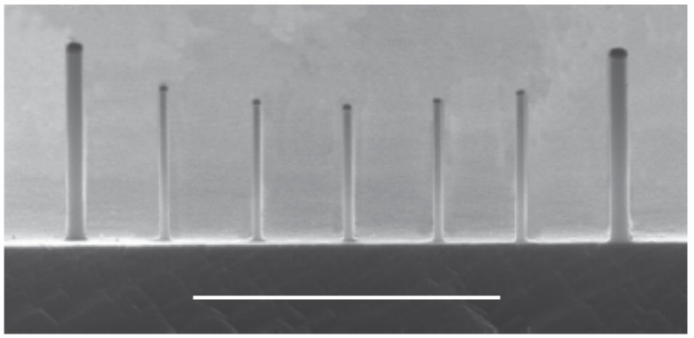

Borgstrom et al., *Nature Nanotechnology* 2:541, 2007.

CNT film growth: limiting steps are C_2H_2 dissociation then diffusion in the catalyst

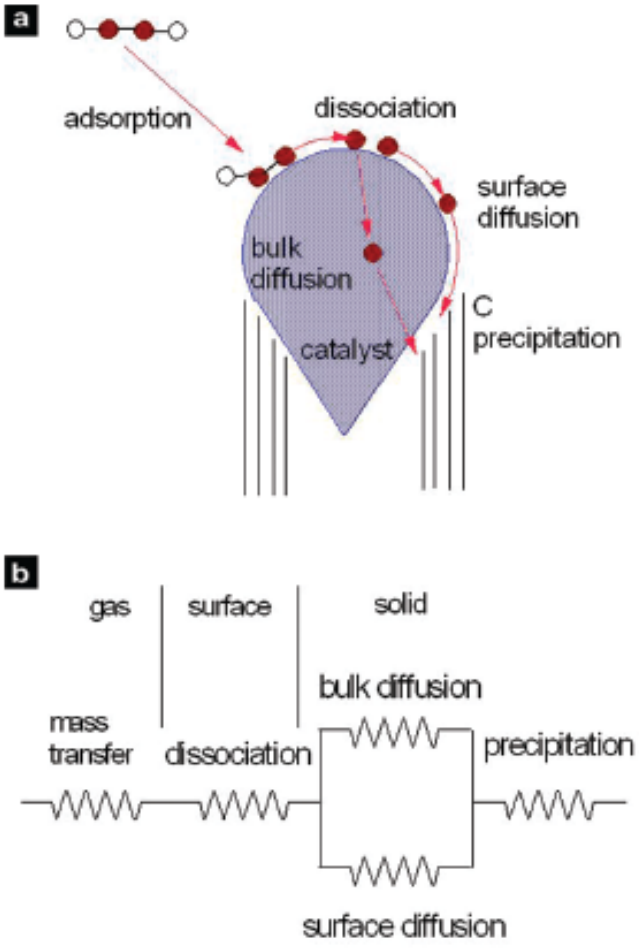

Rate ~Pressure$^{0.6}$

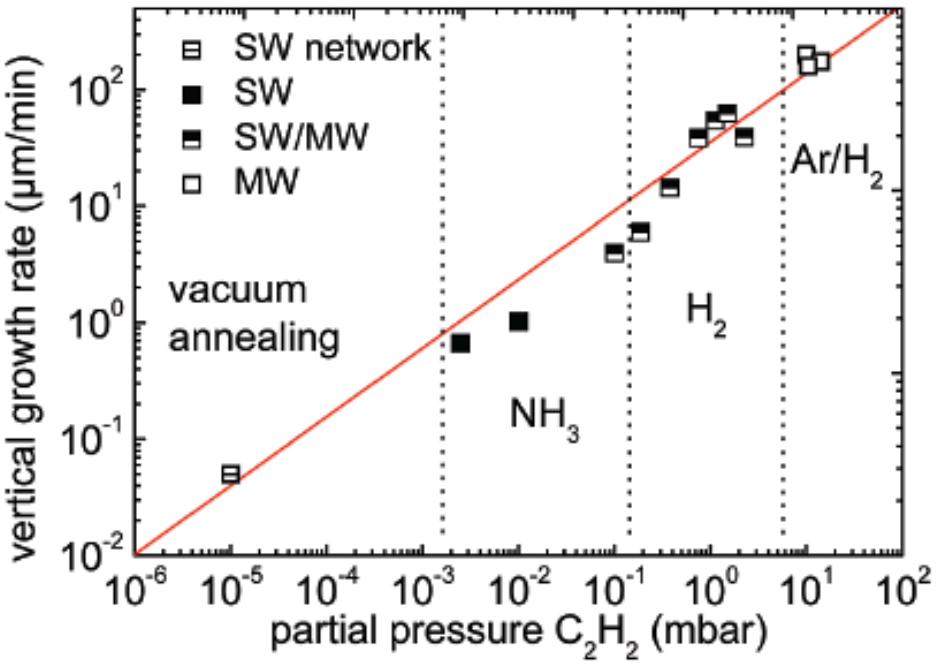

Figure 3. C_2H_2 partial pressure dependence of CNT growth rate in cold-wall conditions, $P^{0.61\pm0.03}$. CNTs were grown from an Fe/Al_2O_3 catalyst at 700 °C for 5 min. For low pressures, the growth gas is pure acetylene, and the Fe film was activated in an NH_3 atmosphere. For the higher pressure regime, growth was performed in a H_2 mixture and above 10 mbar in an Ar/H_2 mixture.

Wirth et al., *ACS Nano* 3(11):3560-3566, 2009.

Apparent activation energies at different pressures are the same (≈0.95 eV)

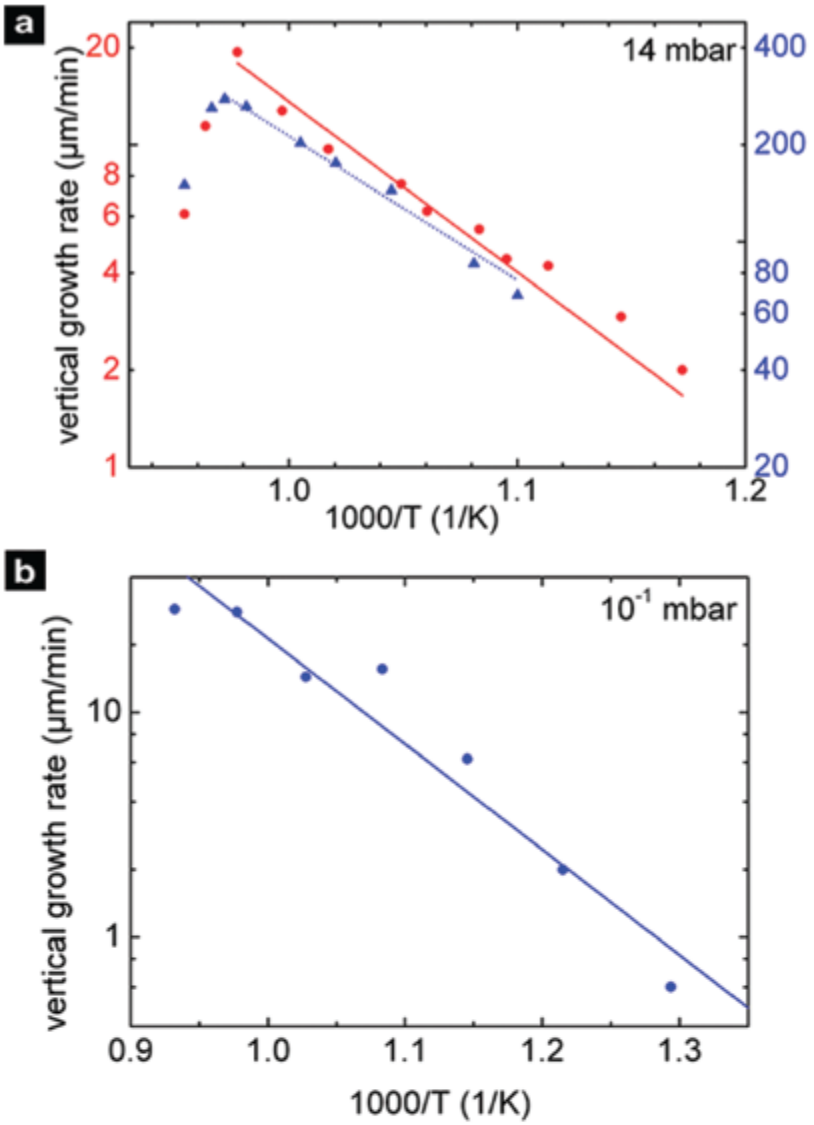

Arrhenius equation $k = Ae^{-E_a/RT}$

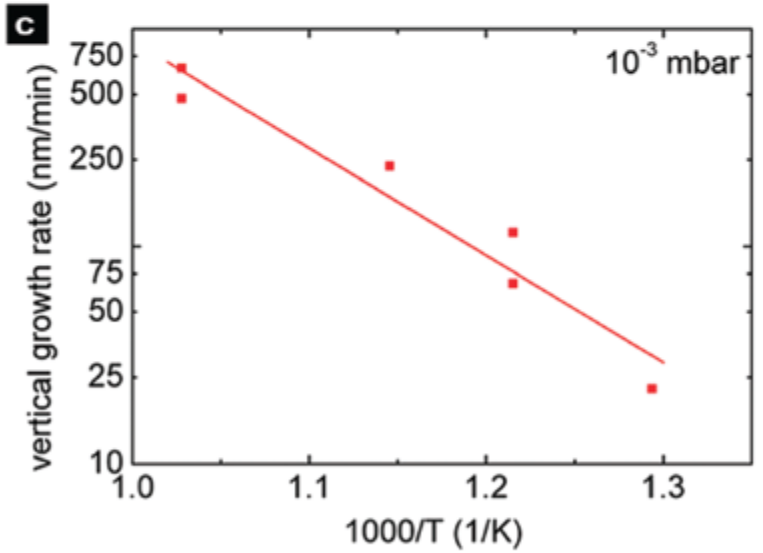

Figure 4. (a) Arrhenius plots for CNT growth rates for atmospheric pressure (●) hot-walled furnace growth and (▲) cold-walled direct heating method from an Fe−Al_2O_3 catalyst in Ar/H_2/C_2H_2 (14 mbar partial pressure C_2H_2). The activation energies are calculated from the slope of the linear fit to the data, (●) $\Delta E = 0.95 \pm 0.04$ eV, (▲) $\Delta E = 0.92 \pm 0.04$ eV. (b) Arrhenius plot at a pressure of 15 mbar in a H_2/C_2H_2 mixture (0.37 mbar partial pressure C_2H_2), $\Delta E = 0.93 \pm 0.1$ eV. The catalyst was heated in H_2 before C_2H_2 was fed into the system. (c) Arrhenius plot at a pressure of 10^{-3} mbar C_2H_2, $\Delta E = 0.98 \pm 0.1$ eV. The C_2H_2 was undiluted during growth. The catalyst film was annealed in NH_3 prior to growth for 5 min.

Wirth et al., *ACS Nano* 3(11):3560-3566, 2009.

Is diffusion by surface or bulk?

Arrhenius equation $k = Ae^{-E_a/RT}$

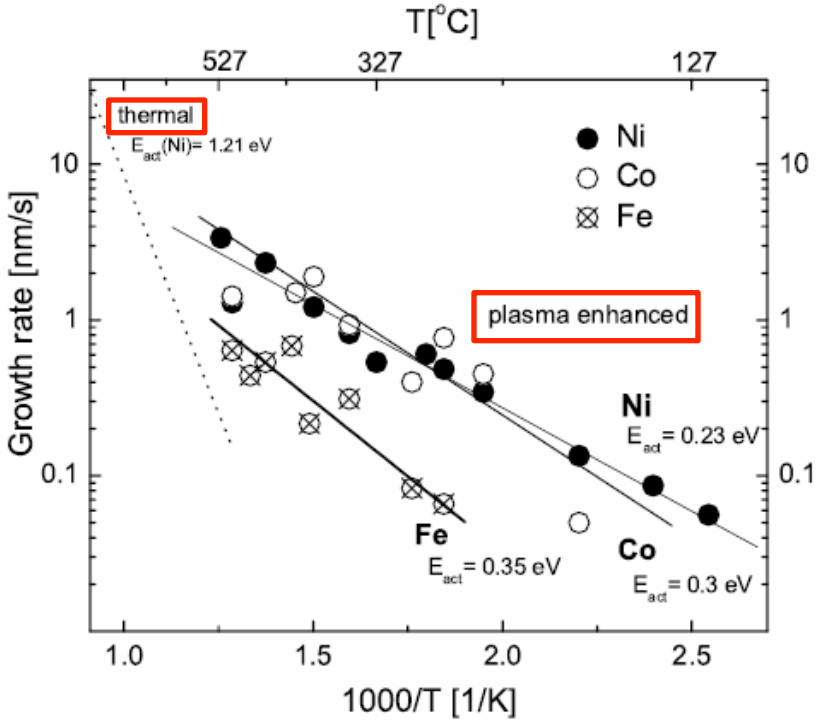

FIG. 2. Arrhenius plots for CNF growth rates on different catalysts in NH_3 diluted C_2H_2. The activation energies are calculated from the slope of the linear fit to the data. Temperature dependent changes in the CNFs crystallinity are not considered. The dotted line is the growth rate variation for Ni thermal CVD (E_{act} = 1.21 eV [11,42]).

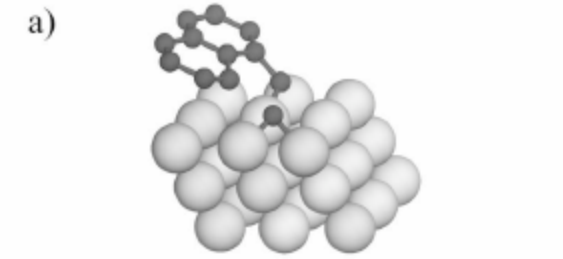

C_2H_2 dissociation

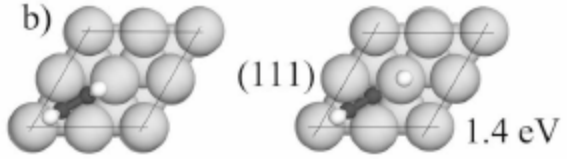

C surface diffusion

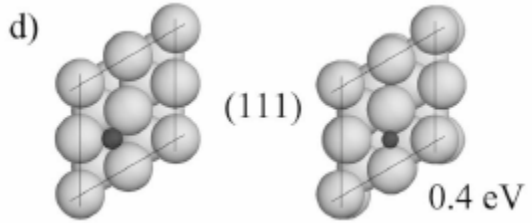

Hofmann et al., *Physical Review Letters*, 95(3):036101 2005.

Catalyst ripening and migration during CNT film growth

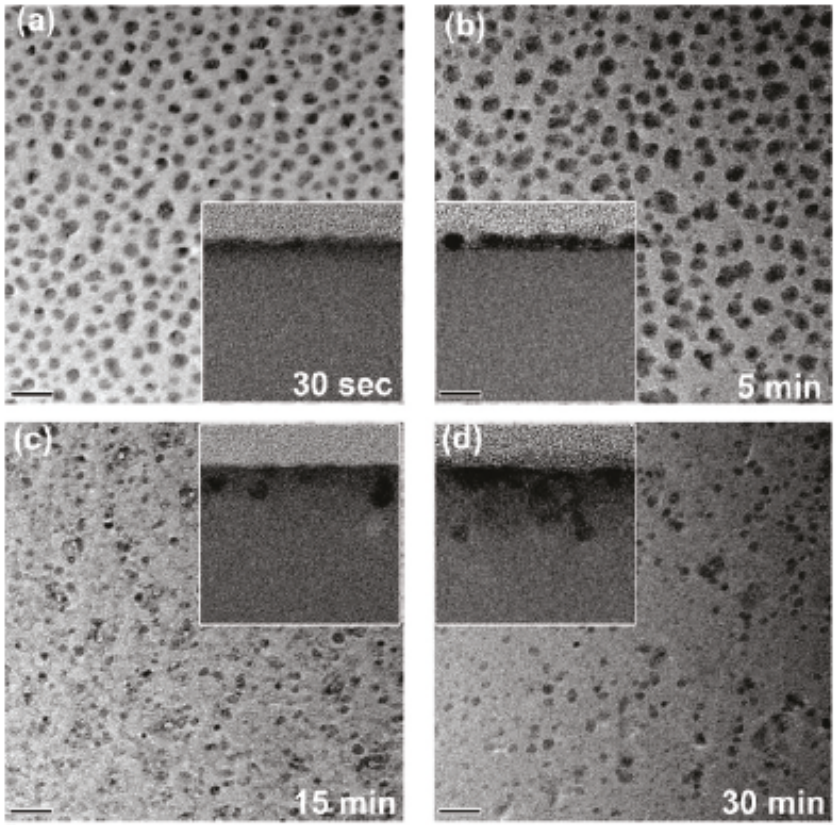

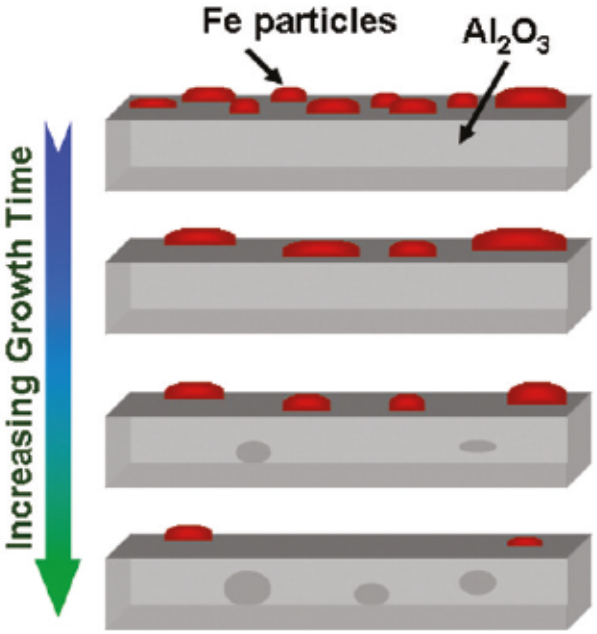

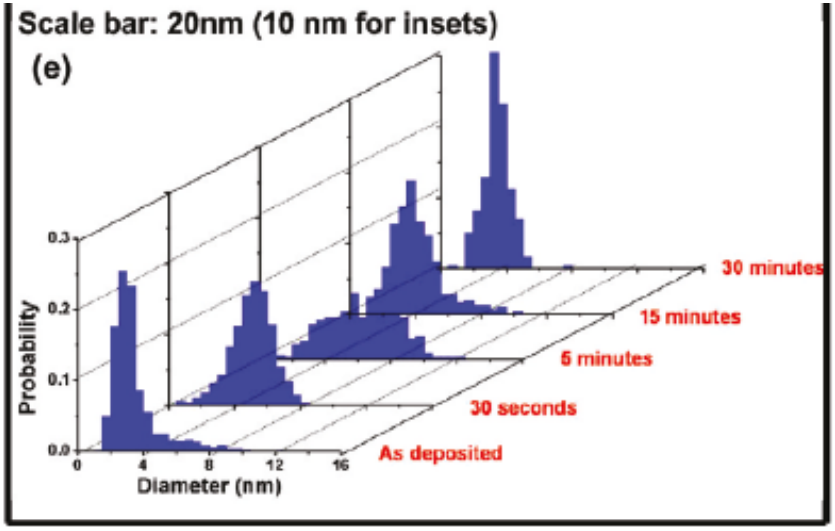

Figure 1. Plan-view TEM images of annealed Fe/Al_2O_3 catalyst layers at 750 °C for various labeled times for (a) 30 s, (b) 5 min, (c) 15 min, and (d) 30 min. Insets are cross-sectional views demonstrating subsurface diffusion of Fe into the Al_2O_3 layer. (e) Statistical representation of the catalyst particle size distribution for the four cases shown in (a)–(d) and the as-deposited Fe sample.

Kim et al., *JPC Letters* (in press), 2010.

Graphene growth and transfer printing

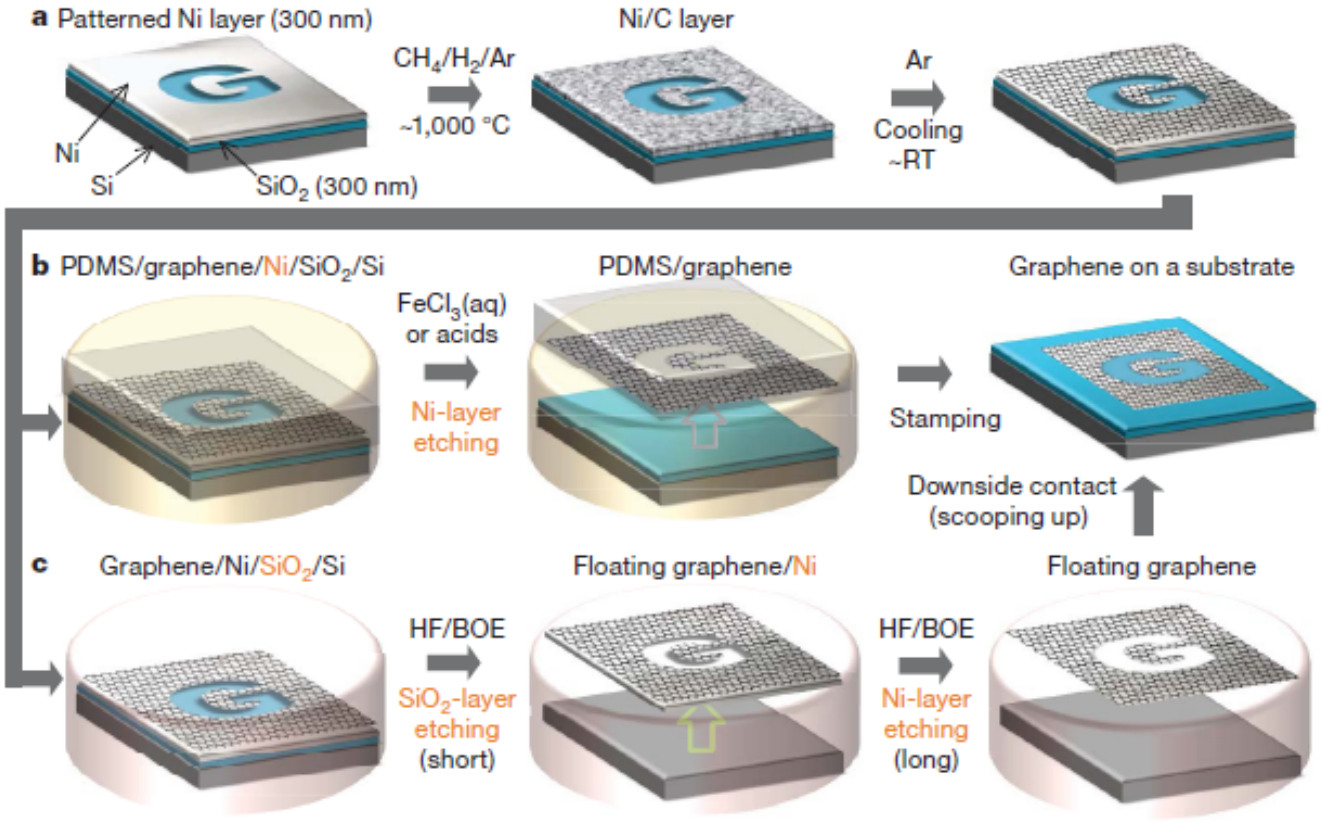

Figure 1 | Synthesis, etching and transfer processes for the large-scale and patterned graphene films. **a**, Synthesis of patterned graphene films on thin nickel layers. **b**, Etching using $FeCl_3$ (or acids) and transfer of graphene films using a PDMS stamp. **c**, Etching using BOE or hydrogen fluoride (HF) solution and transfer of graphene films. RT, room temperature (~25 °C).

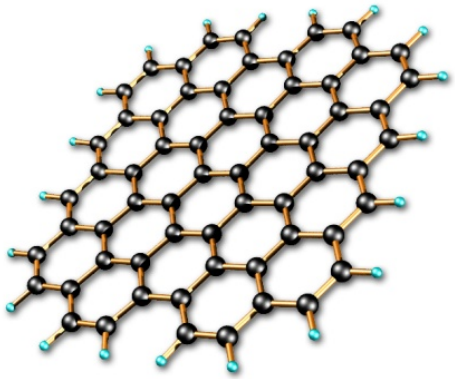

Kim et al., *Nature* 457:706-710, 2009.

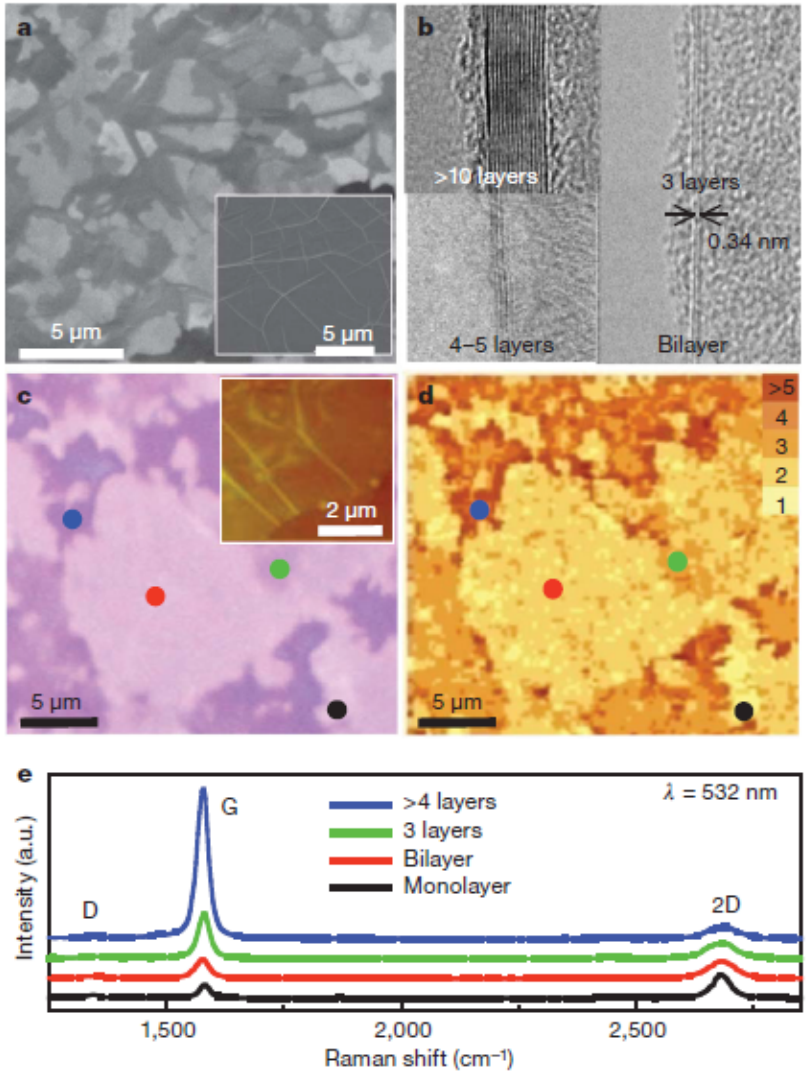

Figure 2 | Various spectroscopic analyses of the large-scale graphene films grown by CVD. **a**, SEM images of as-grown graphene films on thin (300-nm) nickel layers and thick (1-mm) Ni foils (inset). **b**, TEM images of graphene films of different thicknesses. **c**, An optical microscope image of the graphene film transferred to a 300-nm-thick silicon dioxide layer. The inset AFM image shows typical rippled structures. **d**, A confocal scanning Raman image corresponding to **c**. The number of layers is estimated from the intensities, shapes and positions of the G-band and 2D-band peaks. **e**, Raman spectra (532-nm laser wavelength) obtained from the corresponding coloured spots in **c** and **d**. a.u., arbitrary units.

Graphene growth mechanisms

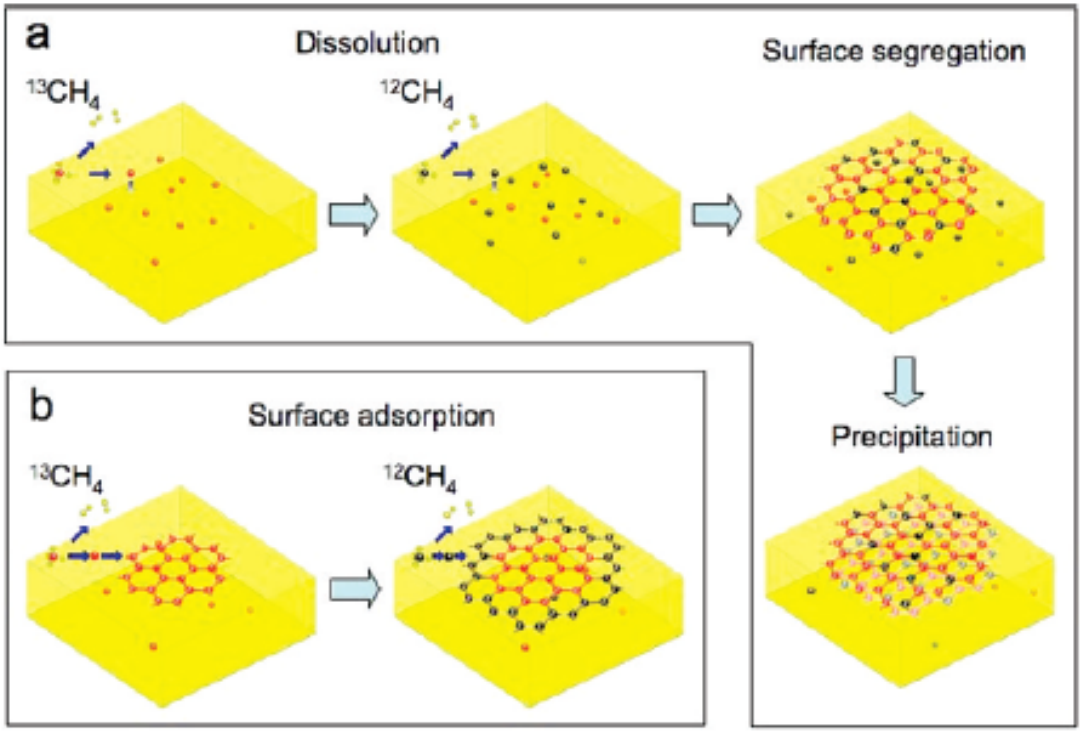

Figure 1. Schematic diagrams of the possible distribution of C isotopes in graphene films based on different growth mechanisms for sequential input of C isotopes. (a) Graphene with randomly mixed isotopes such as might occur from surface segregation and/or precipitation. (b) Graphene with separated isotopes such as might occur by surface adsorption.

Li et al., *Nano Letters* 9(12):4268-4272, 2009.

Summary: key process conditions and trends

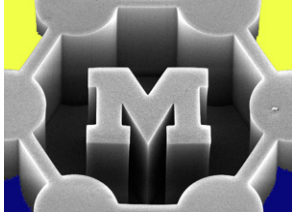

Key variables for CVD growth:

- Reactant composition, supply rate, temperature, pressure, catalyst composition, particle size, substrate

Three important stages:

- Prepare catalyst
- Nucleate
- Grow

Trends:

↑ Catalyst size = ↑ CNT diameter

↑ Temperature = ↑ CNT diameter

↑ Carbon feed = ↑ CNT diameter

CVD growth systems

Horizontal tube, fixed catalyst

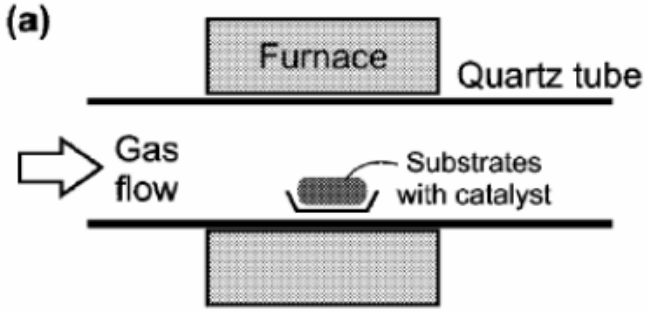

Vertical tube, floating catalyst

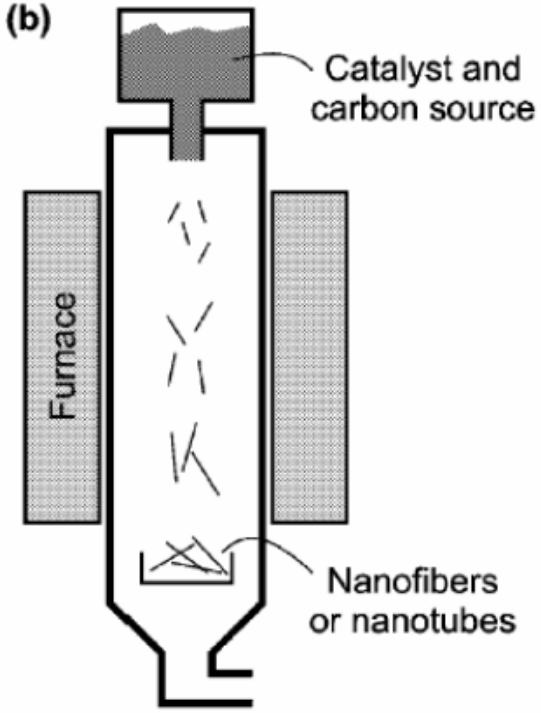

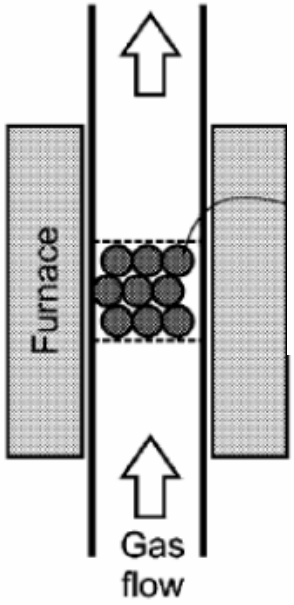

Plasma-enhanced

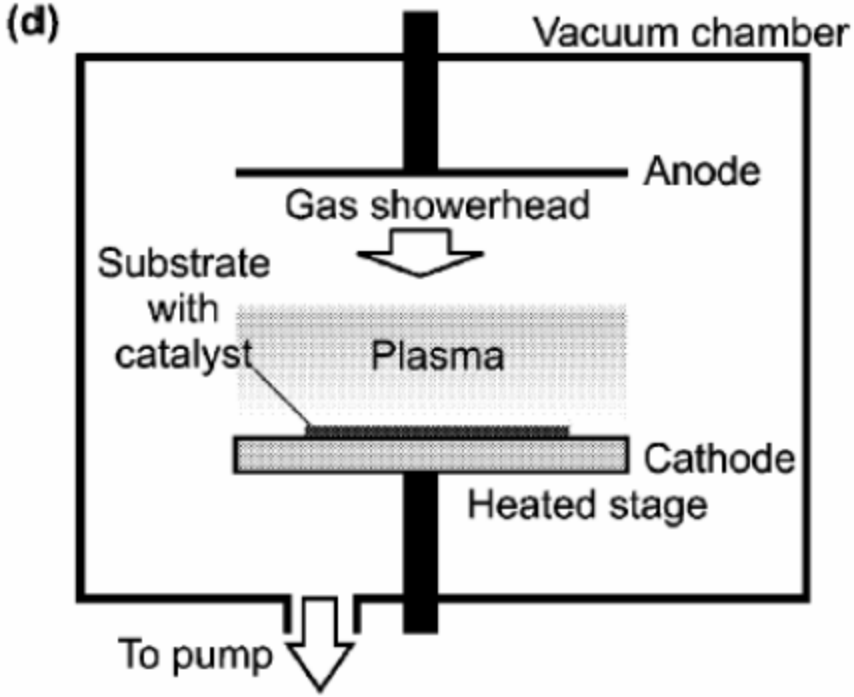

Precursor can be
- **Gas (e.g., pressurized tank)**
- **Liquid (e.g., spray, evaporate)**
- **Solid (evaporate or sublime)**

Vertical tube, fluidized bed

Teo, 2003.

Reactor design: fluidized bed

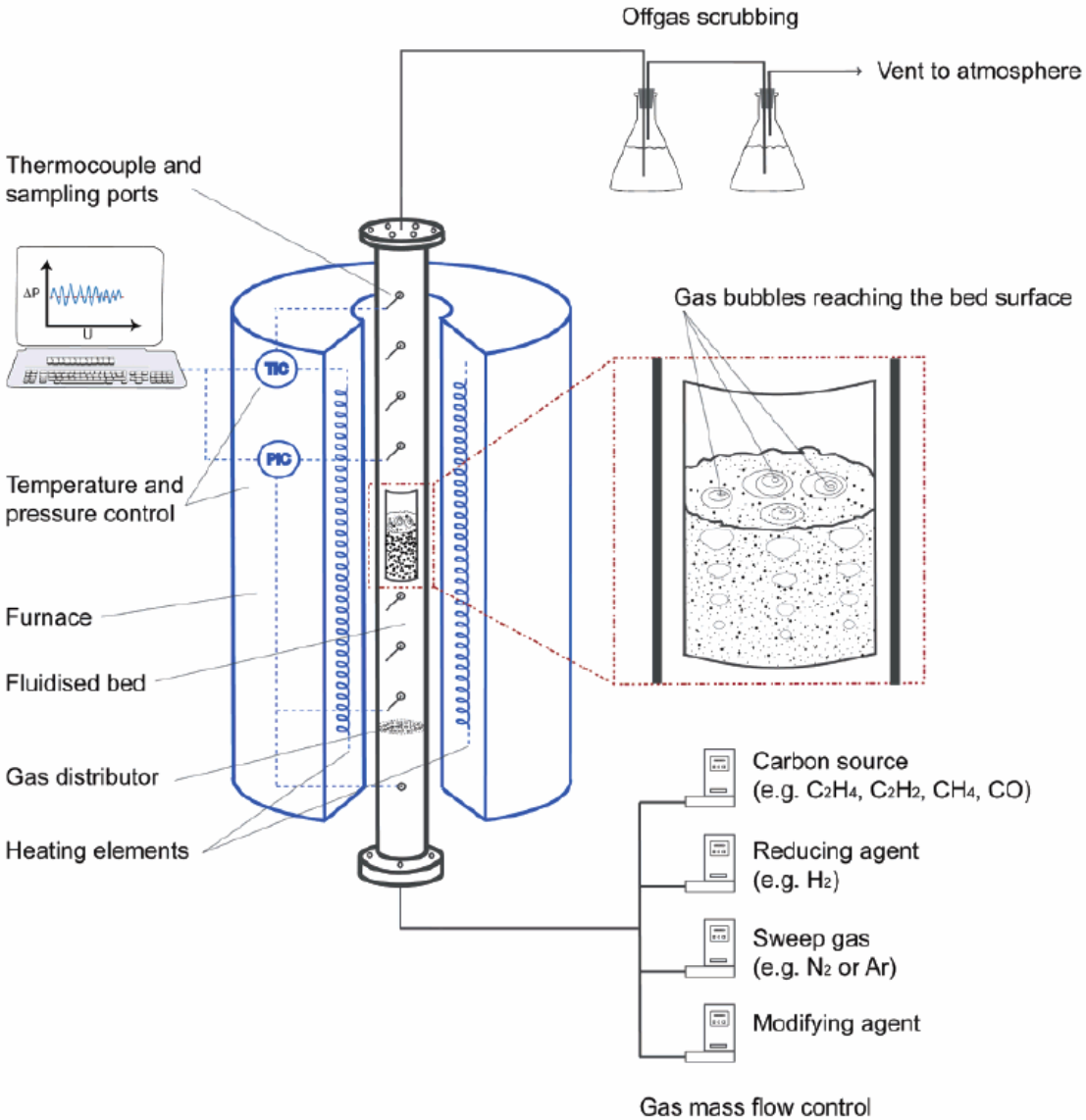

Figure 4. Sketch of a typical fluidized-bed reactor setup. A cylindrical reactor is affixed within a high-temperature furnace with appropriate temperature, pressure, and gas flow controls, connected to a data logging system. Environmental mitigation systems are incorporated to remove entrained solid particles in the off-gas before venting to atmosphere.

See et al., *Ind. Eng. Chem. Res.* 46:997, 2007.

Large fluidized bed reactor

Fluidized bed reactor: 30 kg/h MWNTs = 265 tons/yr @24-7
(F. Wei, Tsinghua Univ)

Worldwide MWNT production (2006 estimate)

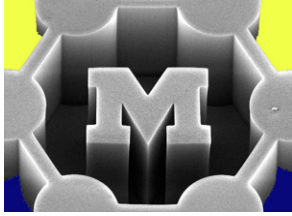

Geography	Country	Company	Capacity (kg/hr)	Capacity (tpy) *
Asia	China	NTP	5	10
Asia	China	Sun	0.625	5
Asia	China	Tsinghua (Prof. Fei Wei)	15	15
Asia	Korea	Iljin	10	10
Asia	Japan	NCT	5	30
Asia	Japan	Showa Denko	16.7	100
Europe		Not Disclosed	0.833	5
Europe		Not Disclosed	2.5	15
Europe		Not Disclosed	0.167	1
Europe		Not Disclosed	1	6
North America	USA	Hyperion	8.3	50
North America	USA	Not Disclosed	4	24
North America			**12.3**	**74**
Europe			**4.5**	**27**
Asia			**52.3**	**170**
Total Capacity			**69.1**	**271**

MWNT total ≈ 270 tons/yr
SWNT total <10 tons/yr

Large scale CNT manufacturing process: growth, annealing, mixing

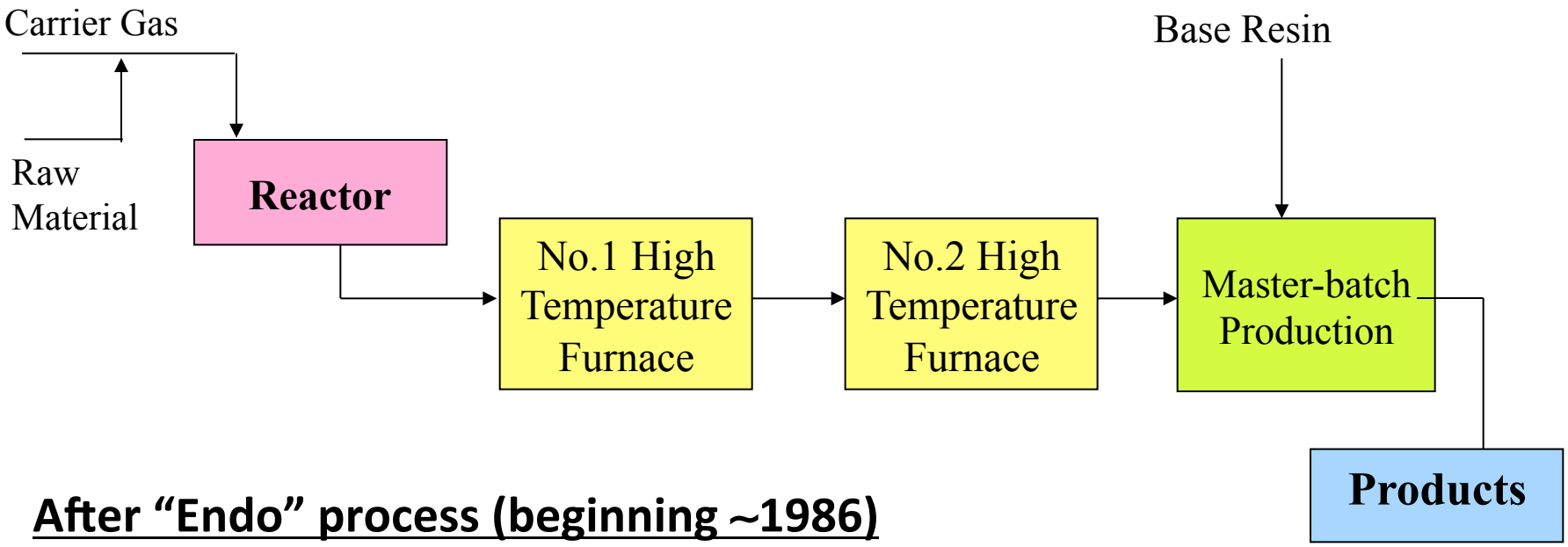

After "Endo" process (beginning ~1986)

- Floating catalyst CVD
- Followed by two stages of high temperature treatment
- Now > 300 tons/yr
- High purity: 99.5 wt% as carbon
- CNT diameter 40-90 nm

Healing defects by high-temperature annealing

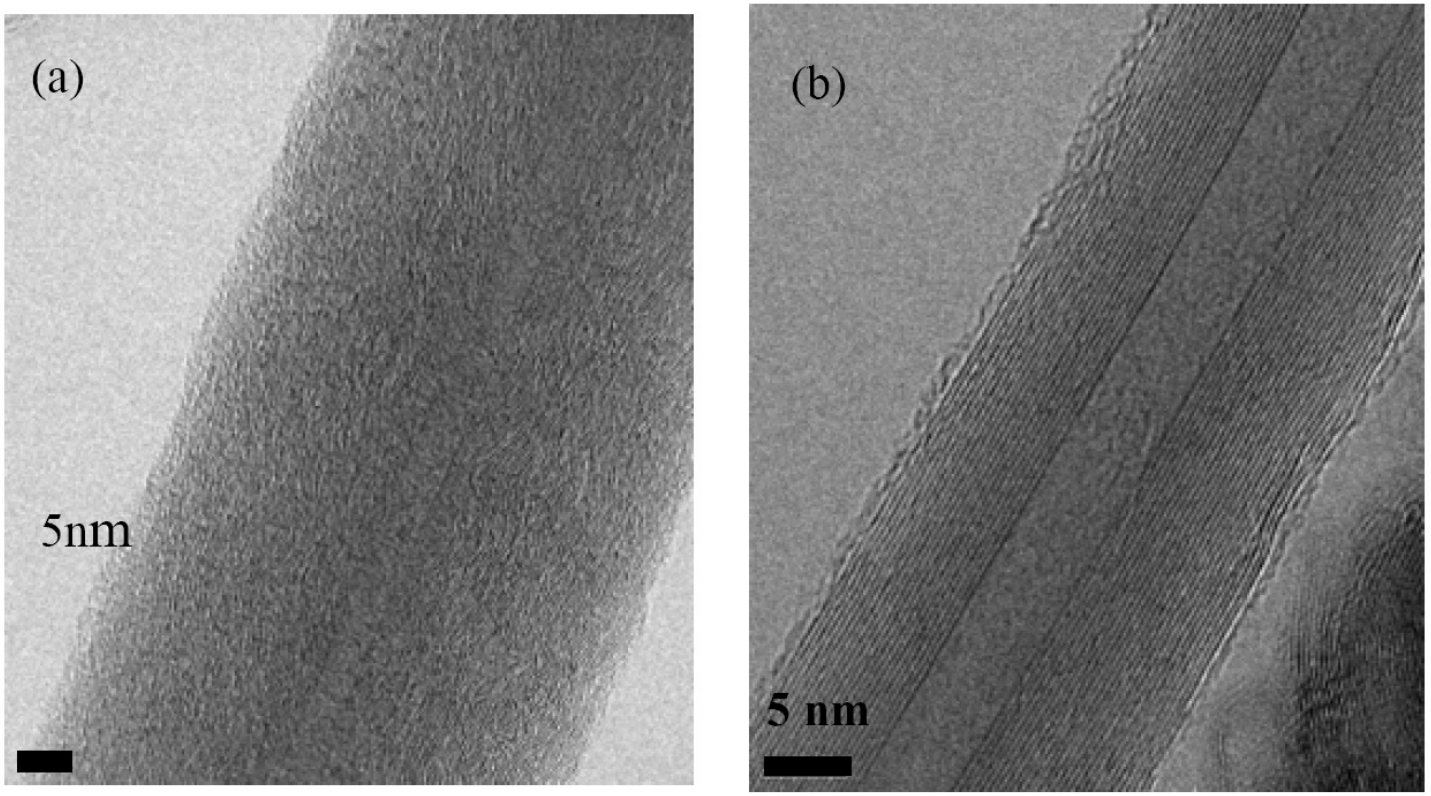

Figure 2.8. HRTEM images of (a) bulk grade and (b) high purity grade MWCNTs (Courtesy of NCT).

Nano Carbon Technologies (NCT), Japan

Toray: Zeolite-templated SWNT Growth

Zeolite : Crystalline inorganic oxide consisting mainly of silicon

Unit cell of zeolite

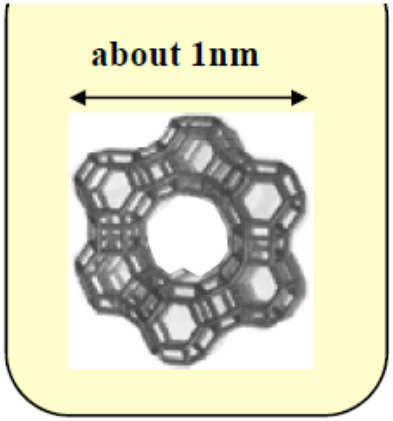

Self-assembly

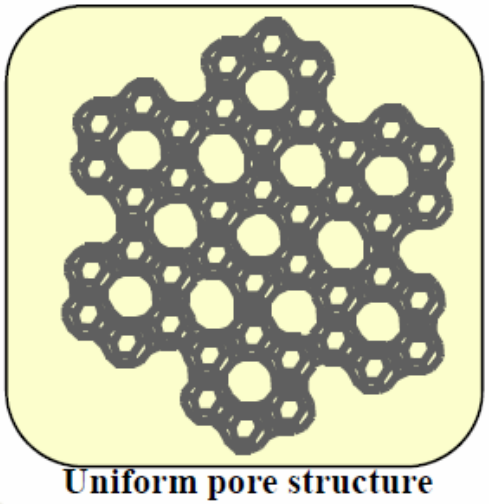

Uniform pore structure

SEM picture of zeolite

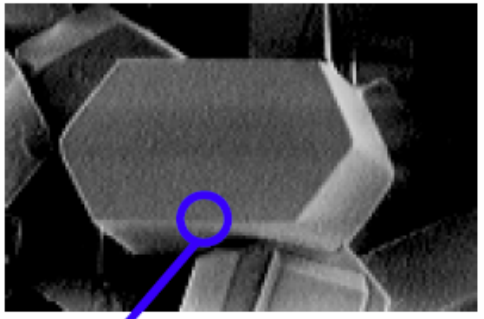

Concept of Toray's CVD method

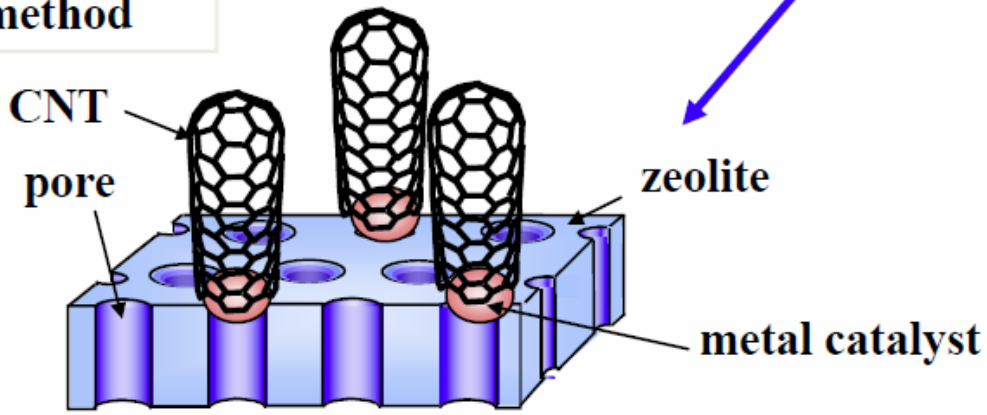

Dispersion of metal catalysts on the surface of zeolites by using uniform nano-structure

'TORAY'

SWNTs from ethanol carbon source, zeolite support

Purified 10 g sample

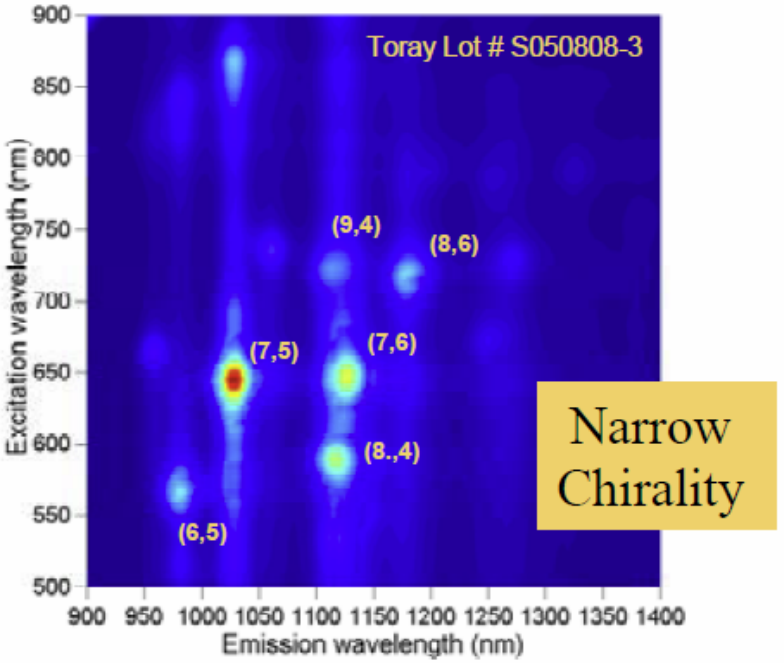

Narrow Chirality

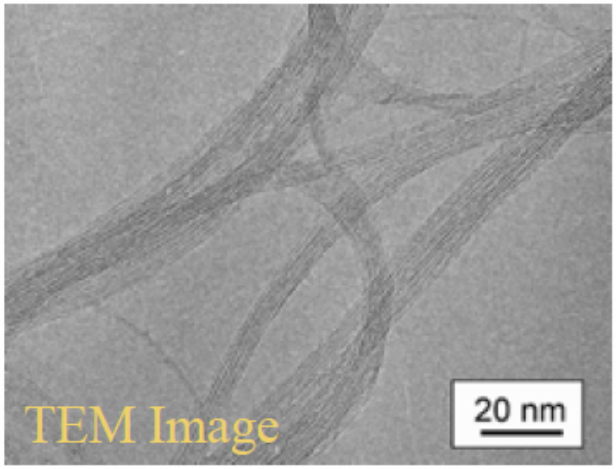

Economics of bulk CNT production

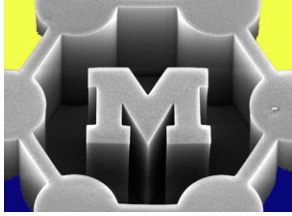

System Type	CNT Capacity (kg/hr)	Total Primary Equipment Investment (K USD)	Installed Investment (8 Year ROI) (USD/kg)	Consumables*		Cost Consumables (USD/kg)	Efficiency of Catalyst Use (Relative Index)	Cost Production (USD/kg) exclusive of Catalyst & Labor
				Electricity (kWhr/kg)	C Source (m^3/kg)			
Rotary Tube 400mm dia.	5	870	5.1	12.5	3.0	8.25	1	13.4
Single Rotary (20 x 400mm)	100	17,550	3.4	12.5	3.0	8.25	1	11.6
Multi-tube Rotary (3 x 400mm dia.)	15	2,090	3.6	10	3.0	8.0	1	11.6
Multi-tube Rotary (7x)	100	14800	2.8	10	3.0	8.0	1	10.8
Cascade Rotaries	5	960	5.5	15	3.0	8.5	1	14.0
Non Quartz Lined Rotary (3 x 1.4m dia.)	100	7800	1.6	6.7	3.5	7.75	1	9.4
Pusher	5	2052	8.8	10	2.0	11.0	< 1	19.8
Pusher (3 x 3000mm W)	100	12900 (3)	2.5	8.6	2.0	10.9	< 1	13.4
Mesh Belt	5	1942	8.4	12.5	2.0	11.4	< 1	19.8
Mesh Belt (2 x 3500mm W)	100	8370 (2)	1.7	7.5	2.0	10.9	< 1	12.6
Fluidized Bed	5	737	4.8	9.5	1.5	4.5	1.25	9.3
Fluidized Bed (3 x 400 mm Dia)	100	3325 (3)	1.0	4.2	1.5	3.5	1.25	4.5

R. Blackmon, Harper International

CVD by plasmon resonance heating

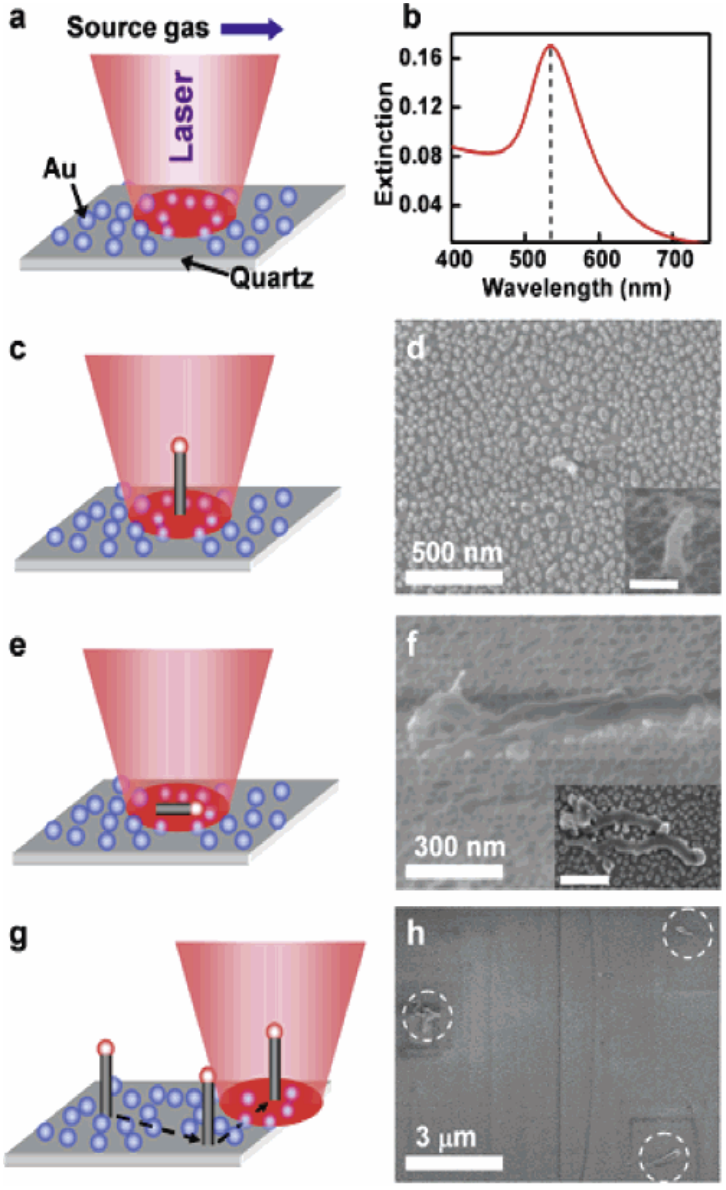

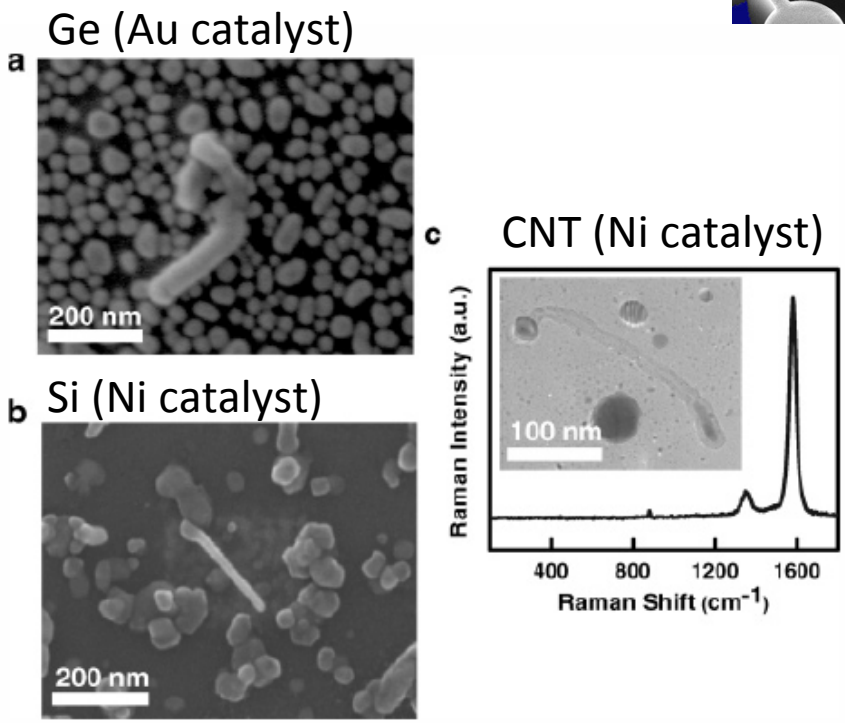

Figure 2. (a) Scanning electron microscopy (SEM) image of gold-catalyzed germanium nanowires. (b) SEM image of nickel-catalyzed silicon nanowires. In experiments, we observed that the nickel catalyst at the top of the nanowire was faceted, suggestive of a vapor−solid−solid growth mechanism. (c) TEM image of a multiwall CNT with an encapsulated catalyst inset into a Raman spectrum taken from the CNT growth region. The Raman spectrum shows two narrow line width peaks at 1352 and 1582 cm^{-1} that are characteristic of CNTs. The absence of the breathing mode peak at ~100−200 cm^{-1} characteristic of single walled CNTs suggests a high fraction of multiwalled CNTs in the area probed with Raman.

Cao et al., *Nano Lett.*, 2007 (ASAP).